J. Fluid Mech. (2017), *vol.* 830, *pp.* 165–210.
doi:10.1017/jfm.2017.534

The effect of inertia on the time period of rotation of an anisotropic particle in simple shear flow

Navaneeth K. Marath[1] **and Ganesh Subramanian**[1,†]

[1]Engineering Mechanics Unit, Jawaharlal Nehru Centre for Advanced Scientific Research, Jakkur, Bangalore, 560 064, India

(Received 19 December 2016; revised 27 July 2017; accepted 29 July 2017; first published online 29 September 2017)

We calculate the leading-order correction to the time period of rotation of a neutrally buoyant spheroid of arbitrary aspect ratio, in a simple shear flow ($\boldsymbol{u}^{\infty} = \dot{\gamma} y \mathbf{1}_1$; $\mathbf{1}_1$ is the unit vector in the flow direction, y being the coordinate along the gradient direction), in its long-time orbit set up by the weak fluid inertial drift at $O(Re)$. Here, Re is the microscale Reynolds number, a dimensionless measure of the fluid inertial effects on the length scale of the spheroid, and is defined as $Re = \dot{\gamma} L^2 \rho/\mu$, where L is the semimajor axis of the spheroid, μ and ρ are respectively the viscosity and density of the fluid, and $\dot{\gamma}$ is the shear rate. This long-time orbit is the tumbling orbit for prolate spheroids; for oblate spheroids, it is the spinning orbit for aspect ratios greater than 0.137, and can be either the tumbling or the spinning orbit for oblate spheroids of aspect ratios less than 0.137. We also calculate the leading-order correction to the time period of rotation of a neutrally buoyant triaxial ellipsoid in a simple shear flow, rotating with its intermediate principal axis aligned along the vorticity of the flow; the latter calculation is in light of recent evidence, by way of numerical simulations (Rosen, PhD dissertation, 2016, Stockholm), of the aforementioned rotation being stabilized by weak inertia. The correction to the time period for arbitrary Re is expressed as a volume integral using a generalized reciprocal theorem formulation. For $Re \ll 1$, it is shown that the correction at $O(Re)$ is zero for spheroids (with aspect ratios of order unity) as well as triaxial ellipsoids in their long-time orbits. The first correction to the time period therefore occurs at $O(Re^{3/2})$, and has a singular origin, arising from fluid inertial effects in the outer region (distances from the spheroid or triaxial ellipsoid of the order of the inertial screening length of $O(LRe^{-1/2})$), where the leading-order Stokes approximation ceases to be valid. Since the correction comes from the effects of inertia in the far field, the rotating spheroid (triaxial ellipsoid) is approximated as a time-dependent point-force-dipole singularity, allowing for the reciprocal theorem integral to be evaluated in Fourier space. It is shown for all relevant cases that fluid inertia at $O(Re^{3/2})$ leads to an increase in the time period of rotation compared with that in the Stokes limit, consistent with the results of recent numerical simulations at finite Re. Finally, combination of the $O(Re^{3/2})$ correction derived here with the $O(Re)$ correction derived earlier by Dabade *et al.* (*J. Fluid Mech.*, vol. 791, 2016, 631703)

† Email address for correspondence: sganesh@jncasr.ac.in

yields a uniformly valid description of the first effects of inertia for spheroids of all aspect ratios, including prediction of the arrest of rotation for extreme-aspect-ratio spheroids.

Key words: low-Reynolds-number flows, multiphase and particle-laden flows, suspensions

1. Introduction

In the Stokes limit, it is well known that, in simple shear flow, a spheroid rotates in any of a one-parameter family of orbits (Jeffery 1922), eponymously called the Jeffery orbits. The generic Jeffery orbit is a spherical ellipse corresponding to a time-dependent three-dimensional precessional motion of the orientation vector about the vorticity axis. The limiting members of the aforementioned family are the tumbling orbit, a great circle in the flow–gradient plane, and the spinning orbit, where the angular velocity vector is time-independent and aligned with the ambient vorticity (see figure 1*a*,*b*,*d*). In the Stokes limit, a spheroid will continue to rotate in a Jeffery orbit determined by its initial orientation for all time. It was shown recently that weak inertia in the suspending fluid and that of the particle, at $O(Re)$ and $O(St)$ respectively, stabilize either the spinning or the tumbling orbit (Einarsson *et al.* 2015; Dabade, Marath & Subramanian 2016; Marath, Dwivedi & Subramanian 2017). Here, Re and St are the Reynolds and Stokes numbers, with $Re = \dot{\gamma}L^2\rho/\mu$ and $St = \dot{\gamma}L^2\rho_p/\mu$, where $\dot{\gamma}$ is the shear rate corresponding to the ambient flow given by $\boldsymbol{u}^\infty = \dot{\gamma}y\mathbf{1}_1$ (see figure 1*a*), L is the length of the semimajor axis of the spheroid, μ is the viscosity of the fluid, and ρ and ρ_p are the densities of the fluid and particle respectively. Marath *et al.* (2017), in particular, showed that the orientation dynamics in the presence of both inertia and rotary Brownian motion allows for an elegant thermodynamic interpretation which has similarities to the coil–stretch transition described in the polymer physics literature (De Gennes 1974; Hinch 1974). In Dabade *et al.* (2016), it was pointed out that weak inertial effects at $O(Re)$ and $O(St)$ do not alter the time period of rotation from its leading-order Stokesian value given by $T_{jeff} = 2\pi\dot{\gamma}^{-1}(\kappa + 1/\kappa)$ and $T_{jeff} = 4\pi$ respectively for the tumbling and spinning orbits. Here, $\kappa = L/b(b/L)$ is the aspect ratio of the prolate (oblate) spheroid, where b is the semiminor axis of the spheroid. As shown later, for a spheroid rotating in the tumbling orbit, the aforementioned vanishing of the $O(Re)$ correction is true only for spheroids with aspect ratios of order unity.

Dabade *et al.* (2016) also calculated the $O(St^2)$ correction to the tumbling period, a simpler calculation due to its regular nature, and showed that the time period decreases from the aforementioned Jeffery value at the said order. This decrease is on account of the inertial persistence of the angular velocity maximum in the vicinity of the gradient–vorticity plane for a prolate spheroid (the flow–vorticity plane for an oblate one). On account of being a singular perturbation problem, the correction due to fluid inertia, which comes at $O(Re^{3/2})$ for spheroids with order-unity aspect ratios, needs a more elaborate analysis and was not investigated in Dabade *et al.* (2016). A recent simulation effort (Mao & Alexeev 2014) has shown that, in contrast to particle inertia, fluid inertia increases the time period of rotation in the stable orbits from its leading-order Jeffery value, although the simulations largely explored Re values of order unity and only aspect ratios of 0.5, 0.8, 1.2 and 2; the small-Re regime, characterizing the first effects of inertia, has not been systematically investigated. In this paper, we calculate the first effects of fluid inertia at $O(Re^{3/2})$ on the time period

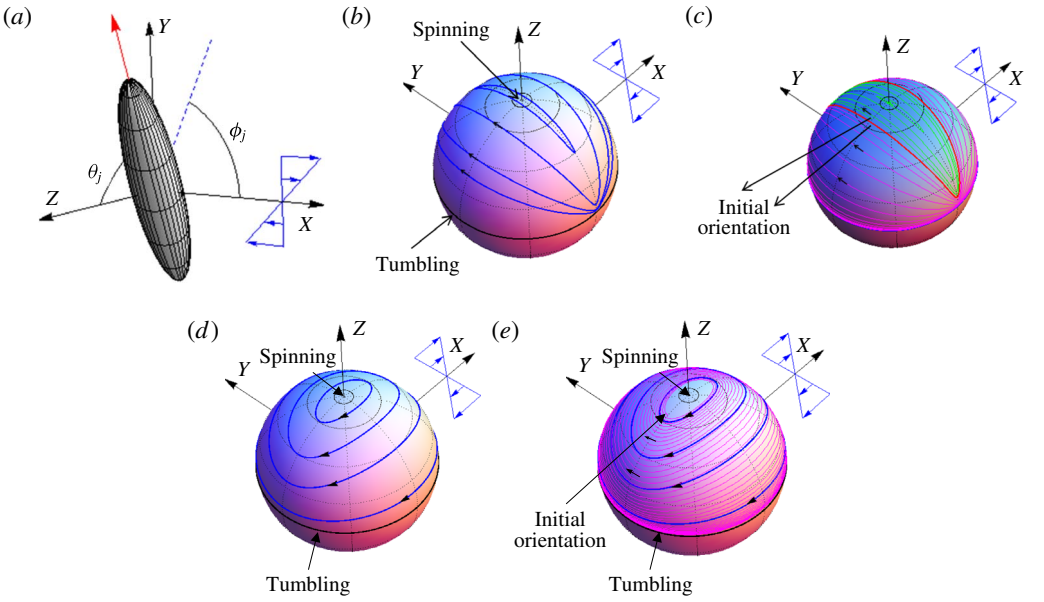

FIGURE 1. (Colour online) (*a*) The orientation vector (red) defined by the angles θ_j and ϕ_j in the space-fixed coordinate system XYZ. The X, Y and Z axes correspond to the flow, the gradient and the vorticity directions of the simple shear flow. (*b*) Jeffery orbits (blue) for an oblate spheroid of aspect ratio 0.05 for different initial conditions. The limiting orbits, that is the tumbling and spinning modes, are indicated. (*c*) The repeller (red) for an oblate spheroid of aspect ratio 0.05, which divides the unit hemisphere into two distinct basins of attractions. The trajectories of the spheroid due to fluid inertial drift at $O(Re)$, starting from either side of the repeller and ending at the attractors of the corresponding basins, are shown as purple and green curves. (*d*) Jeffery orbits (blue) for a prolate spheroid of aspect ratio 2. (*e*) The $O(Re)$ inertial trajectory (purple), which ends in the tumbling orbit, for the same prolate spheroid.

of rotation as a function of the aspect ratio for both prolate and oblate spheroids, and for triaxial ellipsoids over a restricted range of two-axis ratios which includes the value examined in a recent numerical investigation (Rosen 2016). Towards the end of the paper, the $O(Re^{3/2})$ analysis is combined with the $O(Re)$ analysis given in Dabade *et al.* (2016). The latter continues to predict the critical Reynolds number for the arrest of rotation of extreme-aspect-ratio spheroids (both slender fibres and flat disks). The critical Reynolds number is $O(\kappa)$ for flat disks and $O(\ln\kappa/\kappa)$ for slender fibres, the latter being the same as that originally predicted by Subramanian & Koch (2005) based on slender-body theory.

In a simple shear flow, the $O(Re^{3/2})$ correction arises due to fluid inertia becoming important in a region of the order of and beyond the inertial screening length, defined as $LRe^{-1/2}$ ($Re \ll 1$). In this so-called outer region, the Stokes approximation breaks down and inertial forces balance viscous forces at leading order. The aforementioned inertial screening length can be obtained from this balance as follows: the Stokes disturbance field due to a freely rotating spheroid in simple shear flow decays as $O(1/r^2)$. Here, r is the distance (scaled with L) from the centre of the spheroid. The inertial terms, for instance $\boldsymbol{\Gamma}\cdot\boldsymbol{r}\cdot\nabla\boldsymbol{u}$, would scale as Re/r^2 and the viscous term would scale as $1/r^4$; a balance gives $r\sim Re^{-1/2}$ ($\boldsymbol{\Gamma}$ is the non-dimensional velocity gradient

tensor for simple shear, and $\boldsymbol{u}$ is the spheroid disturbance velocity field). Calculation of the effects of fluid inertia based on an analysis of the outer region is non-trivial. Saffman was one of the first to use an analysis based on the outer region to calculate the lift force on a translating sphere 'slipping' past an ambient simple shear flow (Saffman 1965). The Fourier-space analysis in Saffman (1965) was earlier employed by Childress (1964) in the context of estimating the correction to the well-known Stokes drag formula for the slow translation of a sphere along the axis of rotation of a rotating ambient flow. In the rheological context, Lin, Peery & Schowalter (1970) (see also Stone, Brady & Lovalenti 2000) analysed the effects of fluid inertia to $O(Re^{3/2})$ in order to characterize the $O(\phi)$ rheology of a dilute suspension of rigid neutrally buoyant spheres; here, ϕ is the volume fraction of the suspended spheres. Specifically, in Lin *et al.* (1970), a matched asymptotic expansion approach was used to determine both the normal stress differences at $O(\phi Re)$ and $O(\phi Re^{3/2})$, and the correction to the suspension shear viscosity that appears at the latter order; the inertial correction to the viscosity contributes to a shear thickening rheology. Stone *et al.* (2000) performed the $O(\phi Re^{3/2})$ calculation again using a concise Fourier-space formulation based on a reciprocal theorem formulation by treating the sphere as a force-dipole singularity. The concise formulation was used by Subramanian *et al.* (2011) to characterize the complete non-Newtonian rheology of an emulsion to $O(\phi Re^{3/2})$ for arbitrary ratios of the disperse (drop) to continuous phase viscosities, including the $O(\phi Re^{3/2})$ Reynolds stress contributions neglected by earlier authors.

In all of the cases mentioned above, the disturbance velocity field due to the particle is steady on account of its spherical shape. This steady velocity field may also be used to determine the inertial correction to the angular velocity of a freely rotating sphere. The absence of a regular correction at $O(Re)$, in simple shear flow, is easily seen. Such a correction would have to be quadratic in the shear rate, and, being a pseudovector, would have to be proportional to $\boldsymbol{\omega}\cdot\boldsymbol{E}$, where $\boldsymbol{E}$ and $\boldsymbol{\omega}$ are the rate-of-strain tensor and the vorticity vector in the ambient simple shear respectively. Since $\boldsymbol{\omega}$ is perpendicular to the plane of the flow, $\boldsymbol{\omega}\cdot\boldsymbol{E}=0$. This remains true in the absence of ambient vortex stretching, and, therefore, for the one-parameter family of planar linear flows (Subramanian & Koch 2006*b*). It should be noted that, for linear flows other than simple shear, the sphere will deviate from the fluid streamlines at finite Re due to an inertial lag, but the angular velocity correction is unchanged at leading order since the velocity gradient tensor is a constant. The first effects of inertia therefore appear at $O(Re^{3/2})$, Re being defined based on the sphere radius, and the inertial correction has been found to be $-0.054Re^{3/2}$ (Stone *et al.* 2000; Subramanian *et al.* 2011). Thus, for small but finite Re, the time period of rotation of a sphere increases by $1.355Re^{3/2}$.

The disturbance velocity field for a spheroid in a spinning orbit is steady, and therefore the scaling of the inertial correction to the angular velocity would be similar to that of a sphere. Indeed, as shown in a later section, the detailed calculation is easily carried out based on the $O(Re^{3/2})$ Fourier-space formulation, and predicts slowing down of the spinning spheroid due to inertial effects. The inertial correction to the spin is, in fact, proportional to the correction for a sphere, the multiplicative constant being given by a function of the aspect ratio. The $O(Re^{3/2})$ correction in the spinning orbit has recently been determined using the traditional matched asymptotic expansion approach (Meibohm *et al.* 2016), and we validate our calculation with this result. In the tumbling orbit, however, the disturbance velocity field due to the spheroid is unsteady, and the torque-free spheroid acts as a time-dependent force-dipole singularity in the outer region. This dependence, when represented in frequency space, is an infinite Fourier series, and this makes evaluation of the

$O(Re^{3/2})$ correction to the angular velocity, as a function of the instantaneous spheroid orientation, a difficult proposition. However, as is shown later, if one only has to evaluate the time period correction at $O(Re^{3/2})$, one only needs the Jeffery-averaged angular velocity correction. The relevant infinite series then reduces to three terms, allowing one to determine the correction without the need for truncation.

The correctness of the angular velocity correction, predicted at $O(Re^{3/2})$ for a sphere, and the associated increase in time period have been confirmed in a numerical investigation by Mikulencak & Morris (2004). These authors extended the results for the inertial correction to Re values of order unity, with inertia continuing to slow down the rotation. As mentioned earlier, Mao & Alexeev (2014) have recently investigated the effect of inertia on the time period of rotation of spheroids with different aspect ratios using the lattice Boltzmann method. This work concluded that the time period of rotation increases with the Reynolds number, but the authors found the scaling for the inertial correction to be $O(Re)$ for small Reynolds numbers. However, based on the $O(Re)$ correction of the angular velocity derived in Einarsson *et al.* (2015) and Dabade *et al.* (2016), it can be easily seen that the correction to the time period at this order is zero for spheroids with order-unity aspect ratios. This apparent contradiction might arise due to the bounded domain used in the simulations. An accurate estimation of the $O(Re^{3/2})$ inertial correction, in a numerical effort, is not easy since the correction originates in the outer region and requires that the outer boundary for the computational domain be much farther away than the (large) inertial screening length.

It is of interest to note that the arguments leading to the $O(Re^{3/2})$ scaling for the angular velocity correction remain valid even for a general triaxial ellipsoid provided that one of its principal axes remains aligned with the ambient vorticity. It is known that for $Re = 0$, and for sufficiently long times, the orientation dynamics of a triaxial ellipsoid differs significantly from that of a spheroid even for small departures from axisymmetry. For a general triaxial ellipsoid, quasiperiodic and chaotic trajectories coexist in orientation space, and an ellipsoid may exhibit dynamics of either type depending on its initial orientation. Nearly axisymmetric ellipsoids, and those with moderate aspect ratios, exhibit a quasiperiodic orientation dynamics for the most part, as shown originally by Hinch & Leal (1979); on the other hand, the orientation dynamics is largely chaotic for slender ellipsoids (Yarin, Gottlieb & Roisman 1997). It has been shown very recently, using Lattice Boltzmann simulations (Rosen 2016), that the first effects of inertia render the rotation about the intermediate axis stable for certain values of the axis ratios ($\kappa_1 = b/a = 1/3$ and $\kappa_2 = c/a = 1/4$), where $2a$, $2b$ and $2c$ are the lengths of the three axes of the triaxial ellipsoid, with $a > b > c$ (the analogous rotation in the Stokesian limit is neutrally stable). The natural question to ask is with regard to the time period of rotation in this inertially stabilized configuration. We show that the correction to the time period for a triaxial ellipsoid in this configuration again arises at $O(Re^{3/2})$, and evaluate the correction. Assuming stability of the intermediate-axis-aligned rotation, we also examine a sequence of triaxial ellipsoids approaching a tumbling ellipse, and characterize the divergence of the time period in this limit.

The inertial correction above remains $O(Re^{3/2})$ provided that the inertial screening length of $O(Re^{-1/2})$ is much larger than any of the principal axes. At the other extreme, when the largest axis is much larger than the inertial screening length (which is still much larger than the other two axes), and is in addition parallel to the ambient vorticity, the determination of the inertial correction reduces to a two-dimensional scenario involving a freely rotating elliptic cylinder in simple shear flow. The inertial

correction is now larger, being $O(Re)$, due to the more gradual $O(1/r)$ decay of the force-dipole velocity field in two dimensions. An analytical determination of the $O(Re)$ angular velocity correction has been carried out for a circular cylinder by Robertson & Acrivos (1970); the analogous scaling for an elliptic cylinder has been verified in computations by Mikulencak & Morris (2004).

This paper is organized as follows. In § 2, we derive the expression for the inertial correction to the angular velocity of a spheroid using a reciprocal theorem formulation. We express the reciprocal theorem in terms of Fourier-space integrals similarly to Stone *et al.* (2000) and Subramanian *et al.* (2011). In § 3, we summarize the Stokesian scenario and the results of the $O(Re)$ calculation made in Dabade *et al.* (2016). Aside from determining the $O(Re)$ drift across orbits, this latter calculation shows that the time period correction vanishes at $O(Re)$ in the stabilized (spinning or tumbling) orbits. We then consider the simpler case of the spinning spheroid in § 4, and show that the Fourier-space integral for the $O(Re^{3/2})$ angular velocity correction reduces to that of the sphere, as given in Stone *et al.* (2000). A numerical evaluation of this integral yields the spinning correction over the relevant range of aspect ratios. As mentioned above, this is expected since a torque-free spinning spheroid acts as a time-independent force-dipole singularity. In § 5, we evaluate the reciprocal theorem integral for the more involved case of the tumbling orbit, the difficulty arising from the time-dependent nature of the force-dipole singularity. The inertial correction to the tumbling time period reduces to a sum of a three- and a four-dimensional integral. These integrals are evaluated numerically and the results are presented in § 6. In § 7, we calculate the time period correction for a triaxial ellipsoid rotating about its intermediate principal axis for a restricted set of axis-ratio pairs. In § 8, we first summarize our results. Then, we combine the findings of the $O(Re)$ analysis in Dabade *et al.* (2016) and the current one, to present a description of the effects of weak inertia valid for all aspect ratios. In particular, we show that the $O(Re^{3/2})$ inertial terms do not affect the leading-order estimate of the critical Reynolds number (based on the $O(Re)$ inertial correction) required for arrest of the rotation of extreme-aspect-ratio spheroids.

2. Formulation for the time period: the reciprocal theorem

In this section, we derive the formal expression for the correction to the time period of rotation of a spheroid, in a simple shear flow, for small Re. The time period is related to the angular velocity of the spheroid, and the latter can be evaluated using a generalized reciprocal theorem. The reciprocal theorem relates the velocity and stress fields of two problems, the first being the problem of interest and the second being a simpler test problem with a known solution. The flow physics in the two problems can be different; however, the configuration, size and shape of the particle, a spheroid in an unbounded fluid domain, are the same (Leal 1979; Subramanian & Koch 2005, 2006*a*; Dabade *et al.* 2016). The problem of interest here is a torque-free spheroid rotating in a simple shear flow, accounting for the inertial acceleration of the fluid in an unbounded domain. The objective is to relate its angular velocity, $\boldsymbol{\Omega}_1$, to the time period of rotation, for small Re, and thereby determine the latter to $O(Re^{3/2})$. The test problem corresponds to the Stokesian rotation of a spheroid in a quiescent ambient with an angular velocity $\boldsymbol{\Omega}_2$, and with the same instantaneous orientation as that of the spheroid in the problem of interest. The velocity and stress fields in the problem of interest are denoted by $\boldsymbol{u}^{(1)}$ and $\boldsymbol{\sigma}^{(1)}$, and those in the test problem are $\boldsymbol{u}^{(2)}$ and $\boldsymbol{\sigma}^{(2)}$. The reciprocal theorem is formulated in terms of the scaled

disturbance fields (both stress and velocity) in the problem of interest, which are given by $\boldsymbol{\sigma}'^{(1)} = \boldsymbol{\sigma}^{(1)} - 2\boldsymbol{E}$ and $\boldsymbol{u}'^{(1)} = \boldsymbol{u}^{(1)} - \boldsymbol{\Gamma}\cdot\boldsymbol{x}$, where $\boldsymbol{\Gamma}\cdot\boldsymbol{x}$ is the ambient simple shear defined in a coordinate system whose origin is at the centre of the spheroid. The space-fixed coordinate system has its X, Y and Z axes along the flow, gradient and vorticity directions respectively of the ambient simple shear (see figure 1), with the unit vectors in the X, Y and Z directions being $\mathbf{1}_1$, $\mathbf{1}_2$ and $\mathbf{1}_3$ respectively. The disturbance velocity and stress fields are scaled with $\dot{\gamma}L$ and $\mu\dot{\gamma}L$. Thus, $\boldsymbol{\Gamma} = \mathbf{1}_1\mathbf{1}_2$ and $\boldsymbol{E} = (\mathbf{1}_1\mathbf{1}_2 + \mathbf{1}_2\mathbf{1}_1)/2$ are the transpose of the non-dimensional velocity gradient and the rate-of-strain tensors respectively. The expression for the inertial angular velocity has already been derived in Dabade *et al.* (2016) (equation (2.19)), using a reciprocal theorem formulation, and takes the following form in non-dimensional terms:

$$\boldsymbol{\Omega}_1\cdot\boldsymbol{\mathcal{L}}_2 = \boldsymbol{\Gamma} : \int_{S_p} \boldsymbol{x}(\boldsymbol{\sigma}^{(2)}\cdot\boldsymbol{n})\,\mathrm{d}S + St\,\frac{\mathrm{d}}{\mathrm{d}t}(\boldsymbol{I}_p\cdot\boldsymbol{\Omega}_1)\cdot\boldsymbol{\Omega}_2 + Re\int_V \left[\frac{\partial \boldsymbol{u}'^{(1)}}{\partial t} + (\boldsymbol{\Gamma}\cdot\boldsymbol{x})\cdot\nabla\boldsymbol{u}'^{(1)} + \boldsymbol{\Gamma}\cdot\boldsymbol{u}'^{(1)} + \boldsymbol{u}'^{(1)}\cdot\nabla\boldsymbol{u}'^{(1)}\right]\cdot\boldsymbol{u}^{(2)}\,\mathrm{d}V, \tag{2.1}$$

where $\boldsymbol{\Omega}_1$ and $\boldsymbol{\mathcal{L}}_2$ are respectively the angular velocity of the spheroid in the problem of interest and the torque acting on the spheroid in the test problem. The latter is given by $\boldsymbol{\mathcal{L}}_2 = -8\pi(X_C\boldsymbol{pp} + Y_C(\boldsymbol{I}-\boldsymbol{pp}))\cdot\boldsymbol{\Omega}_2$, $\boldsymbol{p}$ here being the orientation vector of the spheroid, and the torque coefficients being given by $X_C = 4(\xi_0^2-1)/(3\xi_0^3(2\xi_0 - 2(\xi_0^2-1)\coth^{-1}\xi_0))$ and $Y_C = 4(2\xi_0^2-1)/(3\xi_0^3(2(\xi_0^2+1)\coth^{-1}\xi_0 - 2\xi_0))$ for a prolate spheroid (Kim & Karrila 1991), where ξ_0 is the inverse of the eccentricity of the spheroid ($\xi_0 = 1/\sqrt{1-1/\kappa^2}$ for a prolate spheroid). The expressions for X_C and Y_C, for an oblate spheroid, can be obtained by using the transformation $\xi_0 = \mathrm{i}\sqrt{\xi_0^2-1}$ and $d = -\mathrm{i}d$ (d is the interfocal distance) in the dimensional forms of the prolate torque coefficients ($\xi_0 = 1/\sqrt{1-\kappa^2}$ for an oblate spheroid). The term proportional to St in (2.1), where St is the Stokes number defined as $\rho_p\dot{\gamma}L^2/\mu$ and $\boldsymbol{I}_p$ is the moment of inertia of the spheroid, gives the contribution to the angular velocity due to particle inertia. For a neutrally buoyant spheroid, the case considered here, $St = Re$. The volume integral on the right-hand side of (2.1) gives the contribution to the angular velocity due to fluid inertia, the domain of integration being the unbounded fluid volume outside the spheroid. The leading-order contribution due to fluid inertia, at $O(Re)$, can be obtained by replacing $\boldsymbol{u}'^{(1)}$ with the disturbance velocity field in the Stokes limit ($\boldsymbol{u}'^{(s)}$) in the integral. The resulting integral is convergent, implying the regular nature of the $O(Re)$ correction. This correction has been evaluated in Einarsson *et al.* (2015) and Dabade *et al.* (2016), and it stabilizes certain Stokesian orbits of the spheroid. Specifically, while, at $Re = 0$, the spheroid may rotate in any of a one-parameter family of precessional orbits known as Jeffery orbits (Jeffery 1922), for finite Re, only the limiting members of this family (the tumbling and the spinning modes; see figure 1*b*) are rendered stable by the drift induced by inertia at $O(Re)$. As shown in § 3, the $O(Re)$ correction to the angular velocity of a spheroid rotating in either of the asymptotic states above does not change the time period of rotation from its leading-order value given in non-dimensional terms by $T_{jeff} = 2\pi(\kappa^2+1)/\kappa$. However, as mentioned in § 1, numerical simulations have shown a change in the time period in the presence of fluid inertia (Mao & Alexeev 2014), although the scaling for this change has not been rigorously characterized in the limit $Re \ll 1$. Thus, there is

a need to characterize the first correction to the time period. As shown later in this section, this comes at $O(Re^{3/2})$.

To calculate the $O(Re^{3/2})$ correction, we first examine the assumptions made when replacing $\boldsymbol{u}'^{(1)}$ with $\boldsymbol{u}'^{(s)}$ to obtain the $O(Re)$ correction. The equation governing $\boldsymbol{u}'^{(1)}$ is given by

$$\nabla^2\boldsymbol{u}'^{(1)} - \nabla p = Re\left(\frac{\partial \boldsymbol{u}'^{(1)}}{\partial t} + \boldsymbol{u}'^{(1)}\cdot\nabla\boldsymbol{u}'^{(1)} + (\boldsymbol{\Gamma}\cdot\boldsymbol{x})\cdot\nabla\boldsymbol{u}'^{(1)} + \boldsymbol{\Gamma}\cdot\boldsymbol{u}'^{(1)}\right). \tag{2.2}$$

This equation is obtained by taking the difference of the governing equations for the full velocity field $\boldsymbol{u}^{(1)}$ and the ambient $\boldsymbol{\Gamma}\cdot\boldsymbol{x}$. By neglecting the inertial terms proportional to Re in (2.2), one gets the Stokes equations whose solution is $\boldsymbol{u}'^{(s)}$. It is well known that $\boldsymbol{u}'^{(s)}$ is not a uniformly valid approximation for the velocity field throughout the unbounded domain outside the spheroid. The inertial terms on the right-hand side decay as $1/r^2$, and cannot be neglected when $r \approx Re^{-1/2}$, the inertial screening length, and the Stokes solution ceases to be a good approximation to the disturbance velocity field at distances of the order of and beyond this length. The region around the sphere can therefore be divided into two, depending on whether the inertial terms can be neglected compared with the viscous terms: the inner region ($r \sim 1$) and the outer region ($r \sim O(Re^{-1/2})$). The Stokes velocity field is a good approximation to the actual disturbance velocity field only in the inner region. The leading-order velocity field in the outer region should be obtained by solving the linearized version of (2.2). The velocity fields in the inner ($\boldsymbol{u}^{inner}$) and outer ($\boldsymbol{u}^{outer}$) regions, however, reduce to the same functional form ($\boldsymbol{u}^{match}$) in a matching region ($1 \ll r \ll Re^{-1/2}$). To calculate the $O(Re^{3/2})$ correction to the angular velocity, $\boldsymbol{u}'^{(1)}$ is written, formally, as the following uniformly valid expansion (Hinch 1991):

$$\boldsymbol{u}'^{(1)} = \boldsymbol{u}^{inner} + \boldsymbol{u}^{outer} - \boldsymbol{u}^{match}. \tag{2.3}$$

Next, defining $\boldsymbol{u}^f = \boldsymbol{u}^{outer} - \boldsymbol{u}^{match}$, the reciprocal theorem in (2.1) becomes

$$\begin{aligned}\boldsymbol{\Omega}_1\cdot\boldsymbol{\mathcal{L}}_2 \;=\; & \boldsymbol{\Gamma}:\int_{S_p}\boldsymbol{x}(\boldsymbol{\sigma}^{(2)}\cdot\boldsymbol{n})\,\mathrm{d}S + Re\frac{\mathrm{d}}{\mathrm{d}t}(\boldsymbol{I}_p\cdot\boldsymbol{\Omega}_1)\cdot\boldsymbol{\Omega}_2 \\ & + Re\int_V\left[\frac{\partial\boldsymbol{u}^{inner}}{\partial t} + (\boldsymbol{\Gamma}\cdot\boldsymbol{x})\cdot\nabla\boldsymbol{u}^{inner} + \boldsymbol{\Gamma}\cdot\boldsymbol{u}^{inner} + \boldsymbol{u}^{inner}\cdot\nabla\boldsymbol{u}^{inner}\right]\cdot\boldsymbol{u}^{(2)}\,\mathrm{d}V \\ & + Re\int_V\left[\frac{\partial\boldsymbol{u}^{f}}{\partial t} + (\boldsymbol{\Gamma}\cdot\boldsymbol{x})\cdot\nabla\boldsymbol{u}^{f} + \boldsymbol{\Gamma}\cdot\boldsymbol{u}^{f} + \boldsymbol{u}^{f}\cdot\nabla\boldsymbol{u}^{f}\right]\cdot\boldsymbol{u}^{(2)}\,\mathrm{d}V \\ & + Re\int_V\left[\boldsymbol{u}^{f}\cdot\nabla\boldsymbol{u}^{inner} + \boldsymbol{u}^{inner}\cdot\nabla\boldsymbol{u}^{f}\right]\cdot\boldsymbol{u}^{(2)}\,\mathrm{d}V.\end{aligned} \tag{2.4}$$

In the inner region, $\boldsymbol{u}^f$ comes at a higher order, and in the outer region, the nonlinear cross terms, $\boldsymbol{u}^f\cdot\nabla\boldsymbol{u}^{inner}$ and $\boldsymbol{u}^{inner}\cdot\nabla\boldsymbol{u}^f$, decay faster than the linear terms, and therefore the integrals involving the cross terms in (2.4) contribute at a higher order. The third term on the right-hand side in (2.4) gives the $O(Re)$ correction to the angular velocity ($\boldsymbol{\Omega}_1$), arising from the inner region with $\boldsymbol{u}^{inner} = \boldsymbol{u}'^{(s)}$, and is evaluated in Dabade *et al.* (2016). The fourth term on the right-hand side is the contribution to the angular velocity from the outer region. To explicitly see the scaling with respect to Re for this contribution, the velocity fields in the fourth term are written in terms of a rescaled coordinate defined as $\rho = Re^{1/2}r$. The rescaled coordinate is $O(1)$ when

r is of the order of the inertial screening length, and is therefore appropriate for the outer region. The radial vector and the differential volume can be expressed in the outer coordinate as $\boldsymbol{\rho} = Re^{1/2}\boldsymbol{x}$, $\mathrm{d}V_\rho = Re^{3/2}\,\mathrm{d}V$. Since the neutrally buoyant spheroid acts as a force-dipole singularity for $r \gg 1$, the disturbance velocity fields in the problem of interest as well as the test problem decay as $1/r^2$ when $1 \ll r \ll Re^{-1/2}$, and can be written as $\boldsymbol{u}^{f_\rho} = Re^{-1}\boldsymbol{u}^f$ and $\boldsymbol{u}^{(2_\rho)} = Re^{-1}\boldsymbol{u}^{(2)}$. It should be noted that, as defined, $\boldsymbol{u}^{f_\rho} = (\boldsymbol{u}^{outer\rho} - \boldsymbol{u}^{match\rho})$, the superscript ρ indicating that these velocity fields are now expressed in the outer coordinate ρ. The reciprocal theorem statement in (2.4), with the fourth term on the right-hand side expressed in terms of the rescaled outer coordinate, is given by

$$\begin{aligned}\boldsymbol{\Omega}_1 \cdot \boldsymbol{\mathcal{L}}_2 \;=\; \boldsymbol{\Gamma} : \int_{S_p} \boldsymbol{x}(\boldsymbol{\sigma}^{(2)} \cdot \boldsymbol{n})\,\mathrm{d}S + Re\frac{\mathrm{d}}{\mathrm{d}t}(\boldsymbol{I}_p \cdot \boldsymbol{\Omega}_1) \cdot \boldsymbol{\Omega}_2 \\ + Re \int_V \left[\frac{\partial \boldsymbol{u}^{inner}}{\partial t} + (\boldsymbol{\Gamma} \cdot \boldsymbol{x}) \cdot \nabla \boldsymbol{u}^{inner} + \boldsymbol{\Gamma} \cdot \boldsymbol{u}^{inner} + \boldsymbol{u}^{inner} \cdot \nabla \boldsymbol{u}^{inner}\right] \cdot \boldsymbol{u}^{(2)}\,\mathrm{d}V, \\ + Re^{3/2} \int_{V_\rho} \left[\frac{\partial \boldsymbol{u}^{f_\rho}}{\partial t} + (\boldsymbol{\Gamma} \cdot \boldsymbol{\rho}) \cdot \nabla \boldsymbol{u}^{f_\rho} + \boldsymbol{\Gamma} \cdot \boldsymbol{u}^{f_\rho}\right] \cdot \boldsymbol{u}^{(2_\rho)}\,\mathrm{d}V_\rho. \end{aligned} \tag{2.5}$$

It should be noted that the nonlinear term $\boldsymbol{u}^f \cdot \nabla \boldsymbol{u}^f$ in the fourth term in (2.4), when expressed in terms of the outer coordinate, contributes at a higher order, and is neglected in the fourth term on the right-hand side of (2.5). It is evident from (2.5) that the correction from the outer region comes at $O(Re^{3/2})$. The volume of the spheroid expressed in outer variables is $O(Re^{3/2})$, and its omission only leads to an error of $O(Re^3)$. The omission is equivalent to treating the spheroid as an equivalent point-force-dipole singularity. Thus, the outer integral in (2.5) may be extended right until the origin, and the resulting calculation is then more conveniently performed in Fourier space. The convolution theorem (Arfken, Weber & Harris 2011) is applied to the $O(Re^{3/2})$ integral in (2.5) to obtain

$$\begin{aligned}\int_{V_\rho} \left[\frac{\partial \boldsymbol{u}^{f_\rho}}{\partial t} + (\boldsymbol{\Gamma} \cdot \boldsymbol{\rho}) \cdot \nabla \boldsymbol{u}^{f_\rho} + \boldsymbol{\Gamma} \cdot \boldsymbol{u}^{f_\rho}\right] \cdot \boldsymbol{u}^{(2_\rho)}\,\mathrm{d}V_\rho \\ = \int \left[\frac{\partial \hat{\boldsymbol{u}}^f}{\partial t} - (\boldsymbol{\Gamma}^\dagger \cdot \boldsymbol{k}) \cdot \nabla_{\boldsymbol{k}} \hat{\boldsymbol{u}}^f + \boldsymbol{\Gamma} \cdot \hat{\boldsymbol{u}}^f\right] \cdot \hat{\boldsymbol{u}}^{(2)}(-\boldsymbol{k})\,\mathrm{d}\boldsymbol{k}, \end{aligned} \tag{2.6}$$

where the hatted variables denote the Fourier transformed fields, the transform being defined as $\hat{f}(\boldsymbol{k}) = \int f(\boldsymbol{r})\mathrm{e}^{-\mathrm{i}2\pi\boldsymbol{k}\cdot\boldsymbol{r}}\,\mathrm{d}\boldsymbol{r}$. In (2.6), $\hat{\boldsymbol{u}}^{(2)}(-\boldsymbol{k})$ and $\hat{\boldsymbol{u}}^f(\boldsymbol{k})$ are the Fourier transforms of the test velocity field $\boldsymbol{u}^{(2_\rho)}$ and the velocity field in the problem of interest $\boldsymbol{u}^{f_\rho}$. The ambient simple shear flow takes the form $\hat{\boldsymbol{u}}^\infty = -k_1\mathbf{1}_2$ ($\boldsymbol{\Gamma}^\dagger = \mathbf{1}_2\mathbf{1}_1$) in Fourier space. Here, k_1 is the component of the wavevector $\boldsymbol{k}$ in the X direction.

To evaluate (2.6), we need to find $\hat{\boldsymbol{u}}^f(\boldsymbol{k})$ and $\hat{\boldsymbol{u}}^{(2)}(\boldsymbol{k})$. The governing equation for $\boldsymbol{u}^{(2_\rho)}$ is

$$\nabla^2 \boldsymbol{u}^{(2\rho)} - \nabla p^{(2\rho)} = \boldsymbol{S}^{(2)} \cdot \frac{\partial \delta(\boldsymbol{\rho})}{\partial \boldsymbol{\rho}}, \tag{2.7}$$

where $\boldsymbol{S}^{(2)}$ is the time-dependent force-dipole singularity corresponding to a spheroid rotating in a quiescent fluid. The term $\boldsymbol{S}^{(2)}$ is given by

$$\boldsymbol{S}^{(2)} = B_1\,((\boldsymbol{\Omega}^{(2)} \wedge \boldsymbol{p})\boldsymbol{p} + \boldsymbol{p}(\boldsymbol{\Omega}^{(2)} \wedge \boldsymbol{p})) + B_2\,((\boldsymbol{\Omega}^{(2)} \cdot \boldsymbol{p})\boldsymbol{\epsilon} \cdot \boldsymbol{p}) + B_3(\boldsymbol{\epsilon} \cdot \boldsymbol{\Omega}^{(2)}), \tag{2.8}$$

where $\boldsymbol{p}$ is the spheroid orientation vector and the constants B_1, B_2 and B_3 for a prolate spheroid are given by

$$B_1 = \frac{8\pi}{\xi_0^3(-3\xi_0 + 3\ \coth^{-1}\xi_0(1+\xi_0^2))}, \tag{2.9}$$

$$B_2 = \frac{8\pi(2 + 3\xi_0(-\coth^{-1}\xi_0 + \xi_0(-1 + \xi_0 \coth^{-1}\xi_0)))}{3\xi_0^2(-\coth^{-1}[\xi_0]^2 + \xi_0^2(-1 + \xi_0 \coth^{-1}\xi_0)^2)}, \tag{2.10}$$

$$B_3 = \frac{8\pi(1 - 2\xi_0^2)}{\xi_0^3(-3\xi_0 + 3\coth^{-1}\xi_0(1+\xi_0^2))}. \tag{2.11}$$

The terms proportional to B_2 and B_3 correspond to the rotlet singularities and the one multiplying B_1 corresponds to the stresslet induced by the rotating spheroid. In the limit $\xi_0 \to \infty$, that is for a sphere, $B_3 = -4\pi$, and B_1 and B_2 are $O(1/\xi_0^2)$, consistent with a rotating sphere acting as a pure rotlet singularity. As before, the constants for an oblate spheroid can be obtained using the transformation $\xi_0 = \mathrm{i}\sqrt{\xi_0^2 - 1}$ and $d = -\mathrm{i}d$, mentioned below (2.1) (alternatively, see Kim & Karrila (1991)). The Fourier transform of (2.7) gives

$$\hat{\boldsymbol{u}}^{(2)}(-\boldsymbol{k}) = \frac{\mathrm{i}\,\boldsymbol{S}^{(2)}\cdot\boldsymbol{k}}{2\pi k^2}\cdot\left(\boldsymbol{I} - \frac{\boldsymbol{k}\boldsymbol{k}}{k^2}\right). \tag{2.12}$$

To evaluate $\hat{\boldsymbol{u}}^f$, we need the equation governing $\boldsymbol{u}^{f_\rho}$, which can be derived from the equations governing $\boldsymbol{u}^{outer\rho}$ and $\boldsymbol{u}^{match\rho}$, given by

$$\nabla^2\boldsymbol{u}^{outer\rho} - \nabla p^{outer\rho} = \boldsymbol{S}\cdot\frac{\partial\delta(\boldsymbol{\rho})}{\partial\boldsymbol{\rho}} + \left(\frac{\partial\boldsymbol{u}^{outer\rho}}{\partial t} + (\boldsymbol{\Gamma}\cdot\boldsymbol{x})\cdot\nabla\boldsymbol{u}^{outer\rho} + \boldsymbol{\Gamma}\cdot\boldsymbol{u}^{outer\rho}\right) \tag{2.13}$$

and

$$\nabla^2\boldsymbol{u}^{match\rho} - \nabla p^{match\rho} = \boldsymbol{S}\cdot\frac{\partial\delta(\boldsymbol{\rho})}{\partial\boldsymbol{\rho}} \tag{2.14}$$

respectively. Equation (2.13) is the far-field approximation of (2.2), where the boundary conditions on the surface of the freely rotating spheroid are replaced by a singular forcing at the origin. Here, to the order of approximation desired, $\boldsymbol{S}$ is the time-dependent force-dipole singularity corresponding to a torque-free spheroid in a simple shear flow at $Re = 0$, given by

$$\begin{aligned}\boldsymbol{S} = {} & A_1\frac{3}{2}(\boldsymbol{E}:\boldsymbol{pp})\left(\boldsymbol{pp} - \frac{\boldsymbol{I}}{3}\right) + A_2((\boldsymbol{I}-\boldsymbol{pp})\cdot\boldsymbol{E}\cdot\boldsymbol{pp} + \boldsymbol{pp}\cdot\boldsymbol{E}\cdot(\boldsymbol{I}-\boldsymbol{pp})) \\ & + A_3\left((\boldsymbol{I}-\boldsymbol{pp})\cdot\boldsymbol{E}\cdot(\boldsymbol{I}-\boldsymbol{pp}) + (\boldsymbol{I}-\boldsymbol{pp})\frac{(\boldsymbol{E}:\boldsymbol{pp})}{2}\right).\end{aligned} \tag{2.15}$$

To understand $\boldsymbol{S}$ in more detail, we note that the Stokesian disturbance field induced in an ambient linear flow can be split into five component flows corresponding to the five degrees of freedom of the rate-of-strain tensor. These may conveniently be regarded as an axisymmetric extensional flow and pairs of planar extensional flows in the longitudinal (containing $\boldsymbol{p}$) and transverse (orthogonal to $\boldsymbol{p}$) planes (Dabade *et al.* 2016), with the component amplitude dependent on the spheroid orientation. Due to its axisymmetry, a spheroid responds identically to the two extensions in the longitudinal and transverse planes. Therefore, the stresslet singularity in (2.15) can be written as a sum of only three terms, with the terms proportional to A_1, A_2 and A_3 being the stresslets induced by the axisymmetric extension and the longitudinal and transverse

planar extensional flows respectively. The constants for a prolate spheroid (Kim & Karrila 1991) are

$$A_1 = -\frac{16\pi}{9\xi_0^3\left(-3\xi_0 + \coth^{-1}\xi_0\left(-1+3\xi_0^2\right)\right)}, \tag{2.16}$$

$$A_2 = \frac{16\pi\left(-1+\xi_0^2\right)}{3\xi_0^2\left(-1+2\xi_0^2\right)\left(2-3\xi_0^2+3\coth^{-1}\xi_0\xi_0\left(-1+\xi_0^2\right)\right)}, \tag{2.17}$$

$$A_3 = -\frac{32\pi\left(-1+\xi_0^2\right)}{3\xi_0^3\left(5\xi_0 - 3\xi_0^3 + 3\coth^{-1}\xi_0\left(-1+\xi_0^2\right)^2\right)}. \tag{2.18}$$

For a sphere, all three constants equal $-20\pi/3$, so that $\lim_{\xi_0\to\infty}\boldsymbol{S} = -(20\pi/3)\boldsymbol{E}$, corresponding to the well-known stresslet singularity of a freely rotating sphere ($n\lim_{\xi_0\to\infty}\boldsymbol{S}$ yields the well-known Einstein correction). The equation governing $\boldsymbol{u}^{f\rho}$ is derived using (2.13) and (2.14), and is given by

$$\begin{aligned}\nabla^2\boldsymbol{u}^{f\rho} - \nabla p^{f\rho} \;=\; & \frac{\partial\boldsymbol{u}^{f\rho}}{\partial t} + (\boldsymbol{\Gamma}\cdot\boldsymbol{x})\cdot\nabla\boldsymbol{u}^{f\rho} + \boldsymbol{\Gamma}\cdot\boldsymbol{u}^{f\rho} \\ & + \frac{\partial\boldsymbol{u}^{match\rho}}{\partial t} + (\boldsymbol{\Gamma}\cdot\boldsymbol{x})\cdot\nabla\boldsymbol{u}^{match\rho} + \boldsymbol{\Gamma}\cdot\boldsymbol{u}^{match\rho}.\end{aligned} \tag{2.19}$$

The bracketed term on the right-hand side of (2.6) is obtained by taking the Fourier transform of (2.19), and is given by

$$\begin{aligned}\frac{\partial\hat{\boldsymbol{u}}^f}{\partial t} - (\boldsymbol{\Gamma}^\dagger\cdot\boldsymbol{k})\cdot\nabla_{\boldsymbol{k}}\hat{\boldsymbol{u}}^f + \boldsymbol{\Gamma}\cdot\hat{\boldsymbol{u}}^f \;=\; & -4\pi^2k^2\hat{\boldsymbol{u}}^f - \mathrm{i}2\pi\boldsymbol{k}\hat{p}^f \\ & - \left(\frac{\partial\hat{\boldsymbol{u}}^{match}}{\partial t} - (\boldsymbol{\Gamma}^\dagger\cdot\boldsymbol{k})\cdot\nabla_{\boldsymbol{k}}\hat{\boldsymbol{u}}^{match} + \boldsymbol{\Gamma}\cdot\hat{\boldsymbol{u}}^{match}\right).\end{aligned} \tag{2.20}$$

The Fourier transformed matching velocity field ($\hat{\boldsymbol{u}}^{match}$) in (2.20) is obtained by taking the Fourier transform of (2.14), and is given by

$$\hat{\boldsymbol{u}}^{match}(\boldsymbol{k}) = -\frac{\mathrm{i}\,\boldsymbol{S}\cdot\boldsymbol{k}}{2\pi k^2}\cdot\left(\boldsymbol{I} - \frac{\boldsymbol{k}\boldsymbol{k}}{k^2}\right), \tag{2.21}$$

with $\boldsymbol{S}$ given by (2.15). By substituting (2.12) and (2.20) into (2.6), the reciprocal theorem relation in (2.5) becomes

$$\begin{aligned}\boldsymbol{\Omega}_1\cdot\boldsymbol{\mathcal{L}}_2 \;=\; & \boldsymbol{\Gamma} : \int_{S_p}\boldsymbol{x}(\boldsymbol{\sigma}^{(2)}\cdot\boldsymbol{n})\,\mathrm{d}S + Re\frac{\mathrm{d}}{\mathrm{d}t}(\boldsymbol{I}_p\cdot\boldsymbol{\Omega}_1)\cdot\boldsymbol{\Omega}_2 \\ & + Re\int_V\left[\frac{\partial\boldsymbol{u}^{inner}}{\partial t} + (\boldsymbol{\Gamma}\cdot\boldsymbol{x})\cdot\nabla\boldsymbol{u}^{inner} + \boldsymbol{\Gamma}\cdot\boldsymbol{u}^{inner} + \boldsymbol{u}^{inner}\cdot\nabla\boldsymbol{u}^{inner}\right]\cdot\boldsymbol{u}^{(2)}\,\mathrm{d}V \\ & - Re^{3/2}\int\left[4\pi^2k^2\hat{\boldsymbol{u}}^f + \frac{\partial\hat{\boldsymbol{u}}^{match}}{\partial t} - (\boldsymbol{\Gamma}^\dagger\cdot\boldsymbol{k})\cdot\nabla_{\boldsymbol{k}}\hat{\boldsymbol{u}}^{match} + \boldsymbol{\Gamma}\cdot\hat{\boldsymbol{u}}^{match}\right] \\ & \cdot\left(\frac{\mathrm{i}\boldsymbol{S}^{(2)}\cdot\boldsymbol{k}}{2\pi k^2}\cdot\left(\boldsymbol{I} - \frac{\boldsymbol{k}\boldsymbol{k}}{k^2}\right)\right)\mathrm{d}\boldsymbol{k}.\end{aligned} \tag{2.22}$$

It should be noted that the term containing the Fourier transformed pressure field in (2.20), which is proportional to $\boldsymbol{k}$, vanishes when contracted with $\hat{\boldsymbol{u}}^{(2)}(-\boldsymbol{k})$, and,

therefore, does not appear in (2.22). For the test problem, we define two second-order tensors $\boldsymbol{L}_2$ and $\boldsymbol{U}_2$, and two third-order tensors $\boldsymbol{\Sigma}^{(2)}$ and $\boldsymbol{S}^{2t}$, such that $\boldsymbol{\mathcal{L}}_2 = \boldsymbol{L}_2 \cdot \boldsymbol{\Omega}_2$ ($\boldsymbol{\mathcal{L}}_2$ is defined below (2.1)), $\boldsymbol{u}^{(2)} = \boldsymbol{U}_2 \cdot \boldsymbol{\Omega}_2$, $\boldsymbol{\sigma}^{(2)} = \boldsymbol{\Sigma}^{(2)} \cdot \boldsymbol{\Omega}_2$ (see Dabade *et al.* 2016) and $\boldsymbol{S}^{(2)} = \boldsymbol{S}^{2t} \cdot \boldsymbol{\Omega}_2$ ($\boldsymbol{S}^{(2)}$ is defined in (2.8)). In terms of these newly defined tensors, the relation (2.22) becomes independent of the angular velocity of the test spheroid ($\boldsymbol{\Omega}_2$).

Next, the angular velocity in the problem of interest ($\boldsymbol{\Omega}_1$) is expanded as $\boldsymbol{\Omega}_{jeff} + Re\,\boldsymbol{\Omega}_{c1} + Re^{3/2}\boldsymbol{\Omega}_{c2}$, and substitution of the expansion as well as the newly defined tensors in (2.22) leads to

$$\boldsymbol{\Omega}_{jeff} \cdot \boldsymbol{L}_2 = \boldsymbol{\Gamma} : \int_{S_p} \boldsymbol{x}(\boldsymbol{\Sigma}^{(2)} \cdot \boldsymbol{n})\,\mathrm{d}S, \tag{2.23}$$

$$\boldsymbol{\Omega}_{c1} \cdot \boldsymbol{L}_2 = \int_V \left[\frac{\partial \boldsymbol{u}'^{(s)}}{\partial t} + (\boldsymbol{\Gamma} \cdot \boldsymbol{x}) \cdot \nabla \boldsymbol{u}'^{(s)} + \boldsymbol{\Gamma} \cdot \boldsymbol{u}'^{(s)} + \boldsymbol{u}'^{(s)} \cdot \nabla \boldsymbol{u}'^{(s)}\right] \cdot \boldsymbol{U}_2\,\mathrm{d}V + \frac{\mathrm{d}}{\mathrm{d}t}(\boldsymbol{I}_p \cdot \boldsymbol{\Omega}_1), \tag{2.24}$$

and

$$\boldsymbol{\Omega}_{c2} \cdot \boldsymbol{L}_2 = -\int \left[4\pi^2 k^2 \hat{\boldsymbol{u}}^f + \frac{\partial \hat{\boldsymbol{u}}^{match}}{\partial t} - (\boldsymbol{\Gamma}^\dagger \cdot \boldsymbol{k}) \cdot \nabla_{\boldsymbol{k}} \hat{\boldsymbol{u}}^{match} + \boldsymbol{\Gamma} \cdot \hat{\boldsymbol{u}}^{match}\right] \cdot \left(\frac{\mathrm{i}\boldsymbol{S}^{(2t)} \cdot \boldsymbol{k}}{2\pi k^2} \cdot \left(\boldsymbol{I} - \frac{\boldsymbol{kk}}{k^2}\right)\right) \mathrm{d}\boldsymbol{k} \tag{2.25}$$

at successive orders. The detailed expression for $\boldsymbol{u}'^{(s)}$, obtained using a spheroidal harmonics formalism, has already been used to evaluate $\boldsymbol{\Omega}_{c1}$ in Dabade *et al.* (2016). To evaluate the $O(Re^{3/2})$ correction, $\boldsymbol{\Omega}_{c2}$, using (2.25), one needs $\hat{\boldsymbol{u}}^f$, which can be obtained by solving (2.20). This is a rather elaborate calculation, and is presented later in §§ 4 and 5.

3. Summary: time period at leading order and at $O(Re)$

The leading-order angular velocity $\boldsymbol{\Omega}_{jeff}$ in (2.23) may be expressed in terms of the rates of change of the polar and azimuthal angles θ_j and ϕ_j (Jeffery 1922), defined in figure 1(*a*), and these are given by

$$\dot{\phi}_{jeff} = -\frac{1}{2} + \frac{\kappa^2 - 1}{2(\kappa^2 + 1)} \cos 2\phi_j, \tag{3.1}$$

$$\dot{\theta}_{jeff} = \frac{\kappa^2 - 1}{4(\kappa^2 + 1)} \sin 2\theta_j \sin 2\phi_j. \tag{3.2}$$

There is an additional spin component given by $\dot{\psi} = -\cos\theta_j/2 - \dot{\phi}_{jeff}\cos\theta_j$. As is well known, the solution of (3.1) and (3.2) shows that the spheroid rotates in any of a one-parameter family of closed orbits (figure 1*b*), the particular orbit being determined by its initial orientation. The parameter is the orbit constant C, which takes values from 0 to ∞. The orbital or so-called natural coordinates (C, τ) were originally introduced by Leal & Hinch (1971), with the constant-C lines being Jeffery orbits and the constant-τ lines (τ being the phase along the Jeffery orbit) being the constant-ϕ lines on the unit sphere. In these coordinates, the aforementioned rates of change take on a much simpler form, namely $\mathrm{d}C/\mathrm{d}t = 0$ and $\mathrm{d}\tau/\mathrm{d}t = \kappa/(\kappa^2 + 1)$.

If a spheroid is initially aligned with the ambient vorticity axis, it will continue to spin in that orientation. This particular orbit with $C = 0 (\theta_j = 0)$ is called a log-rolling (spinning) orbit for a prolate (oblate) spheroid. At leading order, the angular velocity of the spinning spheroid is a constant, and is therefore independent of the aspect ratio and equal to $-(1/2)\mathbf{1}_3$. The disturbance velocity field is steady in this orbit, just like a sphere, and the time period of rotation is 4π. If the initial orientation of the spheroid is in the flow–gradient plane, the orbit is a unit circle in this plane and is called a tumbling orbit ($\theta_j = \pi/2, C = \infty$). The rotation in a Jeffery orbit is not uniform for any orbits other than the log-rolling (spinning) orbit. The disturbance velocity field due to a spheroid in these orbits, including the tumbling one in particular, is unsteady. The Stokesian disturbance field due to a spheroid rotating in any of these orbits exhibits a periodic dependence on time. The time period of rotation may be obtained based on $\dot{\phi}_{jeff}$, and is given by $T_{jeff} = 2\pi(\kappa^2 + 1)/\kappa$. It should be noted that the period is the same for all orbits because $\dot{\phi}_{jeff}$ is independent of θ_j. Further, the disturbance velocity field in the tumbling orbit has a period of $T_{jeff}/2$, due to the $\boldsymbol{p} \leftrightarrow -\boldsymbol{p}$ symmetry.

As mentioned in § 2, the correction to the angular velocity at $O(Re)$, $\boldsymbol{\Omega}_{c1}$, given in (2.24), is evaluated in Dabade *et al.* (2016). The angular velocity components expressed in terms of the angles defined above are of the form

$$\begin{aligned}\dot{\theta}_{c1} &= \sin\theta_j \cos\theta_j \left[F_1^n(\xi_0) + F_2^n(\xi_0)\cos 2\phi_j + F_3^n(\xi_0)\cos 2\theta_j + F_4^n(\xi_0)\cos 4\phi_j \right.\\ &\quad \left. + F_5^n(\xi_0)\cos(2\theta_j - 4\phi_j) + F_6^n(\xi_0)\cos(2\theta_j + 4\phi_j)\right], \qquad (3.3)\\ \dot{\phi}_{c1} &= \sin\phi_j \cos\phi_j \left[G_1^n(\xi_0) + G_2^n(\xi_0)\cos 2\theta_j + G_3^n(\xi_0)\cos 2\phi_j \right.\\ &\quad \left. + G_4^n(\xi_0)\cos(2\theta_j)\cos(2\phi_j)\right]. \qquad (3.4)\end{aligned}$$

For a neutrally buoyant spheroid, the functions F_i^n and G_i^n are defined as $F_i^n = F_i^p + F_i^f$ and $G_i^n = G_i^p + G_i^f$, with F_i^p, F_i^f, G_i^p and G_i^f defined for a prolate spheroid in Dabade *et al.* (2016); the corresponding functions for an oblate spheroid are obtained using the transformation defined in § 2. The superscripts 'f' and 'p' correspond to fluid and particle inertia contributions respectively. The rates of change defined in (3.3) and (3.4) lead to an inertial drift across Jeffery orbits. The orbital drift, defined as the average change in C over one complete rotation of the spheroid, can be obtained from a multiple time scale analysis and has been used to analyse the effect of inertia at $O(Re)$ in planar linear flows (Subramanian & Koch 2005, 2006*a*; Dabade *et al.* 2016; Marath & Subramanian 2017; Marath *et al.* 2017). For simple shear flow, in particular, it has been found that on time scales of $O(Re^{-1})$, a neutrally buoyant prolate spheroid of any aspect ratio settles into the tumbling orbit, and a neutrally buoyant oblate spheroid with aspect ratio κ in the range $0.137 < \kappa < 1$ asymptotes to the spinning orbit. For neutrally buoyant oblate spheroids with $\kappa < 0.137$, a repeller exists on the unit sphere (see the red curve in figure 1*c*), dividing the orientation hemisphere into two basins of attraction, with the attractors being the spinning and tumbling orbits, and, in the absence of stochastic fluctuations, the spheroid can settle into either of these depending on its initial orientation. In the analysis below, we focus on the effect of inertia on the time periods of rotation of both prolate and oblate spheroids, in the orbits into which they settle for times longer than $O(Re^{-1})$, due to the aforementioned $O(Re)$ drift.

The correction to the spinning period is zero at $O(Re)$. The argument leading to an analogous conclusion for a sphere has already been given in the introduction. The argument remains unchanged for a spheroid since $\boldsymbol{\omega}$ and $\boldsymbol{p}$ are coincident in the spinning mode. In the tumbling orbit, $\dot{\phi}_j$ is not a constant, and depends on $\boldsymbol{p}$, which

is orthogonal to $\boldsymbol{\omega}$. The tumbling time period is given by

$$\Delta T^{tumb} = \int_{\pi}^{-\pi} \frac{\mathrm{d}\phi_j}{\dot{\phi}_{jeff} + Re\,\dot{\phi}_{c1} + Re^{3/2}\,\dot{\phi}_{c2}} = \int_{\pi}^{-\pi} \frac{1}{\dot{\phi}_{jeff}}\,\mathrm{d}\phi_j - Re \int_{\pi}^{-\pi} \frac{\dot{\phi}_{c1}}{\dot{\phi}_{jeff}^2}\,\mathrm{d}\phi_j + O(Re^{3/2}), \tag{3.5}$$

where the expansion is valid for $\kappa \sim O(1)$, when $\dot{\phi}_{c1} Re \ll \dot{\phi}_{jeff}$. The leading-order integral on the right-hand side evaluates to $2\pi(\kappa^2+1)/\kappa$, which is, of course, the Jeffery period. The $O(Re)$ integral in the above equation evaluates to zero after substituting for $\dot{\phi}_{jeff}$ and $\dot{\phi}_{c1}$ from (3.1) and (3.4) respectively. The vanishing of this integral can also be seen by noting that the $O(Re)$ correction to the angular velocity given in (3.4) is antisymmetric about the gradient axis ($\phi_j = \pi/2$). Therefore, the contribution to the integral from the first quadrant (ϕ_j varies from 0 to $\pi/2$) cancels the contribution from the second quadrant (ϕ_j varies from $\pi/2$ to π) (this symmetry follows from the Stokesian velocity field due to the regular nature of the correction).

The correction to the time period due to fluid inertia arises at $O(Re^{3/2})$ for both the tumbling and the spinning orbits. As mentioned in the introduction, the $O(Re^{3/2})$ correction for a rigid sphere is evaluated in Stone *et al.* (2000) and Subramanian *et al.* (2011). The evaluation of the correction for a spheroid in the spinning orbit is simpler in that it follows that for a sphere, and is presented in § 4. The correction for a tumbling spheroid is more involved, in having to account for the unsteadiness of the disturbance velocity field, and is presented in § 5.

4. Evaluation: time period – spinning orbit

In this section, we focus on the effect of fluid inertia on spinning spheroids. The spinning mode is the only steady-state orbit for oblate spheroids with aspect ratios larger than 0.137, and one of two for oblate spheroids with aspect ratio less than 0.137. The leading-order spin is $-(1/2)\mathbf{1}_3$. Defining the correction to the spin, at $O(Re^{3/2})$, as $\dot{\psi}_{c2}\mathbf{1}_3$, $\dot{\psi}_{c2}$ being independent of the spin angle ψ due to symmetry, one obtains

$$\Delta T^{spin} = 8\pi Re^{3/2}\dot{\psi}_{c2}. \tag{4.1}$$

Here, $\dot{\psi}_{c2}$ can be obtained by contracting (2.25) with $\mathbf{1}_3$, and is given by

$$\dot{\psi}_{c2} = \frac{1}{8\pi X_C} \int [4\pi^2 k^2 \hat{\boldsymbol{u}}^f - (\boldsymbol{\Gamma}^\dagger \cdot \boldsymbol{k}) \cdot \nabla_{\boldsymbol{k}} \hat{\boldsymbol{u}}^{match} + \boldsymbol{\Gamma} \cdot \hat{\boldsymbol{u}}^{match}] \cdot \left\{ \frac{\mathrm{i}(\boldsymbol{S}^{(2t)} \cdot \boldsymbol{k}) \cdot \mathbf{1}_3}{2\pi k^2} \cdot \left(\boldsymbol{I} - \frac{\boldsymbol{k}\boldsymbol{k}}{k^2} \right) \right\} \mathrm{d}\boldsymbol{k}, \tag{4.2}$$

where all of the terms in the integrand are evaluated at $\theta_j = 0$, corresponding to the spinning orbit, and X_C is the torque coefficient corresponding to spinning motion, defined in § 2. The Fourier transformed velocity fields $\hat{\boldsymbol{u}}^{match}$ and $\hat{\boldsymbol{u}}^f$ are now independent of time. The integral for the time period in (4.1) then becomes

$$\Delta T^{spin} = -\frac{Re^{3/2}}{X_C} \int [-4\pi^2 k^2 \hat{\boldsymbol{u}}^f + (\boldsymbol{\Gamma}^\dagger \cdot \boldsymbol{k}) \cdot \nabla_{\boldsymbol{k}} \hat{\boldsymbol{u}}^{match} - \boldsymbol{\Gamma} \cdot \hat{\boldsymbol{u}}^{match}] \cdot \left\{ \frac{\mathrm{i}(\boldsymbol{S}^{(2t)} \cdot \boldsymbol{k}) \cdot \mathbf{1}_3}{2\pi k^2} \cdot \left(\boldsymbol{I} - \frac{\boldsymbol{k}\boldsymbol{k}}{k^2} \right) \right\} \mathrm{d}\boldsymbol{k}. \tag{4.3}$$

The term within braces above is again independent of time, and simplifies to

$$\frac{\mathrm{i}(\boldsymbol{S}^{(2t)}\cdot\boldsymbol{k})\cdot\mathbf{1}_3}{2\pi k^2}\cdot\left(\boldsymbol{I}-\frac{\boldsymbol{kk}}{k^2}\right)=\boldsymbol{T}_1^{spin}=\frac{\mathrm{i}(B_2+B_3)}{2k^2\pi}(k_2\,\mathbf{1}_1-k_1\,\mathbf{1}_2)\tag{4.4}$$

using (2.8), and, to within a constant of proportionality, is just the Fourier transformed rotlet field. For a sphere, B_2+B_3 above reduces to -4π, which equals half of the torque exerted by a unit sphere rotating with a unit non-dimensional angular velocity.

The singularity $\boldsymbol{S}$ in the actual problem takes the form $\boldsymbol{S}=A_3\boldsymbol{E}$, and, therefore, $\hat{\boldsymbol{u}}^{match}(\boldsymbol{k})$ is $-\mathrm{i}A_3\boldsymbol{E}\cdot\boldsymbol{k}/(2\pi k^2)\cdot(\boldsymbol{I}-\boldsymbol{kk}/k^2)$ from (2.21), which is the Fourier transformed stresslet velocity field, but with a ξ_0-dependent coefficient ($A_3=-20\pi/3$ for a sphere). The inertial terms in (4.3) involving $\hat{\boldsymbol{u}}^{match}$ take the form

$$(\boldsymbol{\Gamma}^{\dagger}\cdot\boldsymbol{k})\cdot\nabla_{\boldsymbol{k}}\hat{\boldsymbol{u}}^{match}-\boldsymbol{\Gamma}\cdot\hat{\boldsymbol{u}}^{match}=\boldsymbol{R}_1^{spin},\tag{4.5}$$

where $\boldsymbol{R}_1^{spin}$ is given by

$$\boldsymbol{R}_1^{spin}=\frac{A_3}{2k^6\pi}\left(\mathrm{i}k_1^3\left(k^2-4k_2^2\right)\,\mathbf{1}_1+\mathrm{i}k_1^2k_2\left(3k^2-4k_2^2\right)\mathbf{1}_2+\mathrm{i}k_1^2\left(k^2-4k_2^2\right)k_3\,\mathbf{1}_3\right).\tag{4.6}$$

The Fourier transformed velocity field $\hat{\boldsymbol{u}}^f$ in (4.3) is governed by (2.20). After eliminating the pressure term, (2.20) reduces, for the spinning case, to

$$\begin{aligned}-(\boldsymbol{\Gamma}^{\dagger}\cdot\boldsymbol{k})\cdot\nabla_{\boldsymbol{k}}\hat{\boldsymbol{u}}^f+\boldsymbol{\Gamma}\cdot\hat{\boldsymbol{u}}^f\cdot\left(\boldsymbol{I}-2\frac{\boldsymbol{kk}}{k^2}\right)+4\pi^2k^2\hat{\boldsymbol{u}}^f&=\boldsymbol{R}_1^{spin}\cdot\left(\boldsymbol{I}-\frac{\boldsymbol{kk}}{k^2}\right)=\boldsymbol{Q}^{spin}\\&=\frac{A_3}{k^6\pi}\left(-\mathrm{i}k_1^3k_2^2\mathbf{1}_1+\mathrm{i}k_1^2k_2\left(k_1^2+k_3^2\right)\mathbf{1}_2-\mathrm{i}k_1^2k_2^2k_3\mathbf{1}_3\right).\end{aligned}\tag{4.7}$$

The components of (4.7) in a space-fixed coordinate system are given as

$$\frac{\partial\hat{u}_1^f}{\partial k_2}-4\pi^2k^2\frac{\hat{u}_1^f}{k_1}-\left(1-\frac{2k_1^2}{k^2}\right)\frac{\hat{u}_2^f}{k_1}=-\frac{Q_1^{spin}}{k_1},\tag{4.8}$$

$$\frac{\partial\hat{u}_2^f}{\partial k_2}-4\pi^2k^2\frac{\hat{u}_2^f}{k_1}+\left(\frac{2k_1k_2}{k^2}\right)\frac{\hat{u}_2^f}{k_1}=-\frac{Q_2^{spin}}{k_1},\tag{4.9}$$

$$\frac{\partial\hat{u}_3^f}{\partial k_2}-4\pi^2k^2\frac{\hat{u}_3^f}{k_1}+\left(\frac{2k_1k_3}{k^2}\right)\frac{\hat{u}_2^f}{k_1}=-\frac{Q_3^{spin}}{k_1},\tag{4.10}$$

where the subscripts 1, 2 and 3 denote the components along the X, Y and Z axes. While the components along the flow ($\hat{u}_1^f$) and the vorticity ($\hat{u}_3^f$) axes are coupled to the one along the gradient axis ($\hat{u}_2^f$), the equation governing the latter is independent of the other two, and is therefore solved first. In (4.8)–(4.10), one can identify a simple shear flow in Fourier space, given by $\hat{\boldsymbol{u}}^{*\infty}(\boldsymbol{k})=-k_1\mathbf{1}_2$, orthogonal to the one in physical space, ($\boldsymbol{u}^{\infty}(\boldsymbol{x})=x_2\mathbf{1}_1$), convecting the Fourier transformed velocity field. The orthogonality arises because the wavevector is oriented normal to the wavefronts, the latter being turned by the simple shear flow in physical space (see figure 2). The components of the Fourier transformed velocity field are convected by the Fourier-space simple shear flow. This convection has the effect that $\hat{\boldsymbol{u}}^f(\boldsymbol{k})$, for a given $\boldsymbol{k}$, has contributions from all wavevectors turned onto $\boldsymbol{k}$ from orientations further upstream. The viscous term, proportional to $4\pi^2k^2$ in (4.8)–(4.10), causes an exponential decay in amplitude with an argument that involves an integral over the

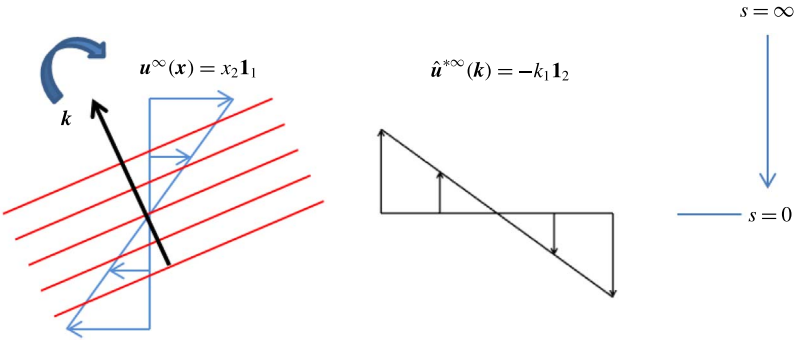

FIGURE 2. (Colour online) The red lines denote the wavefronts. Here, $\boldsymbol{k}$ is the wavevector which gets turned due to a simple shear flow of the form $\boldsymbol{u}^{\infty}(\boldsymbol{x}) = x_2\mathbf{1}_1$. This is equivalent to a convection by a simple shear flow of the form $\hat{\boldsymbol{u}}^{*\infty}(\boldsymbol{k}) = -k_1\mathbf{1}_2$ in the Fourier space.

square of the changing wavevector over this 'turning' period. Defining the streamlines of the Fourier-space simple shear flow as $k_2' = k_2 + k_1 s$, s being a time-like variable, the solutions for the individual components $\hat{u}_2^{f\beta}$, $\hat{u}_1^f$ and $\hat{u}_3^f$ may be written as follows:

$$\hat{u}_2^f(\boldsymbol{k}) = \int_0^{\infty} \exp\left(-4\pi^2\left(k^2 s + k_1 k_2 s^2 + \frac{k_1^2 s^3}{3}\right)\right) \times \left(\frac{1}{k^2}\right) \frac{\mathrm{i}k_1^2(k_2 + k_1 s)\left(k_1^2 + k_3^2\right) A_3}{k'^4\pi}\,\mathrm{d}s, \tag{4.11}$$

$$\hat{u}_1^f(\boldsymbol{k}) = \int_0^{\infty} \exp\left(-4\pi^2\left(k^2 s + k_1 k_2 s^2 + \frac{k_1^2 s^3}{3}\right)\right) \times \left(-\frac{\mathrm{i}k_1^3(k_2 + k_1 s)^2 A_3}{k'^6\pi} - \left(1 - \frac{2k_1^2}{k'^2}\right)\hat{u}_2^f(\boldsymbol{k}')\right)\mathrm{d}s \tag{4.12}$$

and

$$\hat{u}_3^f(\boldsymbol{k}) = \int_0^{\infty} \exp\left(-4\pi^2\left(k^2 s + k_1 k_2 s^2 + \frac{k_1^2 s^3}{3}\right)\right) \times \left(-\frac{\mathrm{i}k_1^2(k_2 + k_1 s)^2 k_3 A_3}{k'^6\pi} + \frac{2k_1 k_3}{k'^2}\hat{u}_2^f(\boldsymbol{k}')\right)\mathrm{d}s, \tag{4.13}$$

where the components in the flow and vorticity directions are coupled to the component in the gradient direction through the term $\hat{u}_2^f(\boldsymbol{k}')$. Here, $\boldsymbol{k}' = (k_1\mathbf{1}_1 + (k_2 + k_1 s)\mathbf{1}_2 + k_3\mathbf{1}_3)$ and $k' = |\boldsymbol{k}'|$, and $\hat{u}_2^f(\boldsymbol{k}')$ in (4.12) and (4.13) is given by

$$\hat{u}_2^f(\boldsymbol{k}') = \int_0^{\infty} \exp\left(-4\pi^2\left(k'^2 s' + k_1(k_2 + k_1 s)s'^2 + \frac{k_1^2 s'^3}{3}\right)\right) \times \left(\frac{1}{k'^2}\right) \frac{\mathrm{i}k_1^2 k_2''\left(k_1^2 + k_3^2\right) A_3}{k''^4\pi}\,\mathrm{d}s', \tag{4.14}$$

where $\boldsymbol{k}'' = (k_1\mathbf{1}_1 + (k_2 + k_1(s + s'))\mathbf{1}_2 + k_3\mathbf{1}_3)$, $k'' = |\boldsymbol{k}''|$ and $k_2'' = (k_2 + k_1(s + s'))$. Thus, $\hat{u}_1^f(\boldsymbol{k}')$ and $\hat{u}_3^f(\boldsymbol{k}')$ given in (4.11) and (4.13) include a one-dimensional and a two-dimensional integral, whereas $\hat{u}_2^f(\boldsymbol{k}')$ given in (4.12) consists of only a one-dimensional integral.

The Fourier transformed test velocity field given in (4.4), the inertial terms involving $\hat{u}^{match}$ given by (4.5)–(4.6) and $\hat{u}^{f}$ given by (4.11)–(4.13) are now substituted in (4.3) to obtain

$$\Delta T^{spin} = -\frac{Re^{3/2}}{X_c}\int [-4\pi^2 k^2(\hat{u}_1^f \mathbf{1}_1 + \hat{u}_2^f \mathbf{1}_2 + \hat{u}_3^f \mathbf{1}_3) + \boldsymbol{R}_1^{spin}] \cdot \boldsymbol{T}_1^{spin}\, \mathrm{d}\boldsymbol{k}. \tag{4.15}$$

The different terms in the integral above can be expressed in a spherical coordinate system with $k_1 = k\sin\theta\cos\phi$, $k_2 = k\sin\theta\sin\phi$, $k_3 = k\cos\theta$ and $\mathrm{d}\boldsymbol{k} = k^2\sin\theta\,\mathrm{d}k\,\mathrm{d}\theta\,\mathrm{d}\phi$ as

$$\begin{aligned}
\int (-4\pi^2 k^2\, \hat{u}_1^f(\boldsymbol{k})\, \mathbf{1}_1 \cdot \boldsymbol{T}_1^{spin})\, \mathrm{d}\boldsymbol{k} &= \int_0^{2\pi}\int_0^{\pi}\int_0^{\infty} 4\pi^2 \left\{ k^2 \frac{\mathrm{i}k_1^3 k_2'^2 A_3}{k'^6\pi} \left[\frac{\mathrm{i}(B_2+B_3)k_2}{2k^2\pi}\right]\right\} \\
&\times \int_0^{\infty} k^2 \exp\left(-4\pi^2\left(k^2 s + k_1 k_2 s^2 + \frac{k_1^2 s^3}{3}\right)\right) \mathrm{d}k\,\mathrm{d}s\,\sin\theta\,\mathrm{d}\theta\,\mathrm{d}\phi \\
&+ \int_0^{2\pi}\int_0^{\pi}\int_0^{\infty}\int_0^{\infty} \left\{ 4\pi^2 k^2 \left[\frac{\mathrm{i}(B_2+B_3)k_2}{2k^2\pi}\right]\left(1 - \frac{2k_1^2}{k'^2}\right)\frac{\mathrm{i}k_1^2 k_2''(k_1^2+k_3^2)A_3}{k''^4 k'^2\pi}\right\} \\
&\times \int_0^{\infty} \exp\left(-4\pi^2\left(k^2 s + k_1 k_2 s^2 + \frac{k_1^2 s^3}{3}\right)\right) \\
&\times \exp\left(-4\pi^2\left(k'^2 s' + k_1 k_2' s'^2 + \frac{k_1^2 s'^3}{3}\right)\right) k^2\,\mathrm{d}k\,\mathrm{d}s'\,\mathrm{d}s\,\sin\theta\,\mathrm{d}\theta\,\mathrm{d}\phi,
\end{aligned} \tag{4.16}$$

$$\begin{aligned}
&\int (-4\pi^2 k^2\, \hat{u}_2^f(\boldsymbol{k})\, \mathbf{1}_2 \cdot \boldsymbol{T}_1^{spin})\, \mathrm{d}\boldsymbol{k} \\
&= -\int 4\pi^2 \left\{ \left[\frac{-\mathrm{i}(B_2+B_3)k_1}{2\pi}\right] \frac{\mathrm{i}k_1^2(k_2+k_1 s)\left(k_1^2+k_3^2\right)A_3}{k^2 k'^4\pi}\right\} \\
&\times \int_0^{\infty} \exp\left(-4\pi^2\left(k^2 s + k_1 k_2 s^2 + \frac{k_1^2 s^3}{3}\right)\right) k^2\,\mathrm{d}k\,\mathrm{d}s\,\sin\theta\,\mathrm{d}\theta\,\mathrm{d}\phi,
\end{aligned} \tag{4.17}$$

$$\int (-4\pi^2 k^2\, \hat{u}_3^f(\boldsymbol{k})\, \mathbf{1}_3 \cdot \boldsymbol{T}_1^{spin})\, \mathrm{d}\boldsymbol{k} = 0 \tag{4.18}$$

and

$$\begin{aligned}
\int \boldsymbol{R}_1^{spin} \cdot \boldsymbol{T}_1^{spin}\, \mathrm{d}\boldsymbol{k} \;=\; &\int_0^{2\pi}\int_0^{\pi}\int_0^{\infty} \left\{ -\frac{A_3 k_1^3 (k^2 - 4k_2^2)}{\pi k^6}\,\frac{(B_2+B_3)k_2}{4\pi} \right. \\
&\left. + \frac{A_3 k_1^2 k_2 (3k^2 - 4k_2^2)}{k^6\pi}\,\frac{(B_2+B_3)k_1}{4\pi}\right\} \mathrm{d}k\,\sin\theta\,\mathrm{d}\theta\,\mathrm{d}\phi,
\end{aligned} \tag{4.19}$$

where we have retained the Cartesian notation for the wavevector components for brevity, and the terms grouped within the braces are such that they are independent of k. The test velocity field does not have a vorticity component, and therefore the contribution to (4.15) due to the term proportional to $\hat{u}_3^f$ is zero.

The right-hand side of (4.16) is sum of a four-dimensional and a five-dimensional integral, whereas that of (4.17) is a single four-dimensional integral. In the four-dimensional integrals, the integration over k gives a term proportional to $1/s^{3/2}$,

which is divergent in the integration over s as $s \to 0$, as follows:

$$\begin{aligned}
&\int_0^\infty k^2 \exp\left(-4\pi^2\left(k^2 s + k_1 k_2 s^2 + \frac{k_1^2 s^3}{3}\right)\right) \mathrm{d}k \\
&\quad = \int_0^\infty k^2 \exp\left(-4\pi^2 k^2\left(s + \sin^2\theta\cos\phi\sin\phi s^2 + \frac{\sin^2\theta\cos^2\phi s^3}{3}\right)\right) \mathrm{d}k \\
&\quad = \frac{1}{32\pi^{5/2}(s + \sin^2\theta\cos\phi\sin\phi s^2 + \sin^2\theta\cos^2\phi s^3/3)^{3/2}}.
\end{aligned} \tag{4.20}$$

The three-dimensional integral on the right-hand side of (4.19) diverges in the limit $k \to \infty$. Although, individually, the abovementioned integrals are divergent, the sum is nevertheless convergent. This divergence arises because, while deriving the expression for the angular velocity in (2.22), we had rewritten the three terms proportional to $\hat{u}^f$ in (2.6) as a sum of a term proportional to $k^2\hat{u}^f$ and three terms proportional to $\hat{u}^{match}$, and each of these four terms is divergent in the limit of $k \to \infty$ (the original terms were convergent with $\hat{u}^f$ decaying as $1/k^3$, the scaling obtained from the large-k limit of (4.11)–(4.13)). To eliminate the divergence, an additional integral over a dummy variable s is introduced in (4.19) as follows:

$$\begin{aligned}
\int \boldsymbol{R}_1^{spin} \cdot \boldsymbol{T}_1^{spin} \,\mathrm{d}\boldsymbol{k} = \int_0^{2\pi}\int_0^{\pi}\int_0^{\infty} &\left\{\frac{-A_3 k_1^3 (k^2 - 4k_2^2)}{\pi k^6}\frac{(B_2 + B_3)k_2}{4\pi}\right. \\
&\left. + \frac{A_3 k_1^2 k_2 (3k^2 - 4k_2^2)}{k^6\pi}\frac{(B_2 + B_3)k_1}{4\pi}\right\} \int_0^\infty 4\pi^2 k^2 \mathrm{e}^{-4\pi^2 k^2 s} \,\mathrm{d}s \,\mathrm{d}k \sin\theta \,\mathrm{d}\theta \,\mathrm{d}\phi.
\end{aligned} \tag{4.21}$$

It should be noted that $\int_0^\infty 4\pi^2 k^2 \exp(-4\pi^2 k^2 s)\,\mathrm{d}s = 1$. The additional integral, when integrated over k, gives a term proportional to $1/s^{3/2}$, and (4.21) takes the form

$$\begin{aligned}
\int \boldsymbol{R}_1^{spin} \cdot \boldsymbol{T}_1^{spin} \,\mathrm{d}\boldsymbol{k} = \int_0^{2\pi}\int_0^{\pi}\int_0^{\infty} &\left\{\frac{-A_3 k_1^3 (k^2 - 4k_2^2)}{\pi k^6}\frac{(B_2 + B_3)k_2}{4\pi}\right. \\
&\left. + \frac{A_3 k_1^2 k_2 (3k^2 - 4k_2^2)}{k^6\pi}\frac{(B_2 + B_3)k_1}{4\pi}\right\} \frac{1}{8\sqrt{\pi}s^{3/2}} \,\mathrm{d}s \sin\theta \,\mathrm{d}\theta \,\mathrm{d}\phi.
\end{aligned} \tag{4.22}$$

The integration over k in the five-dimensional integral in (4.16) gives

$$\begin{aligned}
&\int_0^\infty k^2 \exp\left(-4\pi^2\left(k^2 s + k_1 k_2 s^2 + \frac{k_1^2 s^3}{3}\right)\right) \exp\left(-4\pi^2\left(k'^2 s' + k_1 k_2' s'^2 + \frac{k_1^2 s'^3}{3}\right)\right) \mathrm{d}k \\
&\quad = \int k^2 \exp\left(-4\pi^2 k^2 \frac{s'}{12}\left(3\left(4 + s^2 - s^2\cos 2\theta + 2s\sin^2\theta(s\cos 2\phi + 2\sin 2\phi)\right)\right.\right. \\
&\qquad \left.\left. + 4\cos\phi\sin^2\theta s'\left(3\sin\phi + \cos\phi\left(3s + s'\right)\right)\right)\right) \\
&\qquad \times \exp\left(-4\pi^2 k^2\left(s + \sin^2\theta\cos\phi\sin\phi s^2 + \frac{\sin^2\theta\cos^2\phi s^3}{3}\right)\right) \mathrm{d}k \\
&\quad = \frac{1}{32\pi^{5/2}(f^{exp}(s, s', \theta, \phi))^{3/2}},
\end{aligned} \tag{4.23}$$

where f^{exp} is the function that multiplies $-4\pi^2k^2$ in the exponent of the integrand. It should be noted that there is no divergence for the five-dimensional integral in the limit of $s \to 0$ or $s' \to 0$. The integration over k for the four-dimensional integrals given in (4.16) and (4.17) is substituted from (4.20), and the sum of the resulting three-dimensional integral together with the matching term contribution given in (4.22) is convergent in the limit of $s \to 0$. This sum, which is a three-dimensional integral (over s, θ, ϕ) and a four-dimensional integral (over s, s', θ, ϕ) obtained from the five-dimensional ones in (4.16) and (4.17), after substituting from (4.23), is evaluated numerically using Gaussian quadrature to give the time period correction as

$$\Delta T^{spin} = Re^{3/2}\frac{A_3(B_2+B_3)}{X_C}\,0.00516. \tag{4.24}$$

The angular velocity correction at $O(Re^{3/2})$ can be obtained by using (4.1) and is given by $\Delta T^{spin}/(8\pi)$, which leads to

$$\dot{\psi} = -\frac{1}{2} + Re^{3/2}\frac{A_3(B_2+B_3)}{8\pi X_C}0.00516. \tag{4.25}$$

For an oblate spheroid, $A_3(B_2+B_3)/X_c = 128\pi^2/(9\,\mathrm{cosec}^{-1}\xi_0\xi_0^5 - 6\xi_0\sqrt{-1+\xi_0^2} - 9\xi_0^3\sqrt{-1+\xi_0^2})$. For a sphere, $A_3(B_2+B_3)/X_c = 80\pi^2/3$ and the angular velocity reduces to that obtained by Stone *et al.* (2000) and Subramanian *et al.* (2011). The reason for the absence of the $O(Re)$ correction in (4.25) has already been pointed out in §§ 1 and 3. The correction given in (4.25) matches with that derived using a matched asymptotic expansion approach in Meibohm *et al.* (2016). The plot of the correction to the time period in (4.24) against eccentricity is given in § 6.

The correction derived in (4.24) is also valid for a spinning prolate spheroid, with $A_3(B_2+B_3)/X_c = 128\pi^2(\xi_0^2-1)/(3\xi_0^3(-3\xi_0^3+3(\xi_0^2-1)^2\coth^{-1}\xi_0+5\xi_0))$. Although not relevant to inertial correction in three dimensions, consideration of this mode allows one to connect to the effect of inertia in the two-dimensional scenario. As mentioned in the introduction, the inertial correction for a circular cylinder arises at $O(Re)$, as shown by Robertson & Acrivos (1970). This scaling emerges from the $O(Re^{3/2})$ correction for a spinning prolate spheroid in the limit of $\kappa \to \infty$. To see this, one first writes (4.24) in terms of the Reynolds number based on the spheroid minor axis ($\tilde{Re}$), yielding $\Delta T^{spin} = \tilde{Re}^{3/2}\kappa^3 A_3(B_2+B_3)/X_c$, which in the large-aspect-ratio limit is proportional to $\tilde{Re}^{3/2}\kappa$. As expected, the transition from $O(Re^{3/2})$ to the two-dimensional $O(Re)$ scaling occurs when κ is $O(\tilde{Re}^{-1/2})$.

5. Evaluation: time period – tumbling orbit

In this section, we focus on the tumbling orbit, which is the long-time orbit for prolate spheroids of any aspect ratio and one of two for oblate spheroids with aspect ratios less than 0.137. The inertial correction to the tumbling time period may be obtained by considering the explicit form of the $O(Re^{3/2})$ term in (3.5), and is given by

$$\Delta T^{tumb} = -Re^{3/2}\int_{\pi}^{-\pi}\frac{\dot{\phi}_{c2}}{\dot{\phi}_{jeff}^2}\,\mathrm{d}\phi_j = -Re^{3/2}\int_0^{T_{jeff}}\frac{\dot{\phi}_{c2}}{\dot{\phi}_{jeff}}\,\mathrm{d}t. \tag{5.1}$$

In (5.1), we have changed the variable of integration back to time based on $\mathrm{d}\phi_j/\mathrm{d}t = \dot{\phi}_{jeff}$, since the error affects the time period only at $O(Re^{5/2})$. The angular velocity of

the tumbling spheroid, at $O(Re^{3/2})$, $\dot{\phi}_{c2}$, may be obtained by contracting (2.25) with $\mathbf{1}_3$, which gives

$$\dot{\phi}_{c2} = \frac{1}{8\pi Y_C}\int\left[4\pi^2 k^2\hat{\boldsymbol{u}}^f + \frac{\partial\hat{\boldsymbol{u}}^{match}}{\partial t} - (\boldsymbol{\Gamma}^\dagger\cdot\boldsymbol{k})\cdot\nabla_{\boldsymbol{k}}\hat{\boldsymbol{u}}^{match} + \boldsymbol{\Gamma}\cdot\hat{\boldsymbol{u}}^{match}\right] \cdot\left\{\frac{\mathrm{i}(\boldsymbol{S}^{(2t)}\cdot\boldsymbol{k})\cdot\mathbf{1}_3}{2\pi k^2}\cdot\left(\boldsymbol{I}-\frac{\boldsymbol{kk}}{k^2}\right)\right\}\mathrm{d}\boldsymbol{k}, \tag{5.2}$$

where all of the terms in the integrand are evaluated at $\theta_j = \pi/2$ (tumbling orbit), and Y_c, the torque coefficient corresponding to transverse rotation, is defined in § 2. Substitution of (5.2) into (5.1) leads to the $O(Re^{3/2})$ correction to the time period, given by

$$\Delta T^{tumb} = \frac{Re^{3/2}}{8\pi Y_c}\int\int_0^{T_{jeff}}\left[-4\pi^2 k^2\hat{\boldsymbol{u}}^f - \frac{\partial\hat{\boldsymbol{u}}^{match}}{\partial t} + (\boldsymbol{\Gamma}^\dagger\cdot\boldsymbol{k})\cdot\nabla_{\boldsymbol{k}}\hat{\boldsymbol{u}}^{match} - \boldsymbol{\Gamma}\cdot\hat{\boldsymbol{u}}^{match}\right] \cdot\left\{\frac{\mathrm{i}(\boldsymbol{S}^{(2t)}\cdot\boldsymbol{k})\cdot\mathbf{1}_3}{2\pi k^2\,\dot{\phi}_{jeff}}\cdot\left(\boldsymbol{I}-\frac{\boldsymbol{kk}}{k^2}\right)\right\}\mathrm{d}t\,\mathrm{d}\boldsymbol{k}. \tag{5.3}$$

The integral above is evaluated in the space-fixed coordinate system (XYZ in figure 1*a*) and the details are presented in §§ 5.1–5.4 below. The reciprocal theorem restricts the orientation of the spheroid in the test problem to be the same as that of the spheroid in the problem of interest. Therefore, in the tumbling orbit, the velocity field is unsteady in the test problem too. The singularities corresponding to both problems are time-dependent point-force-dipole singularities (a stresslet in the actual problem and both a stresslet and a rotlet in the test problem), the time dependence arising from the motion of $\boldsymbol{p}$ along the tumbling orbit. The time-dependent $\boldsymbol{p}$ determines $\boldsymbol{S}^{(2t)}$, $\boldsymbol{S}$ and thence $\hat{\boldsymbol{u}}^{match}$ and $\hat{\boldsymbol{u}}^f$ via (2.21) and (2.20). Thus, the term involving the test velocity field, given within braces in (5.3), and the inertial terms in the problem of interest, given in square brackets, are functions of time.

To evaluate the integral in (5.3), in § 5.1, the term within braces is expressed in the aforementioned coordinate system as a Fourier time series which involves a combination of three Fourier modes, namely the mode independent of time that is already present for a sphere, and modes proportional to $\cos(4\pi t/T_{jeff})$ and $\sin(4\pi t/T_{jeff})$, T_{jeff} being the Jeffery period. The combination $\boldsymbol{S}^{(2t)}/\dot{\phi}_{jeff}$ leads to a finite Fourier series, a fact crucial to the evaluation of the time period correction; the time dependence of $\boldsymbol{S}^{(2t)}$ alone, for instance, would have led to an infinite Fourier time series. The two time-dependent modes have a frequency that is twice the Jeffery frequency ($\omega_g = 2\pi/T_{jeff}$), this being due to the fore–aft symmetry of the spheroid, which leads to the same disturbance field for orientations $\boldsymbol{p}$ and $-\boldsymbol{p}$. In (5.3), since one is only interested in the integration over a time period, only the terms corresponding to these three Fourier modes in the Fourier expansion of the inertial acceleration terms will lead to non-zero contributions. The expansions for the inertial terms involving $\hat{\boldsymbol{u}}^{match}$ are made in § 5.2, and that for the inertial term proportional to $\hat{\boldsymbol{u}}^f$ is made in § 5.3. The details of the evaluation of the integral are presented in § 5.4.

5.1. *The term proportional to the singularity in the test problem*

In the tumbling orbit, $\boldsymbol{p}$ has the form $\cos\phi_j\mathbf{1}_1 + \sin\phi_j\mathbf{1}_2$, with $\tan\phi_j = 1/(\kappa\tan(\omega_g t))$, which is the solution of the Jeffery equations (3.1)–(3.2). This relation is used for

both the orientation in the test problem and that in the problem of interest. The term corresponding to the test velocity field in braces, in (5.3), simplifies to

$$\begin{aligned}\frac{\mathrm{i}(\boldsymbol{S}^{(2t)}\cdot\boldsymbol{k})\cdot\mathbf{1}_3}{2\pi k^2\dot{\phi}_{jeff}}\cdot\left(\boldsymbol{I}-\frac{\boldsymbol{kk}}{k^2}\right)&=\boldsymbol{T}_1^{tumb}+\boldsymbol{T}_2^{tumb}\cos(2\omega_g t)+\boldsymbol{T}_3^{tumb}\sin(2\omega_g t)\\&=-\boldsymbol{T}_1\frac{(\kappa^2+1)^2}{2\kappa^2}+\boldsymbol{T}_2\frac{(1-\kappa^4)}{2\kappa^2}+\left(\boldsymbol{T}_1\frac{(\kappa^4-1)}{2\kappa^2}+\boldsymbol{T}_2\frac{(\kappa^2+1)^2}{2\kappa^2}\right)\\&\quad\times\cos(2\omega_g t)-\boldsymbol{T}_3\frac{\kappa^2+1}{\kappa}\sin(2\omega_g t),\end{aligned}\tag{5.4}$$

with $\omega_g=2\pi/T_{jeff}$. The vectors $\boldsymbol{T}_1$, $\boldsymbol{T}_2$ and $\boldsymbol{T}_3$ above are given by

$$\boldsymbol{T}_1=\left(\frac{\mathrm{i}k_2}{2k^2\pi}\mathbf{1}_1-\frac{\mathrm{i}k_1}{2k^2\pi}\mathbf{1}_2\right)B_3,\tag{5.5}$$

$$\boldsymbol{T}_2=\left(\frac{\mathrm{i}(k^2-2k_1^2)k_2}{2k^4\pi}\mathbf{1}_1+\frac{\mathrm{i}k_1(k^2-2k_2^2)}{2k^4\pi}\mathbf{1}_2-\frac{\mathrm{i}k_1k_2k_3}{k^4\pi}\mathbf{1}_3\right)B_1,\tag{5.6}$$

$$\boldsymbol{T}_3=\left(-\frac{\mathrm{i}(k^2-k_1^2+k_2^2)k_1}{2k^4\pi}\mathbf{1}_1+\frac{\mathrm{i}k_2(k^2+k_1^2-k_2^2)}{2k^4\pi}\mathbf{1}_2+\frac{\mathrm{i}(k_1^2-k_2^2)k_3}{2k^4\pi}\mathbf{1}_3\right)B_1.\tag{5.7}$$

The constants B_1 and B_3 above are defined in (2.9) and (2.11) for a prolate spheroid. In the tumbling mode, one need not consider the axial spin singularity corresponding to B_2, since the orientation vector is perpendicular to the angular velocity and, thus, equation (5.4) is independent of B_2. As is evident in (5.4), there are only three Fourier modes for an arbitrary-aspect-ratio spheroid. In the limiting case of a sphere ($\kappa\to1$), $B_1\to0$, and therefore $\boldsymbol{T}_2^{tumb}$, $\boldsymbol{T}_3^{tumb}\to0$, and only the time-independent mode survives. In the limit of a flat disk ($\kappa\to0$), $B_1=B_3=-16/3$, and $\boldsymbol{T}_3^{tumb}$ is $O(\kappa)$ smaller than both $\boldsymbol{T}_1^{tumb}$ and $\boldsymbol{T}_2^{tumb}$, and can therefore be neglected. Therefore, for a flat disk, (5.4) scales as $O(1/\kappa^2)$. In the limit of a slender fibre ($\kappa\to\infty$), $B_1=-B_3=4\pi/(3\log\kappa)$, consistent with viscous slender-body theory, and $\boldsymbol{T}_3^{tumb}$ is $O(1/\kappa)$ smaller than both $\boldsymbol{T}_1^{tumb}$ and $\boldsymbol{T}_2^{tumb}$, and can again be neglected. Therefore, for a slender fibre, (5.4) scales as $O(\kappa^2/\log\kappa)$. The scalings for ΔT^{tumb}, for these extreme-aspect-ratio particles, are further analysed in § 5.5.

5.2. *The inertial terms with* $\hat{\boldsymbol{u}}^{match}$

In this section, we expand the three terms involving $\hat{\boldsymbol{u}}^{match}$, in the integrand in (5.3), as a Fourier series. The general Fourier expansion has an infinite number of terms, but one only needs to retain terms corresponding to the three modes in (5.4). As for the test velocity field, the expression for $\hat{\boldsymbol{u}}^{match}$ given in (2.21) now depends on time through the stresslet singularity coefficient $\boldsymbol{S}$. Hence, we expand $\boldsymbol{S}$ as a Fourier series in time and retain only the aforementioned terms. This truncated expansion takes the form

$$\begin{aligned}\boldsymbol{S}\;=\;&-2A_{112}\sin(2\omega_g t)\mathbf{1}_1\mathbf{1}_1+(A_{120}+2A_{122}\cos(2\omega_g t))(\mathbf{1}_1\mathbf{1}_2+\mathbf{1}_2\mathbf{1}_1)\\&-2A_{222}\sin(2\omega_g t)\mathbf{1}_2\mathbf{1}_2-2A_{332}\sin(2\omega_g t)\mathbf{1}_3\mathbf{1}_3,\end{aligned}\tag{5.8}$$

where

$$A_{112}=-\left(\frac{3A_1}{2}-2A_2+\frac{A_3}{2}\right)\frac{\kappa^2}{(1+\kappa)^3}-\left(A_2-\frac{A_3+A_1}{2}\right)\frac{\kappa}{(1+\kappa)^2},\tag{5.9}$$

$$A_{120} = \left(\frac{A_2}{2} + \left(\frac{3A_1}{2} - 2A_2 + \frac{A_3}{2}\right)\frac{\kappa}{2(1+\kappa)^2}\right), \tag{5.10}$$

$$A_{122} = -\left(\frac{3A_1}{2} - 2A_2 + \frac{A_3}{2}\right)\frac{\kappa(1-\kappa)}{2(1+\kappa)^3}, \tag{5.11}$$

$$A_{222} = -\left(\frac{3A_1}{2} - 2A_2 + \frac{A_3}{2}\right)\frac{\kappa}{(1+\kappa)^3} - \left(A_2 - \frac{A_3+A_1}{2}\right)\frac{\kappa}{(1+\kappa)^2}, \tag{5.12}$$

$$A_{332} = \left(\frac{A_1 - A_3}{2}\right)\frac{\kappa}{(1+\kappa)^2}, \tag{5.13}$$

where the A_i terms are defined in (2.16)–(2.18). In deriving (5.8), we have again used the Jeffery solution for ϕ_j (see § 5.1). For a sphere, $A_1 = A_2 = A_3 = -20\pi/3$, and therefore $\boldsymbol{S}$ in (5.8) reduces to $-10\pi/3(\mathbf{1}_1\mathbf{1}_2 + \mathbf{1}_2\mathbf{1}_1) = -(20\pi/3)\boldsymbol{E}$. For a flat disk, $2A_1 = A_3 = -64/9$ and A_2 is $-8\pi\kappa/3$, therefore (5.8) is $O(\kappa)$. For a slender fibre, $A_1 = -8\pi/(9\log\kappa)$, A_2 and A_3 are $O(1/\kappa^2)$, and (5.8) is therefore $O(1/(\kappa\log\kappa))$.

Using (2.21) and (5.8), the truncated Fourier expansion of the terms involving $\hat{\boldsymbol{u}}^{match}$, to be used in (5.3), is obtained as

$$(\boldsymbol{\Gamma}^{\dagger}\cdot\boldsymbol{k})\cdot\nabla_{\boldsymbol{k}}\hat{\boldsymbol{u}}^{match} - \frac{\partial\hat{\boldsymbol{u}}^{match}}{\partial t} - \boldsymbol{\Gamma}\cdot\hat{\boldsymbol{u}}^{match} = \boldsymbol{R}_1^{tumb} + \boldsymbol{R}_2^{tumb}\cos(2\omega_g t) + \boldsymbol{R}_3^{tumb}\sin(2\omega_g t), \tag{5.14}$$

where $\boldsymbol{R}_1^{tumb}$, $\boldsymbol{R}_2^{tumb}$ and $\boldsymbol{R}_3^{tumb}$ are functions of k_1, k_2, k_3, ω_g and the A_{ijk} terms defined in (5.9)–(5.13), and are given by

$$\boldsymbol{R}_1^{tumb} = \frac{\mathrm{i}A_{120}k_1^3\left(k^2-4k_2^2\right)}{k^6\pi}\mathbf{1}_1 + \frac{\mathrm{i}A_{120}k_1^2k_2\left(3k^2-4k_2^2\right)}{k^6\pi}\mathbf{1}_2 + \frac{\mathrm{i}A_{120}k_1^2\left(k^2-4k_2^2\right)k_3}{k^6\pi}\mathbf{1}_3, \tag{5.15}$$

$$\begin{aligned}\boldsymbol{R}_2^{tumb} = {} & \frac{2\mathrm{i}k_1\left(A_{122}k_1^2\left(k^2-4k_2^2\right)+\omega_g k^2\left(A_{112}\left(-k^2+k_1^2\right)+A_{222}k_2^2+A_{332}k_3^2\right)\right)}{k^6\pi}\mathbf{1}_1 \\ & + \frac{2\mathrm{i}k_2\left(A_{122}k_1^2\left(3k^2-4k_2^2\right)+\omega_g k^2\left(A_{112}k_1^2+A_{222}\left(-k^2+k_2^2\right)+A_{332}k_3^2\right)\right)}{k^6\pi}\mathbf{1}_2 \\ & + \frac{2\mathrm{i}k_3\left(A_{122}k_1^2\left(k^2-4k_2^2\right)+\omega_g k^2\left(A_{112}k_1^2+A_{222}k_2^2+A_{332}\left(-k^2+k_3^2\right)\right)\right)}{k^6\pi}\mathbf{1}_3,\end{aligned} \tag{5.16}$$

$$\begin{aligned}\boldsymbol{R}_3^{tumb} = {} & \left(-\frac{2\mathrm{i}\omega_g A_{122}\left(k^2-2k_1^2\right)k_2}{k^4\pi} + \frac{\mathrm{i}A_{112}k_1^2\left(-k^2+4k_1^2\right)k_2}{k^6\pi}\right. \\ & \left. + \frac{\mathrm{i}A_{222}k_2\left(-k^2\left(k^2+2k_1^2\right)+\left(k^2+4k_1^2\right)k_2^2\right)}{k^6\pi} + \frac{\mathrm{i}A_{332}\left(k^2+4k_1^2\right)k_2k_3^2}{k^6\pi}\right)\mathbf{1}_1 \\ & + \left(-\frac{2\mathrm{i}\omega_g A_{122}k_1\left(k^2-2k_2^2\right)}{k^4\pi} + \frac{\mathrm{i}A_{112}k_1^3\left(-k^2+4k_2^2\right)}{k^6\pi}\right. \\ & \left. - \frac{\mathrm{i}A_{222}k_1\left(k-k_2\right)\left(k+k_2\right)\left(-k^2+4k_2^2\right)}{k^6\pi} - \frac{\mathrm{i}A_{332}k_1\left(k^2-4k_2^2\right)k_3^2}{k^6\pi}\right)\mathbf{1}_2\end{aligned} \tag{5.17}$$

$$+\left(\frac{4\mathrm{i}\omega_g A_{122}k_1k_2k_3}{k^4\pi}+\frac{4\mathrm{i}A_{112}k_1^3k_2k_3}{k^6\pi}+\frac{2\mathrm{i}A_{222}k_1k_2\left(-k^2+2k_2^2\right)k_3}{k^6\pi}\right.$$
$$\left.+\frac{2\mathrm{i}A_{332}k_1k_2k_3\left(-k^2+2k_3^2\right)}{k^6\pi}\right)\mathbf{1}_3. \tag{5.17}$$

Again, for a sphere, only the time-independent mode survives in (5.14). In the limit of extreme aspect ratios, that is, for a fibre or a flat disk, one needs to consider only the constant term and the one proportional to $\cos(2\omega_g t)$ in (5.14), since the test singularity has only those two modes, as seen later in § 5.5.

5.3. *The inertial term proportional to* $\hat{\boldsymbol{u}}^f$

In this section, we expand the lone term proportional to $\hat{\boldsymbol{u}}^f$ in the integrand in (5.3) as a Fourier series. As in the previous section, we only need to find the coefficients of the three modes present in (5.4). To begin with, (2.20) is contracted with $(\boldsymbol{I}-\boldsymbol{kk}/k^2)$ to eliminate the pressure, leading to the following governing equation for $\hat{\boldsymbol{u}}^f$:

$$\frac{\partial\hat{\boldsymbol{u}}^f}{\partial t}-(\boldsymbol{\Gamma}^\dagger\cdot\boldsymbol{k})\cdot\nabla_k\hat{\boldsymbol{u}}^f+\boldsymbol{\Gamma}\cdot\hat{\boldsymbol{u}}^f\cdot\left(\boldsymbol{I}-2\frac{\boldsymbol{kk}}{k^2}\right)+4\pi^2k^2\hat{\boldsymbol{u}}^f$$
$$=-\left(\frac{\partial\hat{\boldsymbol{u}}^{match}}{\partial t}-(\boldsymbol{\Gamma}^\dagger\cdot\boldsymbol{k})\cdot\nabla\hat{\boldsymbol{u}}^{match}+\boldsymbol{\Gamma}\cdot\hat{\boldsymbol{u}}^{match}\right)\cdot\left(\boldsymbol{I}-\frac{\boldsymbol{kk}}{k^2}\right). \tag{5.18}$$

The expression on the right-hand side above is evaluated using (5.14) to give

$$\frac{\partial\hat{\boldsymbol{u}}^f}{\partial t}-(\boldsymbol{\Gamma}^\dagger\cdot\boldsymbol{k})\cdot\nabla\hat{\boldsymbol{u}}^f+\boldsymbol{\Gamma}\cdot\hat{\boldsymbol{u}}^f\cdot\left(\boldsymbol{I}-2\frac{\boldsymbol{kk}}{k^2}\right)+4\pi^2k^2\hat{\boldsymbol{u}}^f$$
$$=(\boldsymbol{R}_1^{tumb}+\boldsymbol{R}_2^{tumb}\cos(2\omega_g t)+\boldsymbol{R}_3^{tumb}\sin(2\omega_g t))\cdot\left(\boldsymbol{I}-\frac{\boldsymbol{kk}}{k^2}\right)$$
$$=\sum_{\beta\in\{0,2,-2\}}\boldsymbol{Q}^\beta\mathrm{e}^{\mathrm{i}\beta\omega_g t}, \tag{5.19}$$

where $\boldsymbol{Q}^0=\boldsymbol{R}_1^{tumb}-(\boldsymbol{R}_1^{tumb}\cdot\boldsymbol{k})\boldsymbol{k}/k^2$, $\boldsymbol{Q}^2=((\boldsymbol{R}_2^{tumb}-\mathrm{i}\boldsymbol{R}_3^{tumb})/2)\cdot(\boldsymbol{I}-(\boldsymbol{kk}/k^2))$ and $\boldsymbol{Q}^{-2}=((\boldsymbol{R}_2^{tumb}+\mathrm{i}\boldsymbol{R}_3^{tumb})/2)\cdot(\boldsymbol{I}-(\boldsymbol{kk}/k^2))$. The $\boldsymbol{Q}^\beta$ terms for $\beta=0$, 2 and -2 are given as follows:

$$\boldsymbol{Q}^0=-\frac{2\mathrm{i}A_{120}k_1^3k_2^2}{k^6\pi}\mathbf{1}_1+\frac{2\mathrm{i}A_{120}k_1^2k_2\left(k^2-k_2^2\right)}{k^6\pi}\mathbf{1}_2-\frac{2\mathrm{i}A_{120}k_1^2k_2^2k_3}{k^6\pi}\mathbf{1}_3, \tag{5.20}$$
$$\boldsymbol{Q}^2=\boldsymbol{Q}^{2Re}+\mathrm{i}\boldsymbol{Q}^{2i}, \tag{5.21}$$
$$\boldsymbol{Q}^{-2}=-\boldsymbol{Q}^{2Re}+\mathrm{i}\boldsymbol{Q}^{2i}, \tag{5.22}$$

$$\boldsymbol{Q}^{2Re}=\left(\frac{k_2\left(-k^4A_{222}-2\omega_g k^2A_{122}\left(k^2-2k_1^2\right)+A_{112}k_1^2\left(-k^2+2k_1^2\right)\right)}{2k^6\pi}\right.$$
$$\left.+\frac{k_2\left(A_{222}\left(k^2+2k_1^2\right)k_2^2+A_{332}\left(k^2+2k_1^2\right)k_3^2\right)}{2k^6\pi}\right)\mathbf{1}_1$$

$$+\left(-\frac{k_1\left(k^2-2k_2^2\right)A_{112}k_1^2}{2k^6\pi}\right.$$
$$\left.-\frac{k_1\left(k^2-2k_2^2\right)\left(+A_{222}k_2^2+A_{332}k_3^2+k^2\left(-A_{222}+2A_{122}\omega_g\right)\right)}{2k^6\pi}\right)\mathbf{1}_2$$
$$+\frac{k_1k_2k_3\left(2\omega_gk^2A_{122}+A_{112}k_1^2+A_{222}k_2^2+A_{332}\left(-k^2+k_3^2\right)\right)}{k^6\pi}\mathbf{1}_3, \tag{5.23}$$

$$\boldsymbol{Q}^{2i} = \frac{k_1\left(-2A_{122}k_1^2k_2^2+k^2\left(A_{112}\left(-k^2+k_1^2\right)+A_{222}k_2^2+A_{332}k_3^2\right)\omega_g\right)}{k^6\pi}\mathbf{1}_1$$
$$+\frac{k_2\left(2A_{122}k_1^2\left(k^2-k_2^2\right)+k^2\left(A_{112}k_1^2+A_{222}\left(-k^2+k_2^2\right)+A_{332}k_3^2\right)\omega_g\right)}{k^6\pi}\mathbf{1}_2$$
$$+\frac{k_3\left(-2A_{122}k_1^2k_2^2+k^2\left(A_{112}k_1^2+A_{222}k_2^2+A_{332}\left(-k^2+k_3^2\right)\right)\omega_g\right)}{k^6\pi}\mathbf{1}_3. \tag{5.24}$$

We have written the Fourier modes in complex exponential form in (5.19) to simplify the analysis that follows. To reiterate, the general solution for $\hat{\boldsymbol{u}}^f$ would contain a forcing on the right-hand side of (5.19) that involves an infinite Fourier series. However, only the three terms corresponding to the values of β above (0, 2, −2) contribute to the change in the time period of rotation.

To obtain the solution of (5.19), $\hat{\boldsymbol{u}}^f$ is expanded as a complex exponential Fourier series, given by

$$\hat{\boldsymbol{u}}^f = \sum_{\beta\in\{0,2,-2\}}\hat{\boldsymbol{u}}^{f\beta}\mathrm{e}^{\mathrm{i}\beta\omega_gt}. \tag{5.25}$$

By substituting the expansion above into (5.19), the governing equations for each of the components of the Fourier transformed velocity field may be written as

$$\frac{\partial\hat{u}_1^{f\beta}}{\partial k_2}-(4\pi^2k^2+\mathrm{i}\omega_g\beta)\frac{\hat{u}_1^{f\beta}}{k_1}-\left(1-\frac{2k_1^2}{k^2}\right)\frac{\hat{u}_2^{f\beta}}{k_1}=-\frac{Q_1^\beta}{k_1}, \tag{5.26}$$
$$\frac{\partial\hat{u}_2^{f\beta}}{\partial k_2}-(4\pi^2k^2+\mathrm{i}\omega_g\beta)\frac{\hat{u}_2^{f\beta}}{k_1}+\left(\frac{2k_1k_2}{k^2}\right)\frac{\hat{u}_2^{f\beta}}{k_1}=-\frac{Q_2^\beta}{k_1}, \tag{5.27}$$
$$\frac{\partial\hat{u}_3^{f\beta}}{\partial k_2}-(4\pi^2k^2+\mathrm{i}\omega_g\beta)\frac{\hat{u}_3^{f\beta}}{k_1}+\left(\frac{2k_1k_3}{k^2}\right)\frac{\hat{u}_2^{f\beta}}{k_1}=-\frac{Q_3^\beta}{k_1}. \tag{5.28}$$

The equations above are similar to the ones seen for the spinning case in (4.8)–(4.10) except for an additional frequency-dependent term (involving ω_g) on the left-hand side and a frequency-dependent forcing amplitude on the right-hand side. Obtainment of the solution to (5.26)–(5.28) therefore proceeds in a manner similar to that of the spinning case, and the gradient component, being independent of the others, is solved first. The solution of (5.26)–(5.28) arising from the substitution of (5.25) corresponds to the neglect of an exponentially decaying transient, which governs the relaxation from a general initial condition, and a restriction to the long-time dynamics corresponding to the frequencies present in the applied forcing. The steady linear flow ensures that there is a one-to-one correspondence between the Fourier amplitudes of the forcing and the velocity field, with inertia determining the frequency-dependent phase lag between the two via the terms proportional to $\mathrm{i}\omega_g$ in (5.26)–(5.28). It should be noted again that $\sum_{\beta\in\{0,2,-2\}}\boldsymbol{Q}^\beta\mathrm{e}^{\mathrm{i}\beta\omega_gt}$ does not determine the complete outer velocity field, but the part that is relevant for the determination of ΔT^{tumb}.

Again, defining $k_2' = k_2 + k_1 s$, where s is a time-like variable, the solutions for the individual components $\hat{u}_2^{f\beta}$, $\hat{u}_1^{f\beta}$ and $\hat{u}_3^{f\beta}$ are written in terms of s as follows:

$$\hat{u}_2^{f\beta}(\boldsymbol{k}) = \int_0^\infty \exp\left(-4\pi^2\left(k^2 s + k_1 k_2 s^2 + \frac{k_1^2 s^3}{3}\right)\right)\left(\frac{k^2 + k_1^2 s^2 + 2k_1 k_2 s}{k^2}\right) \times \mathrm{e}^{-\mathrm{i}\omega_g \beta s} Q_2^\beta(k_1, k_2 + k_1 s, k_3)\,\mathrm{d}s, \tag{5.29}$$

$$\hat{u}_1^{f\beta}(\boldsymbol{k}) = \int_0^\infty \exp\left(-4\pi^2\left(k^2 s + k_1 k_2 s^2 + \frac{k_1^2 s^3}{3}\right)\right)\mathrm{e}^{-\mathrm{i}\omega_g \beta s} Q_1^\beta(k_1, k_2 + k_1 s, k_3)\,\mathrm{d}s - \int_0^\infty \mathrm{e}^{-\mathrm{i}\omega_g \beta s}\exp\left(-4\pi^2\left(k^2 s + k_1 k_2 s^2 + \frac{k_1^2 s^3}{3}\right)\right) \times \left(1 - \frac{2k_1^2}{\left(k^2 + k_1^2 s^2 + 2k_1 k_2 s\right)}\right)\hat{u}_2^{f\beta}(k_1, k_2 + k_1 s, k_3)\,\mathrm{d}s, \tag{5.30}$$

$$\hat{u}_3^{f\beta}(\boldsymbol{k}) = \int_0^\infty \exp\left(-4\pi^2\left(k^2 s + k_1 k_2 s^2 + \frac{k_1^2 s^3}{3}\right)\right)\mathrm{e}^{-\mathrm{i}\omega_g \beta s} Q_3^\beta(k_1, k_2 + k_1 s, k_3)\,\mathrm{d}s + \int_0^\infty \mathrm{e}^{-\mathrm{i}\omega_g \beta s}\exp\left(-4\pi^2\left(k^2 s + k_1 k_2 s^2 + \frac{k_1^2 s^3}{3}\right)\right) \times \left(\frac{2k_1 k_3}{k^2 + k_1^2 s^2 + 2k_1 k_2 s}\right)\hat{u}_2^{f\beta}(k_1, k_2 + k_1 s, k_3)\,\mathrm{d}s. \tag{5.31}$$

The solutions for $\hat{u}_1^{f\beta}$ and $\hat{u}_3^{f\beta}$ are coupled with $\hat{u}_2^{f\beta}$, as expected, and are given as a sum of a one-dimensional and a two-dimensional integral, with the latter integral arising from the coupling with $\hat{u}_2^{f\beta}$. The contributions in (5.29)–(5.31), for the different β terms, are substituted in (5.25) to obtain the components of $\hat{\boldsymbol{u}}^f$ in the space-fixed coordinate system, and are given by

$$\hat{u}_2^f(\boldsymbol{k}) = \hat{u}_2^{f0}(k_1, k_2, k_3) + \hat{u}_2^{ft}(k_1, k_2, k_3, t), \tag{5.32}$$

$$\hat{u}_1^f(\boldsymbol{k}) = \hat{u}_1^{f0}(k_1, k_2, k_3) + \hat{u}_1^{ft}(k_1, k_2, k_3, t), \tag{5.33}$$

$$\hat{u}_3^f(\boldsymbol{k}) = \hat{u}_3^{f0}(k_1, k_2, k_3) + \hat{u}_3^{ft}(k_1, k_2, k_3, t), \tag{5.34}$$

where we have written the components as a sum of a time-independent term (superscript '$f0$') and time-dependent term (superscript 'ft'). Denoting the convected wavevector, $k_1\mathbf{1}_1 + (k_2 + k_1 s)\mathbf{1}_2 + k_3\mathbf{1}_3$, as $\boldsymbol{k}'$ and $k' = |\boldsymbol{k}'|$, the time-dependent and time-independent contributions in (5.32)–(5.34) may be conveniently expressed in the form

$$\hat{u}_2^{f0}(\boldsymbol{k}) = \int_0^\infty \exp\left(-4\pi^2\left(k^2 s + k_1 k_2 s^2 + \frac{k_1^2 s^3}{3}\right)\right)\left(\frac{k^2 + k_1^2 s^2 + 2k_1 k_2 s}{k^2}\right) Q_2^0(\boldsymbol{k}')\,\mathrm{d}s, \tag{5.35}$$

$$\hat{u}_2^{ft}(\boldsymbol{k}, t) = \int_0^\infty \mathrm{i}2\exp\left(-4\pi^2\left(k^2 s + k_1 k_2 s^2 + \frac{k_1^2 s^3}{3}\right)\right)\left(\frac{k^2 + k_1^2 s^2 + 2k_1 k_2 s}{k^2}\right) \times \left(\left(Q_2^{2i}(\boldsymbol{k}')\cos(2\omega_g s) - Q_2^{2Re}(\boldsymbol{k}')\sin(2\omega_g s)\right)\cos(2\omega_g t) + \left(Q_2^{2Re}(\boldsymbol{k}')\cos(2\omega_g s) + Q_2^{2i}(\boldsymbol{k}')\sin(2\omega_g s)\right)\sin(2\omega_g t)\right)\mathrm{d}s \tag{5.36}$$

$$= \hat{u}_2^{ftcos}(\boldsymbol{k}, t)\cos(2\omega_g t) + \hat{u}_2^{ftsin}(\boldsymbol{k}, t)\sin(2\omega_g t), \tag{5.37}$$

$$\hat{u}_1^{f0}(\boldsymbol{k}) = \int_0^\infty \exp\left(-4\pi^2\left(k^2 s + k_1 k_2 s^2 + \frac{k_1^2 s^3}{3}\right)\right)\left(Q_1^0(\boldsymbol{k}') - \left(1 - \frac{2k_1^2}{k'^2}\right)\hat{u}_2^{f0}(\boldsymbol{k}')\right) \mathrm{d}s, \tag{5.38}$$

$$\begin{aligned}\hat{u}_1^{ft}(\boldsymbol{k}) \;=\; & \int_0^\infty \mathrm{i}2 \exp\left(-4\pi^2\left(k^2 s + k_1 k_2 s^2 + \frac{k_1^2 s^3}{3}\right)\right) \\ & \times \left(\left(Q_1^{2i}(\boldsymbol{k}')\cos(2\omega_g s) - Q_1^{2Re}(\boldsymbol{k}')\sin(2\omega_g s)\right)\cos(2\omega_g t)\right. \\ & \left. + \left(Q_1^{2Re}(\boldsymbol{k}')\cos(2\omega_g s) + Q_1^{2i}(\boldsymbol{k}')\sin(2\omega_g s)\right)\sin(2\omega_g t)\right) \mathrm{d}s \\ & - \int_0^\infty \exp\left(-4\pi^2\left(k^2 s + k_1 k_2 s^2 + \frac{k_1^2 s^3}{3}\right)\right)\left(1 - \frac{2k_1^2}{k'^2}\right)\hat{u}_2^{ft}(\boldsymbol{k}', t)\,\mathrm{d}s\end{aligned} \tag{5.39}$$

$$= \hat{u}_1^{ftcos}(\boldsymbol{k}, t)\cos(2\omega_g t) + \hat{u}_1^{ftsin}(\boldsymbol{k}, t)\sin(2\omega_g t), \tag{5.40}$$

$$\hat{u}_3^{f0}(\boldsymbol{k}) = \int_0^\infty \exp\left(-4\pi^2\left(k^2 s + k_1 k_2 s^2 + \frac{k_1^2 s^3}{3}\right)\right)\left(Q_3^0(\boldsymbol{k}') + \frac{2k_1 k_3}{k'^2}\hat{u}_2^{f0}(\boldsymbol{k}')\right) \mathrm{d}s, \tag{5.41}$$

$$\begin{aligned}\hat{u}_3^{ft}(\boldsymbol{k}, t) \;=\; & \int_0^\infty \mathrm{i}2 \exp\left(-4\pi^2\left(k^2 s + k_1 k_2 s^2 + \frac{k_1^2 s^3}{3}\right)\right) \\ & \times \left(\left(Q_3^{2i}(\boldsymbol{k}')\cos(2\omega_g s) - Q_3^{2Re}(\boldsymbol{k}')\sin(2\omega_g s)\right)\cos(2\omega_g t)\right. \\ & \left. + \left(Q_3^{2Re}(\boldsymbol{k}')\cos(2\omega_g s) + Q_3^{2i}(\boldsymbol{k}')\sin(2\omega_g s)\right)\sin(2\omega_g t)\right) \mathrm{d}s \\ & + \int_0^\infty \exp\left(-4\pi^2\left(k^2 s + k_1 k_2 s^2 + \frac{k_1^2 s^3}{3}\right)\right)\left(\frac{2k_1 k_3}{k'^2}\right)\hat{u}_2^{ft}(\boldsymbol{k}', t)\,\mathrm{d}s\end{aligned} \tag{5.42}$$

$$= \hat{u}_3^{ftcos}(\boldsymbol{k}, t)\cos(2\omega_g t) + \hat{u}_3^{ftsin}(\boldsymbol{k}, t)\sin(2\omega_g t), \tag{5.43}$$

where the terms Q_j^{2Re}, Q_j^{2i} are given in (5.23)–(5.24), with 'j' denoting the component along the 1, 2 and 3 directions. The coefficients of $\cos(2\omega_g t)$ and $\sin(2\omega_g t)$ in (5.36) and (5.42) are denoted by $\hat{u}^{ftcos}$ and $\hat{u}^{ftsin}$. The flow and vorticity components are coupled to the gradient component through $\hat{u}_2^{ft}(\boldsymbol{k}', t)$ and $\hat{u}_2^{f0}(\boldsymbol{k}')$, which are given by

$$\begin{aligned}\hat{u}_2^{ft}(\boldsymbol{k}', t) \;=\; & \int_0^\infty \mathrm{i}2 \exp\left(-4\pi^2\left(k'^2 s' + k_1 k_2' s'^2 + \frac{k_1^2 s'^3}{3}\right)\right)\left(\frac{k'^2 + k_1^2 s'^2 + 2k_1 k_2' s'}{k'^2}\right) \\ & \times \left(\left(Q_2^{2i}(\boldsymbol{k}'')\cos(2\omega_g(s+s')) - Q_2^{2Re}(\boldsymbol{k}'')\sin(2\omega_g(s+s'))\right)\cos(2\omega_g t)\right. \\ & \left. + \left(Q_2^{2Re}(\boldsymbol{k}'')\cos(2\omega_g(s+s')) + Q_2^{2i}(\boldsymbol{k}'')\sin(2\omega_g(s+s'))\right)\sin(2\omega_g t)\right) \mathrm{d}s'\end{aligned} \tag{5.44}$$

and

$$\hat{u}_2^{f0}(\boldsymbol{k}') = \int_0^\infty \exp\left(-4\pi^2\left(k'^2 s' + k_1 k_2' s'^2 + \frac{k_1^2 s'^3}{3}\right)\right)\left(\frac{k'^2 + k_1^2 s^2 + 2k_1 k_2' s}{k'^2}\right) Q_2^0(\boldsymbol{k}'')\,\mathrm{d}s \tag{5.45}$$

respectively. As defined in § 4, the primed variables in (5.44) and (5.45) are given as $\boldsymbol{k}'' = k_1\mathbf{1}_1 + (k_2 + k_1(s+s'))\mathbf{1}_2 + k_3\mathbf{1}_3$, $k_2' = k_2 + k_1 s$ and $k'' = |\boldsymbol{k}''|$. The coefficients of $\cos(2\omega_g t)$ and $\sin(2\omega_g t)$ in the time-dependent terms are defined as $\hat{u}_i^{ftcos}(\boldsymbol{k}, t)$ and $\hat{u}_i^{ftsin}(\boldsymbol{k}, t)$ respectively. The components along the flow and vorticity directions given in (5.38)–(5.43) are therefore sums of a one-dimensional integral and a two-dimensional

integral. The two-dimensional integrals in (5.38)–(5.43) are coupled with the velocity in the gradient direction and are given by (5.44) and (5.45).

5.4. *Evaluation of integrals*

The integral for the tumbling time period given in (5.3) is evaluated in this section. The inertial terms given in (5.14) along with the term involving the singularity in the test problem in (5.4) are substituted in (5.3) to obtain the final form of the integral as

$$\begin{aligned}\Delta T^{tumb} \;=\; & \frac{Re^{3/2}}{8\pi Y_c} \\ & \times \int\int_0^{T_{jeff}} [-4\pi^2 k^2(\hat{u}_1^f \mathbf{1}_1 + \hat{u}_2^f \mathbf{1}_2 + \hat{u}_3^f \mathbf{1}_3) + \boldsymbol{R}_1 + \boldsymbol{R}_2 \cos(2\omega_g t) + \boldsymbol{R}_3 \sin(2\omega_g t)] \\ & \cdot \left(\boldsymbol{T}_1^{tumb} + \boldsymbol{T}_2^{tumb} \cos(2\omega_g t) + \boldsymbol{T}_3^{tumb} \sin(2\omega_g t)\right) \mathrm{d}t\, \mathrm{d}\boldsymbol{k}, \end{aligned} \tag{5.46}$$

where the components of $\hat{\boldsymbol{u}}^f$ are given in (5.32)–(5.34). The integration over time in (5.46) is straightforward, and leads to

$$\begin{aligned}\Delta T^{tumb} \;=\; & \frac{Re^{3/2}}{8\pi Y_C} \int \left[\frac{2\pi}{\omega_g} \boldsymbol{T}_1^{tumb} \cdot (\boldsymbol{R}_1 - 4\pi^2 k^2 (\hat{u}_1^{f0} \mathbf{1}_1 + \hat{u}_2^{f0} \mathbf{1}_2 + \hat{u}_3^{f0} \mathbf{1}_3)) \right. \\ & + \frac{\pi}{\omega_g} \boldsymbol{T}_2^{tumb} \cdot (\boldsymbol{R}_2 - 4\pi^2 k^2 (\hat{u}_1^{ftcos} \mathbf{1}_1 + \hat{u}_2^{ftcos} \mathbf{1}_2 + \hat{u}_3^{ftcos} \mathbf{1}_3)) \\ & \left. + \frac{\pi}{\omega_g} \boldsymbol{T}_3^{tumb} \cdot (\boldsymbol{R}_3 - 4\pi^2 k^2 (\hat{u}_1^{ftsin} \mathbf{1}_1 + \hat{u}_2^{ftsin} \mathbf{1}_2 + \hat{u}_3^{ftsin} \mathbf{1}_3)) \right] \mathrm{d}\boldsymbol{k}. \end{aligned} \tag{5.47}$$

The expressions for $\hat{u}^{fi}$ ($i =$ '0','cos','sin') are given in (5.35)–(5.43). Each of the terms proportional to $\hat{u}_1^{fi}$ and $\hat{u}_3^{fi}$ ($i =$ '0','cos','sin') in (5.47) is a sum of four-dimensional and five-dimensional integrals. The terms proportional to $\hat{u}_2^{fi}$ are four-dimensional integrals and the terms proportional to $\boldsymbol{R}_1$, $\boldsymbol{R}_2$ and $\boldsymbol{R}_3$ involve three-dimensional integrals. The numerical evaluation of the integrals proceeds in a manner similar to that of the spinning case in § 4. In a spherical coordinate system, the three-dimensional and four-dimensional integrals involved in (5.47) are again seen to be divergent (after a k integration), with the combination of the integrals nevertheless being convergent, as explained in § 4. These integrals are evaluated numerically to obtain the time period.

To illustrate the aforementioned simplification of (5.47) to an equation involving convergent integrals alone, we focus on the evaluation of the integrals proportional to $\hat{u}_1^{f0}$, $\boldsymbol{R}_1$, $\boldsymbol{R}_2$ and $\boldsymbol{R}_3$. The simplification of the other terms in the integral follows the same method as presented below. We present the final simplified form of the integrals for the other terms in appendix A. We write the four-dimensional and five-dimensional integrals for the term proportional to $\hat{u}_1^{f0}$ as follows:

$$\begin{aligned} & \int (-4\pi^2 k^2\, \hat{u}_1^{f0}(\boldsymbol{k})\, \mathbf{1}_1 \cdot \boldsymbol{T}_1^{tumb})\, \mathrm{d}\boldsymbol{k} \\ & \quad = -\int 4\pi^2 k^2 \left[-\frac{(\kappa^2+1)^2}{2\kappa^2} \frac{\mathrm{i}B_3 k_2}{2k^2\pi} + \frac{\mathrm{i}B_1 (k^2 - 2k_1^2) k_2}{2k^4\pi} \frac{(1-\kappa^4)}{2\kappa^2} \right] \\ & \qquad \times \int_0^\infty \exp\left(-4\pi^2 \left(k^2 s + k_1 k_2 s^2 + \frac{k_1^2 s^3}{3} \right) \right) Q_1^0(\boldsymbol{k}')\, \mathrm{d}s\, \mathrm{d}\boldsymbol{k} \end{aligned}$$

$$+\int 4\pi^2 k^2\left[-\frac{(\kappa^2+1)^2}{2\kappa^2}\frac{\mathrm{i}B_3 k_2}{2k^2\pi}+\frac{\mathrm{i}B_1(k^2-2k_1^2)k_2}{2k^4\pi}\frac{(1-\kappa^4)}{2\kappa^2}\right]$$
$$\times\int_0^\infty \exp\left(-4\pi^2\left(k^2 s+k_1k_2s^2+\frac{k_1^2s^3}{3}\right)\right)\left(1-\frac{2k_1^2}{k'^2}\right)$$
$$\times\int_0^\infty \exp\left(-4\pi^2\left(k'^2 s'+k_1k_2's'^2+\frac{k_1^2s'^3}{3}\right)\right)\left(\frac{k'^2+k_1^2s'^2+2k_1k_2's'}{k'^2}\right)$$
$$\times Q_2^0(\boldsymbol{k}'')\,\mathrm{d}s'\,\mathrm{d}s\,\mathrm{d}\boldsymbol{k}. \tag{5.48}$$

The first and second integrals on the right-hand side are respectively four-dimensional and five-dimensional integrals. The five-dimensional integral arises due to the coupling with the velocity component in the gradient direction. When writing the five-dimensional integral, we have used the definition of $\hat{u}_2^{f0}$ in (5.45) and substituted in (5.38). The term in the square brackets in (5.47) corresponds to the $\mathbf{1}_1$ component of $\boldsymbol{T}_1^{tumb}$ and is obtained from (5.4). The integrals in (5.47) can be expressed in a spherical coordinate system with $k_1 = k\sin\theta\cos\phi$, $k_2 = k\sin\theta\sin\phi$, $k_3 = k\cos\theta$ and $\mathrm{d}\boldsymbol{k} = k^2\sin\theta\,\mathrm{d}k\,\mathrm{d}\theta\,\mathrm{d}\phi$. Rewriting (5.48) to isolate the k integral in the spherical coordinate system (again, for brevity, we have retained the notation k_1, k_2 and k_3), one obtains

$$\int(-4\pi^2k^2\,\hat{u}_1^{f0}(\boldsymbol{k})\,\mathbf{1}_1\cdot\boldsymbol{T}_1^{tumb})\,\mathrm{d}\boldsymbol{k}$$
$$=-\int_0^{2\pi}\int_0^{\pi}\int_0^{\infty}4\pi^2\left\{k^2Q_1^0(\boldsymbol{k}')\left[-\frac{(\kappa^2+1)^2}{2\kappa^2}\frac{\mathrm{i}B_3k_2}{2k^2\pi}\right.\right.$$
$$\left.\left.+\frac{\mathrm{i}B_1(k^2-2k_1^2)k_2}{2k^4\pi}\frac{(1-\kappa^4)}{2\kappa^2}\right]\right\}$$
$$\times\int_0^\infty k^2\exp\left(-4\pi^2\left(k^2s+k_1k_2s^2+\frac{k_1^2s^3}{3}\right)\right)\mathrm{d}k\,\mathrm{d}s\,\sin\theta\,\mathrm{d}\theta\,\mathrm{d}\phi$$
$$+\int_0^{2\pi}\int_0^{\pi}\int_0^{\infty}\int_0^{\infty}\left\{4\pi^2k^2\left[-\frac{(\kappa^2+1)^2}{2\kappa^2}\frac{\mathrm{i}B_3k_2}{2k^2\pi}+\frac{\mathrm{i}B_1(k^2-2k_1^2)k_2}{2k^4\pi}\frac{(1-\kappa^4)}{2\kappa^2}\right]\right.$$
$$\times\left(1-\frac{2k_1^2}{k'^2}\right)Q_2^0(\boldsymbol{k}'')\left(\frac{k'^2+k_1^2s'^2+2k_1k_2's'}{k'^2}\right)\Bigg\}$$
$$\times\int_0^\infty\exp\left(-4\pi^2\left(k^2s+k_1k_2s^2+\frac{k_1^2s^3}{3}\right)\right)$$
$$\times\exp\left(-4\pi^2\left(k'^2s'+k_1k_2's'^2+\frac{k_1^2s'^3}{3}\right)\right)k^2\,\mathrm{d}k\,\mathrm{d}s'\,\mathrm{d}s\,\sin\theta\,\mathrm{d}\theta\,\mathrm{d}\phi, \tag{5.49}$$

where the term in the braces is independent of k because Q_1^0 (the '1' component of $\boldsymbol{Q}^0$, see (5.20)) and the term in the square brackets above are proportional to $1/k$. The k integrals above are evaluated for the four-dimensional case, given by

$$\int_0^\infty k^2\exp\left(-4\pi^2\left(k^2s+k_1k_2s^2+\frac{k_1^2s^3}{3}\right)\right)\mathrm{d}k$$
$$=\int_0^\infty k^2\exp\left(-4\pi^2k^2\left(s+\sin^2\theta\cos\phi\sin\phi s^2+\frac{\sin^2\theta\cos^2\phi s^3}{3}\right)\right)\mathrm{d}k$$
$$=\frac{1}{32\pi^{5/2}(s+\sin^2\theta\cos\phi\sin\phi s^2+\sin^2\theta\cos^2\phi s^3/3)^{3/2}}, \tag{5.50}$$

and the five-dimensional case, given by

$$\begin{aligned}
&\int_0^\infty k^2 \exp\left(-4\pi^2\left(k^2 s + k_1 k_2 s^2 + \frac{k_1^2 s^3}{3}\right)\right) \exp\left(-4\pi^2\left(k'^2 s' + k_1 k_2' s'^2 + \frac{k_1^2 s'^3}{3}\right)\right) \mathrm{d}k \\
&\quad = \int k^2 \exp\left(-4\pi^2 k^2\left(s + \sin^2\theta\cos\phi\sin\phi s^2 + \frac{\sin^2\theta\cos^2\phi s^3}{3}\right)\right) \\
&\qquad \times \exp\left(-4k^2\pi^2\frac{sp}{3}\left(3(4 + s^2 - s^2\cos 2\theta + 2s\sin^2\theta(s\cos 2\phi + 2\sin 2\phi))\right.\right. \\
&\qquad \left.\left. + 4\cos\phi\sin^2\theta s'(3\sin\phi + \cos\phi(3s + s'))\right)\right) \mathrm{d}k \\
&\quad = \frac{1}{32\pi^{5/2}(f^{exp}(s, s', \theta, \phi))^{3/2}},
\end{aligned} \tag{5.51}$$

where f^{exp} is the function that multiplies $-4\pi^2k^2$ in the exponent of the integrand. The result of the k integration for the four-dimensional integral is proportional to $1/s^{3/2}$ and therefore diverges in the limit of $s \to 0$. The sum of all of the four-dimensional divergent integrals in the expressions of terms proportional to $\hat{u}_2^{f0}$, $\hat{u}_2^{f0}$, $\hat{u}_j^{fi}$ ($j = 1, 2$ and 3 and i = 't cos','t sin'), given in appendix (A 1)–(A 9), as well as the one in (5.49) for $\hat{u}_1^{f0}$, and the three-dimensional integral presented below in (5.52), is however convergent. The reason for the divergence has already been explained in § 4. It should be noted that the k integrals in (A 1)–(A 9) are identical to that of (5.49).

The three-dimensional integral proportional to $\boldsymbol{R}_1$, $\boldsymbol{R}_2$ and $\boldsymbol{R}_3$ in (5.48) is

$$\int \left[\frac{2\pi}{\omega_g}\boldsymbol{T}_1^{tumb} \cdot (\boldsymbol{R}_1) + \frac{\pi}{\omega_g}\boldsymbol{T}_2^{tumb} \cdot \boldsymbol{R}_2 + \frac{\pi}{\omega_g}\boldsymbol{T}_3^{tumb} \cdot \boldsymbol{R}_3\right] \mathrm{d}\boldsymbol{k}. \tag{5.52}$$

The terms $\boldsymbol{R}_1$, $\boldsymbol{R}_2$, $\boldsymbol{R}_3$, $\boldsymbol{T}_1^{tumb}$, $\boldsymbol{T}_2^{tumb}$ and $\boldsymbol{T}_3^{tumb}$ (see (5.15)–(5.17) and (5.4)–(5.7)) are proportional to $(1/k)$, and $\mathrm{d}\boldsymbol{k}$ is proportional to $k^2\,\mathrm{d}k$ in (5.52), making the k integral divergent as $k \to \infty$. The divergence here can again be isolated by introducing an integral over a dummy variable s. Noting that $\int_0^\infty 4\pi^2k^2\exp(-4\pi^2k^2s) = 1$, the integrals proportional to $\boldsymbol{R}_1$, $\boldsymbol{R}_2$ and $\boldsymbol{R}_3$ are written as

$$\begin{aligned}
&4\pi^2\int_0^{2\pi}\int_0^{\pi}\int_0^{\infty}\int_0^{\infty}\left[\frac{2\pi}{\omega_g}\boldsymbol{T}_1^{tumb} \cdot \boldsymbol{R}_1 + \frac{\pi}{\omega_g}\boldsymbol{T}_2^{tumb} \cdot \boldsymbol{R}_2 + \frac{\pi}{\omega_g}\boldsymbol{T}_3^{tumb} \cdot \boldsymbol{R}_3\right] \\
&\qquad \times k^2 \mathrm{e}^{-4\pi^2k^2s}\,\mathrm{d}s k^2\,\mathrm{d}k\sin\theta\,\mathrm{d}\theta\,\mathrm{d}\phi,
\end{aligned} \tag{5.53}$$

where we have added an additional integral over s. The k integral can be readily evaluated, and (5.53) becomes

$$\begin{aligned}
&4\pi^2\int_0^{2\pi}\int_0^{\pi}\int_0^{\infty}\left\{\left[\frac{2\pi}{\omega_g}\boldsymbol{T}_1^{tumb} \cdot \boldsymbol{R}_1 + \frac{\pi}{\omega_g}\boldsymbol{T}_2^{tumb} \cdot \boldsymbol{R}_2 + \frac{\pi}{\omega_g}\boldsymbol{T}_3^{tumb} \cdot \boldsymbol{R}_3\right] k^2\right\} \\
&\qquad \times \frac{1}{32\pi^{5/2}s^{3/2}}\,\mathrm{d}s\sin\theta\,\mathrm{d}\theta\,\mathrm{d}\phi,
\end{aligned} \tag{5.54}$$

where the term in the braces above is independent of k.

In (5.49) and (A 1)–(A 9), the results of the k integration from (5.50) and (5.51) are substituted, and they are combined with (5.54), to obtain the final integral for the time period. The final integral is evaluated numerically using Gaussian quadrature. The numerical integration has to be carried out for each of the aspect ratios. This is unlike the spinning case, where the aspect-ratio-dependent term factored out from the integral (see (4.24)). However, in the limit of extreme aspect ratios ($\kappa \to 0$ for an oblate spheroid and $\kappa \to \infty$ for a prolate spheroid), one can again pull out the aspect-ratio dependence and obtain the appropriate limiting forms. This is discussed in § 5.5. The correction to the tumbling period obtained from the numerical integration is presented in § 6.

5.5. *Extreme-aspect-ratio analysis*

In this section, we evaluate the scaling of the $O(Re^{3/2})$ inertial correction to the time period for spheroids with extreme aspect ratios ($\kappa \ll 1$ or $\kappa \gg 1$) rotating in the tumbling orbit. At $Re = 0$, an oblate (prolate) spends a time of $O(1/\kappa)$ ($O(\kappa)$) in the nearly aligned phase, and a time of $O(1)$ in the non-aligned phase (flipping between nearly aligned orientations). The nearly aligned phase for a thin prolate spheroid (slender fibre) corresponds to $\boldsymbol{p}$ being close to the flow axis ($\phi_j \sim O(1/\kappa)$, $\pi + O(1/\kappa)$), while that for a thin oblate spheroid (flat disk) corresponds to $\boldsymbol{p}$ being close to the gradient axis ($\phi_j - \pi/2$ and $\phi_j + \pi/2 \sim O(\kappa)$). In both cases, the Jeffery angular velocity is asymptotically small, of $O(\kappa^2)$ ($O(1/\kappa^2)$) for the oblate (prolate) case. Thus, one would expect inertia to primarily alter the time period during the nearly aligned phase. As mentioned in the introduction, for extreme aspect ratios, the $O(Re)$ correction can balance the slow Stokesian rotation in the aligned phase, leading to a threshold Re beyond which the spheroid is stationary. For a fixed Re, this places a natural restriction on the $O(Re^{3/2})$ analysis for extreme aspect ratios. The relevant aspect-ratio bounds arising from the scalings obtained here are given in § 8.

The integral in (5.3), when expressed in terms of ϕ_j, takes the form

$$\begin{aligned}\Delta T^{tumb} &= -Re^{3/2}\int_{\pi}^{-\pi}\frac{\dot{\phi}_{c2}}{\dot{\phi}^2_{jeff}}\,\mathrm{d}\phi_j \\ &= \int_{\pi}^{-\pi}\frac{1}{8\pi Y_c}\int\left[4\pi^2k^2\hat{\boldsymbol{u}}^f + \frac{\partial\hat{\boldsymbol{u}}^{match}}{\partial t} - (\boldsymbol{\Gamma}^{\dagger}\cdot\boldsymbol{k})\cdot\boldsymbol{\nabla}_{\boldsymbol{k}}\hat{\boldsymbol{u}}^{match}\right. \\ &\quad \left. + \boldsymbol{\Gamma}\cdot\hat{\boldsymbol{u}}^{match}\right]\cdot\left\{\frac{\mathrm{i}(\boldsymbol{S}^{(2t)}\cdot\boldsymbol{k})\cdot\boldsymbol{1}_3}{2\pi k^2}\cdot\left(\boldsymbol{I} - \frac{\boldsymbol{k}\boldsymbol{k}}{k^2}\right)\right\}\frac{1}{\dot{\phi}^2_{jeff}}\,\mathrm{d}\boldsymbol{k}\,\mathrm{d}\phi_j. \end{aligned} \tag{5.55}$$

The dominant contribution arising from the aligned phase may be seen by considering a flat disk with $\kappa = 0$ (a slender fibre with $\kappa = \infty$); it is sufficient to focus on one of the aligned phases, since the contribution of the other phase is identical from symmetry considerations. The angular velocity of a nearly aligned disk (slender fibre) is $O((\pi/2 - \phi_j)^2)$ ($O(\phi_j^2)$). The term in braces in (5.55) is proportional to $\boldsymbol{T}_1 + \boldsymbol{T}_2\cos(2\phi_j) + \boldsymbol{T}_3\sin(2\phi_j)$, with the $\boldsymbol{T}_i$ terms given in (5.5)–(5.7), and therefore reduces to $\boldsymbol{T}_1 + \boldsymbol{T}_2$ and $\boldsymbol{T}_1 - \boldsymbol{T}_2$ respectively, for a slender fibre and a flat disk. In the slender-fibre limit, $\boldsymbol{T}_1$ and $\boldsymbol{T}_2$ scale as $1/\log\kappa$, and in the flat-disk limit, they are constants of order unity. Noting that the velocity field $\hat{\boldsymbol{u}}^f$ is driven by $\hat{\boldsymbol{u}}^{match}$, it can be seen that the term in square brackets in (5.55) is proportional to $\hat{\boldsymbol{u}}^{match}$, which in

the flat-disk limit is proportional to $A_2/2(\mathbf{1}_1\mathbf{1}_2+\mathbf{1}_2\mathbf{1}_1)+(A_1+A_3)(\phi_j-\pi/2)/2\,\mathbf{1}_1\mathbf{1}_1-A_1(\phi_j-\pi/2)\mathbf{1}_2\mathbf{1}_2+(A_1-A_3)(\phi_j-\pi/2)/2\,\mathbf{1}_3\mathbf{1}_3$. In the slender-fibre limit, the term is proportional to $A_1\phi_j\,\mathbf{1}_1\mathbf{1}_1-A_1\phi_j/(2)\,(\mathbf{1}_2\mathbf{1}_2+\mathbf{1}_3\mathbf{1}_3)$; see (2.16)–(2.18) for the definition of the constants A_i. It should be recalled that for a slender fibre, A_1 scales as $1/\log\kappa$, and both A_2 and A_3 scale as $1/\kappa^2$. For a flat disk, A_2 scales as κ, whereas A_1 and A_3 are constants. The integral in (5.55) therefore diverges as $O(\kappa/(\phi_j-\pi/2)^3)$ for a flat disk and as $O(1/(\phi_j^2\log\kappa))$ for a slender fibre. This clearly implies that the contribution comes from the nearly aligned phases in the two cases. The divergence is cut off for ϕ_j of $O(\pi/2-\kappa)$ for a flat disk and ϕ_j of $O(1/\kappa)$ for a slender fibre, leading to inertial time period estimates of $O(1/\kappa^2)$ and $O(\kappa^2/\log\kappa)$ in the two cases.

Having estimated the scalings of the time period, we proceed to calculate the numerical prefactor, which requires evaluation of the integral using a rescaled angular coordinate that remains $O(1)$ in the nearly aligned phase. For the flat disk, this boundary layer variable is given by $\hat{\phi}=(-\pi/2+\phi_j)/\kappa$. In terms of $\hat{\phi}$, one may rewrite (5.55) in the boundary layer variable as

$$\Delta T^{tumb} = \int_{\infty}^{-\infty}\frac{1}{8\pi Y_c}\int\left[4\pi^2k^2\hat{\boldsymbol{u}}^f+\frac{\partial\hat{\boldsymbol{u}}^{match}}{\partial t}-(\boldsymbol{\Gamma}^{\dagger}\cdot\boldsymbol{k})\cdot\nabla_{\boldsymbol{k}}\hat{\boldsymbol{u}}^{match}+\boldsymbol{\Gamma}\cdot\hat{\boldsymbol{u}}^{match}\right]$$
$$\cdot\left\{\frac{\mathrm{i}(\boldsymbol{S}^{(2t)}\cdot\boldsymbol{k})\cdot\mathbf{1}_3}{2\pi k^2}\cdot\left(\boldsymbol{I}-\frac{\boldsymbol{kk}}{k^2}\right)\right\}\frac{1}{\kappa^3(\hat{\phi}^2+1)^2}\,\mathrm{d}\boldsymbol{k}\,\mathrm{d}\hat{\phi}. \tag{5.56}$$

At the leading order in κ, the term within braces in (5.56) becomes

$$\left\{\frac{\mathrm{i}(\boldsymbol{S}^{(2t)}\cdot\boldsymbol{k})\cdot\mathbf{1}_3}{2\pi k^2}\cdot\left(\boldsymbol{I}-\frac{\boldsymbol{kk}}{k^2}\right)\right\}=\boldsymbol{T}_1-\boldsymbol{T}_2, \tag{5.57}$$

where $\boldsymbol{T}_1$ and $\boldsymbol{T}_2$ are defined in (5.5)–(5.6), with $B_1=B_3=-16/3$ in the flat-disk limit. The term proportional to the singularity in the test problem is therefore independent of κ. The leading-order term in $\hat{\boldsymbol{u}}^{match}$ takes the form

$$\hat{\boldsymbol{u}}^{match}=-\frac{\mathrm{i}\left(k^2-2k_1{}^2\right)A_2k_2}{4k^4\pi}\mathbf{1}_1-\frac{\mathrm{i}k_1A_2\left(k^2-2k_2^2\right)}{4k^4\pi}\mathbf{1}_2+\frac{\mathrm{i}k_1A_2k_2k_3}{2k^4\pi}\mathbf{1}_3. \tag{5.58}$$

It should be recalled that A_2 is the coefficient of the longitudinal extension and is equal to $-8\pi\kappa/3$ in the flat-disk limit (see below (5.13)). The inertial term in the square brackets in (5.56) is therefore proportional to κ. Although the contribution from the inertial terms involving the singularities in the axisymmetric extension and transverse extensions, proportional to A_1 and A_3, comes at $O(\kappa)$, this contribution is also proportional to the boundary layer variable $\hat{\phi}$, and the integration over $\hat{\phi}$ in (5.56) is zero for this contribution. The evaluation of the integral in (5.56) leads to

$$\Delta T^{tumb}=Re^{3/2}0.1763/\kappa^2 \tag{5.59}$$

for a flat disk.

The estimation of the correction for the slender-fibre case is slightly non-trivial. If one proceeds in a manner similar to that for the flat disk given above, one can see that the scaling of the leading-order term in (5.55), when expressed in the boundary layer variable ($\hat{\phi}=\phi/\kappa$), is $\kappa^2/\log\kappa$. It should be noted that the scaling of $1/\log\kappa$ arises because the axisymmetric extensional flow with $A_1\propto 1/\log\kappa$ is dominant in the slender-fibre limit (Subramanian & Koch 2005). It turns out, however, that the leading-order term is an odd function of the boundary layer variable ($\hat{\phi}$), and therefore the integral over $\hat{\phi}$ is zero. The correction should therefore come in at a smaller order ($\kappa/\log\kappa$).

6. Results: $O(Re^{3/2})$ correction for spheroids

In this section, we summarize the numerical results obtained using the analytical expressions derived in the previous two sections. The scaled correction to the tumbling time period is plotted against the eccentricity (e) for a prolate spheroid in figure 3(a). For a sphere ($e = 0$), the correction is 1.355, and it first decreases with increasing eccentricity (increasing aspect ratio) until an e of approximately 0.75, as shown in the inset plot, before eventually diverging in the slender-fibre limit. The correction normalized with the Jeffery period, which diverges as $O(\kappa)$ as $\kappa \to \infty$, is plotted against the eccentricity in figure 3(b). As is clear from the dip in the plot for large κ, the divergence of the inertial correction is slower than $O(\kappa)$ for $\kappa \to \infty$. To obtain the scaling for this divergence, we have plotted $\Delta T^{tumb} \log \kappa$ on a log–log scale in figure 3(c) together with a line of slope 1 (red) for purposes of comparison. The plot suggests a scaling of $O(\kappa/\log \kappa)$, consistent with the arguments at the end of § 5.5.

The correction to the time period is plotted against the eccentricity, for an oblate spheroid in the tumbling orbit, in figure 4(a). The correction starts again from that for the sphere ($e = 0$) and, to begin with, decreases slightly with increasing eccentricity (decreasing aspect ratio), as shown in the inset plot, before eventually diverging in the limit of a flat disk. The blue circles in figure 4(a) correspond to the aspect ratios for which the tumbling orbit is always unstable. The correction scaled with the Jeffery period (which diverges as $1/\kappa$ as $\kappa \to 0$) is plotted in figure 4(b), and, in contrast to the prolate case, continues to diverge in the limit $\kappa \to 0$. We have plotted the flat-disk asymptote (red) given by (5.59) as well as the numerical results on a log–log scale in figure 4(c); the asymptote compares well with the numerical results, and validates the predicted $O(\kappa^{-2})$ divergence. In figure 5, we have plotted the correction against the eccentricity for an oblate spheroid in its spinning orbit. Starting from the sphere value of 1.355, the scaled correction decreases with increasing eccentricity, approaching a finite value of 0.47 for the flat disk. This is unlike the case of a prolate spheroid in spinning mode, in which case the correction increases with increasing aspect ratio, eventually leading to a change in the scaling from $O(Re^{3/2})$ to $O(\tilde{Re})$, as is appropriate for a cylinder, where $\tilde{Re}$ is the Reynolds number based on the smallest axis of the spheroid (see § 4).

The $O(Re^{3/2})$ time period corrections for both the prolate and oblate spheroids have been found to be positive, implying an increase in the time period of rotation due to inertia in all relevant cases.

7. Evaluation of the $O(Re^{3/2})$ time period correction for triaxial ellipsoids

In this section, we calculate the inertial correction to the time period of rotation for a triaxial ellipsoid that is rotating in an orbit stabilized by weak inertia. In the Stokes limit, it is known that the orientation dynamics of a triaxial ellipsoid may range from quasiperiodic to chaotic, depending on the axis ratios and the initial orientation (Yarin *et al.* 1997). For $Re = 0$, the angular velocity of a triaxial ellipsoid rotating in a simple shear flow can be written as (Kim & Karrila 1991)

$$\boldsymbol{\Omega}_1 = \boldsymbol{\Omega}_\infty + \frac{1-\kappa_1^2}{1+\kappa_1^2}(\boldsymbol{E}:\boldsymbol{pq})(\boldsymbol{p}\times\boldsymbol{q}) + \frac{\kappa_2^2-1}{1+\kappa_2^2}(\boldsymbol{E}:\boldsymbol{pr})(\boldsymbol{r}\times\boldsymbol{p}) + \frac{\kappa_1^2-\kappa_2^2}{\kappa_1^2+\kappa_2^2}(\boldsymbol{E}:\boldsymbol{qr})(\boldsymbol{q}\times\boldsymbol{r}). \tag{7.1}$$

In (7.1), $\boldsymbol{p}$, $\boldsymbol{q}$ and $\boldsymbol{r}$ are respectively the unit vectors along the longest (of length $2a$), intermediate (of length $2b$) and shortest (of length $2c$) principal axes of the triaxial ellipsoid. Here, κ_1 and κ_2 are the axis ratios of the triaxial ellipsoid,

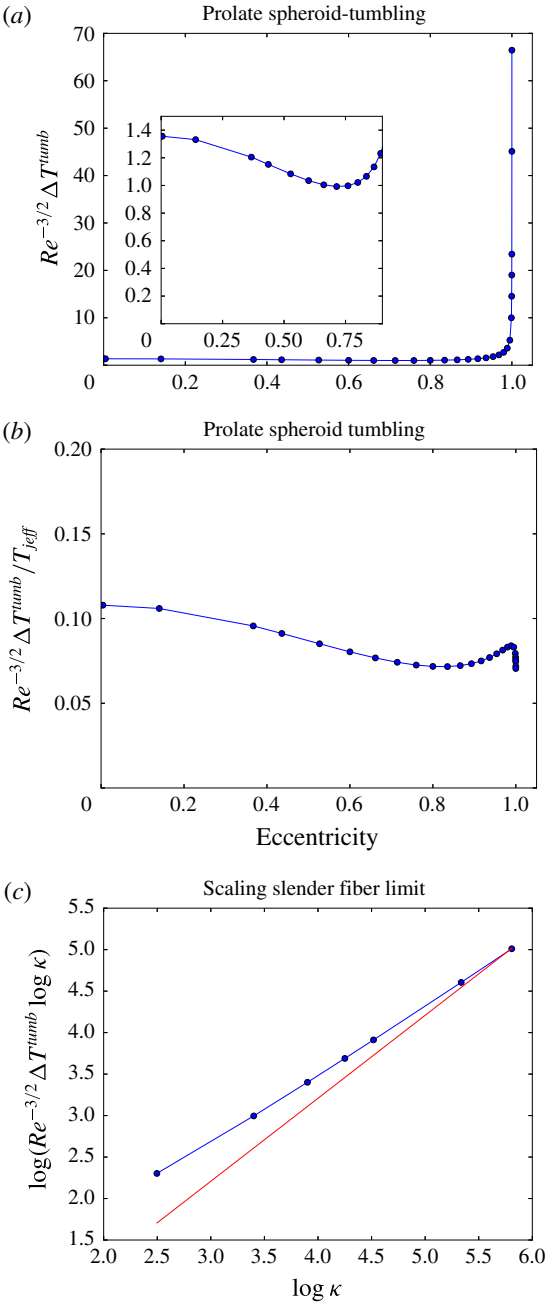

FIGURE 3. (Colour online) (*a*) The $O(Re^{3/2})$ inertial correction plotted against the eccentricity (e) for a prolate spheroid in the tumbling orbit. The inset plot shows a zoomed view of $e < 0.8$. (*b*) The $O(Re^{3/2})$ inertial correction scaled with the Jeffery period plotted as a function of the prolate spheroid eccentricity. (*c*) The inertial correction times $\log\kappa$ is plotted on a log–log scale for large aspect ratios; the red line shown in the plot has a slope of unity.

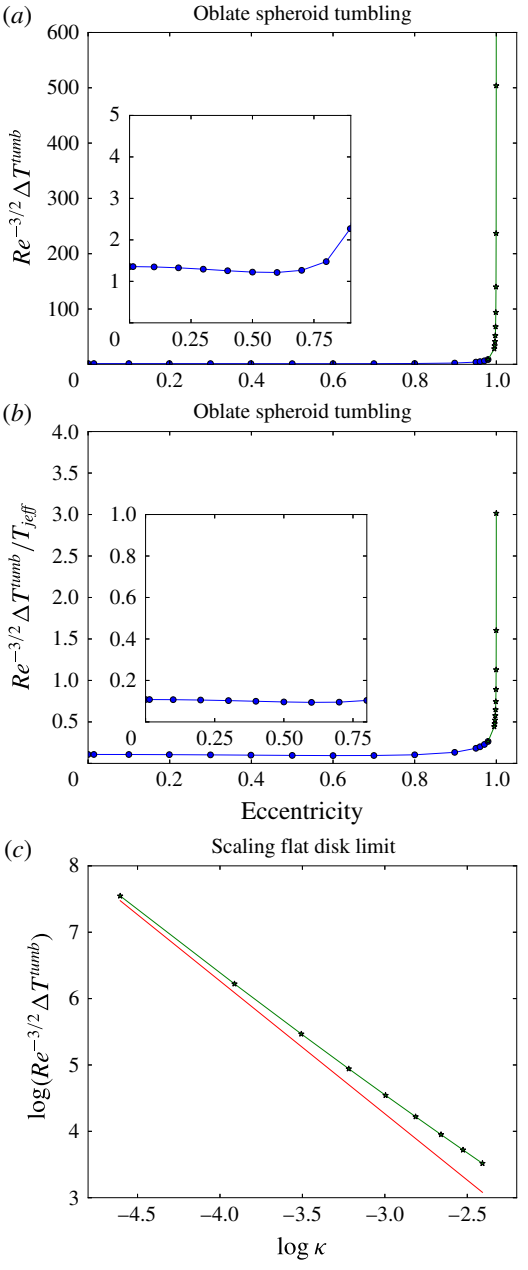

FIGURE 4. (Colour online) (*a*) The $O(Re^{3/2})$ inertial correction plotted against the eccentricity for an oblate spheroid in the tumbling orbit. The blue points indicate the aspect ratios for which the tumbling orbit is unstable; the black points correspond to conditional stability (initial-orientation-dependent). The inset plot shows the zoomed view for $e < 0.8$. (*b*) The $O(Re^{3/2})$ inertial correction scaled with the Jeffery period plotted as a function of the oblate spheroid eccentricity. (*c*) The inertial correction is plotted on a log–log scale for small aspect ratios. The red line is the asymptote given in (5.59).

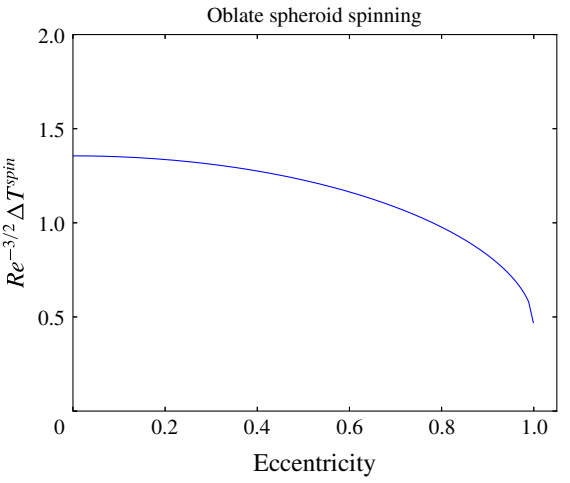

FIGURE 5. (Colour online) The $O(Re^{3/2})$ inertial correction is plotted against the eccentricity for an oblate spheroid in the spinning orbit.

defined as $\kappa_1 = b/a$ and $\kappa_2 = c/a$. For $\kappa_1 = 1$, the ellipsoid becomes an oblate spheroid with aspect ratio κ_2, and for $\kappa_1 = \kappa_2$, the ellipsoid becomes a prolate spheroid with aspect ratio $1/\kappa_1$.

Recently, Rosen (2016) simulated the inertial orientation dynamics of a triaxial ellipsoid in simple shear flow as a function of Re (based on the length of the longest principal axis), using lattice Boltzmann simulations. Rosen (2016) examined the stability of principal-axis-aligned rotations for a triaxial ellipsoid with $\kappa_1 = 1/3$ and $\kappa_2 = 1/4$ for Re ranging from 0 to 100. A particular result was the ability of inertia to stabilize the intermediate-axis-aligned rotation even for small but finite Re, an aspect that comes under the purview of the current small-Re analysis. The triangular region in figure 6 covers all axis ratios of interest for a triaxial ellipsoid, with one of its sides ($\kappa_1 = 1$) corresponding to an oblate spheroid, the other ($\kappa_2 = 0$) corresponding to an elliptical flat disk, and the hypotenuse ($\kappa_1 = \kappa_2$) corresponding to a prolate spheroid. The analysis below can predict the time period correction for an ellipsoid with axis ratios of order unity, provided that the ellipsoid rotates about one of its principal axes. The particular pair of axis ratios examined by Rosen (2016) is shown as a filled (black) circle in figure 6. We also use the analysis to predict the time period corrections for a sequence of axis-ratio pairs approaching an elliptical flat disk (marked using crosses in figure 6). It is known from Dabade *et al.* (2016) that a circular flat disk (an infinitely thin oblate spheroid) tumbles starting from almost any initial orientation. Therefore, it is reasonable to assume that rotation about the intermediate axis remains stable for ellipsoids with axis ratios approaching that of an elliptical flat disk. The stability of such a rotation needs to nevertheless be validated using a numerical approach as given in Rosen (2016) or an $O(Re)$ analytical calculation. It should be noted that the assumption of stable intermediate-axis-aligned rotation cannot be true for triaxial ellipsoids with axis ratios lying close to the blue segment in figure 6 (corresponding to triaxial ellipsoids with axis-ratio pairs close to that of an oblate spheroid with $\kappa_2 > 0.137$). This is because as $\kappa_1 \to 1$, a triaxial ellipsoid approaches the limiting oblate spheroid via the intermediate axis lengthening to equal the longest one. Stable intermediate-axis-aligned rotation would therefore correspond to a tumbling rather than a spinning oblate spheroid.

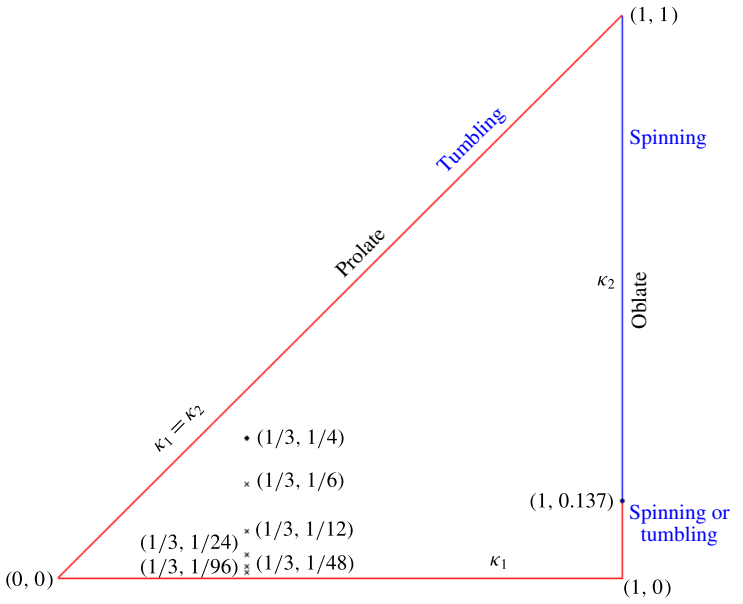

FIGURE 6. (Colour online) The orbits stabilized by inertia from earlier analysis for general triaxial ellipsoids are indicated in the figure. The filled black circle corresponds to the ellipsoid for which the numerical simulation by Rosen (2016) has shown that the rotation about the intermediate axis is stable. The orbits stabilized for prolate and oblate spheroids are indicated (Dabade *et al.* 2016). For the ellipsoids indicated by crosses, we assume that the inertia stabilizes the rotation about the intermediate axis.

To calculate the correction, we again use the reciprocal theorem formulation of § 2, with the problem of interest being a neutrally buoyant triaxial ellipsoid rotating in a simple shear flow with its intermediate axis aligned with the ambient vorticity. In the test problem, we consider the same triaxial ellipsoid rotating in a quiescent fluid. The expression for the angular velocity of a triaxial ellipsoid obtained from the reciprocal theorem is the same as that of a spheroid given in (2.24)–(2.25), with the velocity fields and torque constants replaced with those of the ellipsoid. As for the spheroid, the $O(Re)$ correction to the time period for any triaxial ellipsoid rotating in a principal-axis-aligned orientation is zero. At $O(Re)$, the angular velocity of the triaxial ellipsoid must be quadratic in the flow parameters ($\boldsymbol{E}$ and $\boldsymbol{\omega}$) and be invariant under any of the transformations $\boldsymbol{p} \leftrightarrow -\boldsymbol{p}$, $\boldsymbol{q} \leftrightarrow -\boldsymbol{q}$ and $\boldsymbol{r} \leftrightarrow -\boldsymbol{r}$. The invariance implies that for a rotation with any of the principal axes aligned with the ambient vorticity, the angular dependence of the time period integral at $O(Re)$, given in (3.5), is such that it evaluates to zero when integrated over ϕ_j. For rotation about the intermediate axis $\boldsymbol{q}$, ϕ_j would correspond to the angle made by the vector $\boldsymbol{p}$ with the flow axis (the vectors $\boldsymbol{p}$ and $\boldsymbol{r}$ lie in the flow–gradient plane). Thus, the correction to the time period of rotation about the intermediate axis arises at $O(Re^{3/2})$. The calculation of this correction follows the same steps as that for a tumbling spheroid seen in § 5. We therefore define the singularity coefficients that completely characterize the far-field disturbance forms in the problem of interest and the test problem, and directly state the correction to the time period at $O(Re^{3/2})$ for the ellipsoids shown in figure 6 without going into the details of the calculation.

To calculate the $O(Re^{3/2})$ correction to the time period, one has to evaluate the integral given in (5.3). The singularity coefficient for a triaxial ellipsoid rotating with angular velocity $\boldsymbol{\Omega}^{(2)}$ in a quiescent ambient is given by

$$\begin{aligned}\boldsymbol{S}_{ik}^{(2)} &= \frac{1}{2}\epsilon_{ijk}(H_1(\kappa_1^2+\kappa_2^2)(\boldsymbol{\Omega}^{(2)}\cdot\boldsymbol{p})p_j + H_2(1+\kappa_2^2)(\boldsymbol{\Omega}^{(2)}\cdot\boldsymbol{q})q_j + H_3(\kappa_1^2+1)(\boldsymbol{\Omega}^{(2)}\cdot\boldsymbol{r})r_j)\\ &+ \left(\frac{H_3}{2}(1-\kappa_1^2)(p_iq_k+p_kq_i)(\boldsymbol{\Omega}^{(2)}\cdot(\boldsymbol{p}\times\boldsymbol{q}))\right.\\ &+ \frac{H_1}{2}(\kappa_1^2-\kappa_2^2)(r_iq_k+r_kq_i)(\boldsymbol{\Omega}^{(2)}\cdot(\boldsymbol{q}\times\boldsymbol{r})) \qquad (7.2)\\ &+ \left.\frac{H_2}{2}(\kappa_2^2-1)(p_ir_k+p_kr_i)(\boldsymbol{\Omega}^{(2)}\cdot(\boldsymbol{r}\times\boldsymbol{p}))\right), \qquad (7.3)\end{aligned}$$

with constants H_i defined as (Kim & Karrila 1991)

$$H_1 = \frac{16\pi\kappa_1\kappa_2}{3(\kappa_1^2\beta_0+\kappa_2^2\gamma_0)}, \quad H_2 = \frac{16\pi\kappa_1\kappa_2}{3(\alpha_0+\kappa_2^2\gamma_0)}, \quad H_3 = \frac{16\pi\kappa_1\kappa_2}{3(\alpha_0+\kappa_1^2\beta_0)}, \quad (7.4a\text{–}c)$$

and

$$\alpha_0 = \int_0^\infty \frac{\kappa_1\kappa_2}{(1+t)\sqrt{(1+t)(\kappa_1^2+t)(\kappa_2^2+t)}}\,\mathrm{d}t, \qquad (7.5)$$

$$\beta_0 = \int_0^\infty \frac{\kappa_1\kappa_2}{(\kappa_1^2+t)\sqrt{(1+t)(\kappa_1^2+t)(\kappa_2^2+t)}}\,\mathrm{d}t, \qquad (7.6)$$

$$\gamma_0 = \int_0^\infty \frac{\kappa_1\kappa_2}{(\kappa_2^2+t)\sqrt{(1+t)(\kappa_1^2+t)(\kappa_2^2+t)}}\,\mathrm{d}t. \qquad (7.7)$$

In the limit of a spheroid, the singularity in (7.3) reduces to that given in (2.8), with the first three terms reducing to the rotlet proportional to B_2 and B_3, and the last three terms reducing to the stresslet proportional to B_1. For the particular case of rotation about the intermediate axis, this singularity reduces to

$$\boldsymbol{S}_{ik}^{(2)} = \frac{1}{2}\epsilon_{ijk}(H_2(1+\kappa_2^2)(\boldsymbol{\Omega}^{(2)}\cdot\boldsymbol{q})q_j) + \left(\frac{H_2}{2}(\kappa_2^2-1)(p_ir_k+p_kr_i)(\boldsymbol{\Omega}^2\cdot(\boldsymbol{r}\times\boldsymbol{p}))\right). \qquad (7.8)$$

The stresslet singularity coefficient corresponding to a triaxial ellipsoid rotating in simple shear flow is given by

$$\begin{aligned}\boldsymbol{S}_{ik}^{(1)} &= J_1\alpha_0''(3p_ip_k-\delta_{ik})(\boldsymbol{E}:\boldsymbol{pp}) + J_1\beta_0''(3q_iq_k-\delta_{ik})(\boldsymbol{E}:\boldsymbol{qq}) + J_1\gamma_0''(3r_ir_k-\delta_{ik})(\boldsymbol{E}:\boldsymbol{rr})\\ &- \frac{H_3}{2}\left(\frac{\alpha_0+\beta_0}{\gamma_0'} - \frac{(1-\kappa_1^2)^2}{(1+\kappa_1^2)}\right)(\boldsymbol{E}:\boldsymbol{pq})(p_iq_k+q_ip_k)\\ &- \frac{H_1}{2}\left(\frac{\gamma_0+\beta_0}{\alpha_0'} - \frac{(\kappa_2^2-\kappa_1^2)^2}{(\kappa_2^2+\kappa_1^2)}\right)(\boldsymbol{E}:\boldsymbol{rq})(r_iq_k+q_ir_k)\\ &- \frac{H_2}{2}\left(\frac{\gamma_0+\alpha_0}{\beta_0'} - \frac{(\kappa_2^2-1)^2}{(1+\kappa_1^2)}\right)(\boldsymbol{E}:\boldsymbol{rp})(r_ip_k+p_ir_k), \qquad (7.9)\end{aligned}$$

with the constants above defined as (Kim & Karrila 1991)

$$J_1 = -\frac{16\pi\kappa_1\kappa_2}{9(\alpha_0''\beta_0''+\alpha_0''\gamma_0''+\gamma_0''\beta_0'')}, \qquad (7.10)$$

$$\alpha_0'' = \int_0^\infty \frac{\kappa_1\kappa_2\,\mathrm{d}t}{(\kappa_1^2+t)(\kappa_2^2+t)\sqrt{(1+t)(\kappa_1^2+t)(\kappa_2^2+t)}}, \tag{7.11}$$

$$\beta_0'' = \int_0^\infty \frac{\kappa_1\kappa_2\,\mathrm{d}t}{(1+t)(\kappa_2^2+t)\sqrt{(1+t)(\kappa_1^2+t)(\kappa_2^2+t)}}, \tag{7.12}$$

$$\gamma_0'' = \int_0^\infty \frac{\kappa_1\kappa_2\,\mathrm{d}t}{(\kappa_1^2+t)(1+t)\sqrt{(1+t)(\kappa_1^2+t)(\kappa_2^2+t)}}, \tag{7.13}$$

$$\alpha_0' = \frac{\gamma_0-\beta_0}{(\kappa_1^2-\kappa_2^2)}, \tag{7.14}$$

$$\beta_0' = \frac{\alpha_0-\gamma_0}{(\kappa_2^2-1)}, \tag{7.15}$$

$$\gamma_0' = \frac{\beta_0-\alpha_0}{(1-\kappa_1^2)}. \tag{7.16}$$

It should be noted that, unlike the singularity for a spheroid given in (2.15), there are six constants in (7.9), with three constants corresponding to axisymmetric extensional flows, aligned with each of the ellipsoidal axes (first three terms in (7.9)), and the last three corresponding to planar extensional flows in the planes formed by the three axes (taken two at a time). The first term within the brackets of the latter three constants in (7.9) is obtained by imposing the torque-free condition on the ellipsoid. For the particular case of the rotation about the intermediate axis, (7.9) reduces to

$$\begin{aligned} \boldsymbol{S}_{ik}^{(1)} \;=\; & J_1\alpha_0''(3p_ip_k-\delta_{ik})(\boldsymbol{E}:\boldsymbol{pp}) + J_1\gamma_0''(3r_ir_k-\delta_{ik})(\boldsymbol{E}:\boldsymbol{rr}) \\ & -\frac{H_2}{2}\left(\frac{\gamma_0+\alpha_0}{\beta_0'}-\frac{(\kappa_2^2-1)^2}{(1+\kappa_1^2)}\right)(\boldsymbol{E}:\boldsymbol{rp})(r_ip_k+p_ir_k). \end{aligned} \tag{7.17}$$

The correction to the time period takes the same form as in (5.3), with the constants Y_c (the torque coefficient for the rotation about the intermediate principal axis) and $\dot{\phi}_{jeff}$ (the magnitude of the leading-order angular velocity of the triaxial ellipsoid) given by

$$Y_C = -\frac{2\kappa_1\kappa_2(1+\kappa_2^2)}{3(\alpha_0+\kappa_2^2\gamma_0)}, \tag{7.18}$$

$$\dot{\phi}_{jeff} = -\frac{1}{2}+\frac{1-\kappa_2^2}{1+\kappa_2^2}\cos(2\phi_j). \tag{7.19}$$

The detailed calculation, for the triaxial ellipsoids indicated in figure 6, leads to the time period corrections given in table 1. We have also listed the ratio of the correction(ΔT_{corrE}) to the leading-order time period ($T_{jeff}=2\pi(\kappa_2+\kappa_2^{-1})$) in the table. As shown in figure 7, this ratio scales as $1/\kappa_2^{0.87}$ for $\kappa_2\to 0$. Unlike the case of the prolate spheroid in figure 3, where the ratio decreases with increasing aspect ratio (slender fibres), here it increases with decreasing κ_2 (thin ellipses). This increase is similar to that seen for a tumbling oblate spheroid with decreasing aspect ratio (see figure 4).

In principle, the analogue of the $O(Re)$ integral given in (2.24), for a triaxial ellipsoid, would allow one to analytically determine the stability of the principal-axis-aligned rotations for axis ratios other than the one examined in simulations

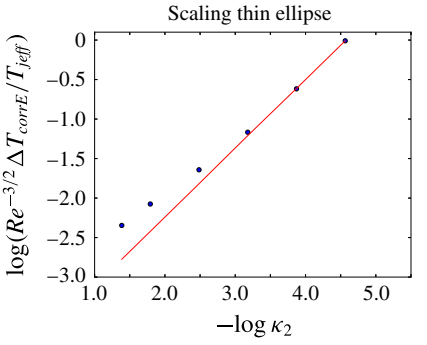

FIGURE 7. (Colour online) The ratio $\Delta T_{corrE}/T_{jeff}$ plotted against $1/\kappa_2$ in a log–log scale. The red line has a slope of 0.87.

κ_1	κ_2	Time period	$\Delta T_{corrE}/T_{jeff}$
$\frac{1}{3}$	$\frac{1}{4}$	$\frac{17\pi}{2} + 2.55\ Re^{3/2}$	$0.095\ Re^{3/2}$
$\frac{1}{3}$	$\frac{1}{6}$	$\frac{37\pi}{3} + 4.86\ Re^{3/2}$	$0.125\ Re^{3/2}$
$\frac{1}{3}$	$\frac{1}{12}$	$\frac{145\pi}{6} + 14.7\ Re^{3/2}$	$0.194\ Re^{3/2}$
$\frac{1}{3}$	$\frac{1}{24}$	$\frac{577\pi}{12} + 47.04\ Re^{3/2}$	$0.311\ Re^{3/2}$
$\frac{1}{3}$	$\frac{1}{48}$	$\frac{2305\pi}{24} + 162.68\ Re^{3/2}$	$0.539\ Re^{3/2}$
$\frac{1}{3}$	$\frac{1}{96}$	$\frac{9217\pi}{48} + 597.43\ Re^{3/2}$	$0.99\ Re^{3/2}$

TABLE 1. Inertial time periods for torque-free triaxial ellipsoids in simple shear flow.

(Rosen 2016). However, the analysis involved is likely to be exceedingly complicated, since the $O(Re)$ correction arises from a region around the ellipsoid of the order of its own size, and thus the Stokes velocity field required for the $O(Re)$ computation would involve nonlinear combinations of the ellipsoidal harmonics used by Jeffery (1922). In contrast, the $O(Re^{3/2})$ correction is insensitive to these details, and, as seen above, one only needs the force-dipole singularity that the ellipsoids in the actual and test problems correspond to. A calculation of the time period correction over the entire parameter space indicated in figure 6 will, however, have to wait until a more comprehensive investigation of inertia-induced stability of the principal-axis-aligned rotations.

8. Conclusions and future work

In this paper, we have evaluated the leading-order fluid inertial correction, at $O(Re^{3/2})$, to the time period of rotation a spheroid, in simple shear flow, rotating in

the tumbling and spinning orbits. The first effects of inertia occur at $O(Re)$, but at this order, inertia only acts to stabilize either one of two Jeffery orbits, depending on the spheroid aspect ratio and its initial orientation, leaving the time period of rotation unchanged. Specifically, it has been shown by Einarsson *et al.* (2015) and Dabade *et al.* (2016) that the stable orbit for a prolate spheroid of any aspect ratio is the tumbling one, and is the spinning one for an oblate spheroid with $\kappa > 0.137$. The stable orbit for an oblate spheroid with $\kappa < 0.137$ is either spinning or tumbling, depending on the initial orientation.

The correction to the angular velocity at $O(Re^{3/2})$ is formulated as an integral in Fourier space, based on a reciprocal theorem formulation, the details of which are given in § 2. The disturbance velocity field around a spinning spheroid is steady, and, therefore, the correction to the angular velocity at $O(Re^{3/2})$ is trivially related to the correction to the time period through (4.1). The calculation proceeds in a manner similar to earlier calculations for a sphere (Stone *et al.* 2000; Subramanian *et al.* 2011), and the result is given in (4.24). The disturbance velocity field around a spheroid is unsteady in the tumbling orbit, and the evaluation of the time period correction is therefore not trivial. However, we show in § 5 that by expanding the integrand in the reciprocal theorem as a Fourier series in time, one can evaluate the correction without the need for truncation. The numerical results for the tumbling and spinning orbits are summarized in § 6. It is shown that the time period of rotation increases with the fluid inertia, at $O(Re^{3/2})$ in both tumbling and spinning orbits, consistent with earlier simulations. It was shown in Dabade *et al.* (2016) that the particle inertia decreases the tumbling time period at $O(St^2)$. For the tumbling neutrally buoyant spheroids considered here, $St = Re$, and the increase due to fluid inertia is therefore dominant. Particle inertia plays no role for spinning spheroids.

Although not considered here, for a general spheroid orientation, the $O(Re^{3/2})$ correction should also contribute to an orbital drift. This correction is of little consequence for the rheology of a dilute suspension of neutrally buoyant prolate spheroids, on account of the stability, at $O(Re)$, of the tumbling mode for all aspect ratios. However, the $O(Re^{3/2})$ correction will affect the rheology of a suspension of oblate spheroids by altering the location of the repeller identified in Dabade *et al.* (2016), and that separates the basins of attraction (on the unit hemisphere) corresponding to the tumbling and spinning modes. The altered repeller location, for aspect ratios lower than 0.137 (this threshold is itself subject to an $O(Re^{1/2})$ correction), will contribute to an $O(Re^{1/2})$ correction to the shear viscosity. This is in contrast to the $O(Re^{3/2})$ modification expected from the direct effects of inertia (via corrections to the stresslet integral, and the acceleration and Reynolds stresses); see Subramanian *et al.* (2011). An analogous effect is expected in the presence of weak Brownian motion, with the critical aspect ratio, corresponding to the tumbling–spinning transition in simple shear flow, being altered by $O(Re^{1/2})$ (see Marath *et al.* 2017).

In § 7, we have evaluated the time period correction for the triaxial ellipsoids indicated in figure 6. The calculation proceeds in a manner similar to that of a tumbling spheroid, and the results are presented in § 7. In performing this calculation, we have assumed that fluid inertia, at $O(Re)$, stabilizes the rotation about the intermediate principal axis for ellipsoids other than the one already analysed in Rosen (2016). Examination of a sequence of triaxial ellipsoids asymptoting to an elliptical disk of eccentricity $(8/9)^{1/2}$, rotating in the assumed manner, leads to the inertial correction to the time period diverging in a manner similar to the oblate spheroid. The assumption of intermediate-axis-aligned rotation is, however, not likely

for axis ratios close to the blue segment in figure 6. Inertial stabilization, at $O(Re)$, of principal-axis-aligned rotations requires a more comprehensive simulation programme than the one given in Rosen (2016), or a small-Re analytical approach. The latter appears to be particularly forbidding, keeping in mind the ellipsoidal harmonics used for constructing the Stokes velocity field around an arbitrarily oriented triaxial ellipsoid (Jeffery 1922).

The analysis of the period of rotation of a tumbling inertial spheroid has thus far assumed an aspect ratio of order unity, and we make this estimate more precise in the arguments that follow. An order-unity aspect ratio leads to the inertial contributions to the angular velocity being asymptotically small in comparison with the Stokesian one, and, as seen in (3.5), the time period may then be expanded in a perturbative manner for small Re. This is no longer possible for extreme-aspect-ratio spheroids. As described in § 5.5, at $Re = 0$, such spheroids rotate very slowly during the aligned phase. Thus, even in the limit $Re \ll 1$, the $O(Re)$ inertial correction becomes comparable to the leading-order Stokesian rotation, and, as first shown by Subramanian & Koch (2005), this leads to an arrest of rotation beyond a modest threshold Re. To analyse this arrest for both slender fibres ($\kappa \to \infty$) and flat disks ($\kappa \to 0$), we consider the asymptotic forms of the equation for $\dot{\phi}_j$, given by

$$\dot{\phi}_j = -\phi_j^2 - \frac{1}{\kappa^2} + Re\phi_j \left[G_1^\infty - G_2^\infty + G_3^\infty - G_4^\infty\right] + \lim_{\kappa\to\infty} Re^{3/2}\dot{\phi}_{c2} \tag{8.1}$$

$$= -\phi_j^2 - \frac{1}{\kappa^2} + Re\frac{\phi_j}{15\log\kappa} + \lim_{\kappa\to\infty} Re^{3/2}\dot{\phi}_{c2} \tag{8.2}$$

and

$$\dot{\phi}_j = -\phi_j^2 - \kappa^2 - Re\phi_j \left[G_1^0 - G_2^0 - G_3^0 + G_4^0\right] + \lim_{\kappa\to 0} Re^{3/2}\dot{\phi}_{c2} \tag{8.3}$$

$$= -{\phi_j}^2 - \kappa^2 + Re\frac{2\phi_j}{15} + \lim_{\kappa\to 0} Re^{3/2}\dot{\phi}_{c2}, \tag{8.4}$$

for slender fibres and flat disks respectively. Here, $G_i^\infty = \lim_{\kappa\to\infty} G_i^n(\xi_0)$, $G_i^0 = \lim_{\kappa\to 0} G_i^n(\xi_0)$, and these terms are given in Dabade *et al.* (2016). We consider a slender fibre to begin with; the arguments for a flat disk follow in an analogous manner. For $\log\kappa/\kappa \ll Re \ll 1$, the arrest of rotation for a fibre occurs when the $O(Re)$ term in (8.2) equals the slender-body contribution of (ϕ_j^2), so the orientation of the nearly aligned stationary fibre is $O(Re/\log\kappa)$. At the onset of arrest, the non-slender-body term proportional to κ^{-2} in (8.2) must also be of the same order, and this leads to a threshold given by $Re_c = ((30\log\kappa)/\kappa)$, the resulting stationary orientation being $O(1/\kappa)$ (see Subramanian & Koch 2005). We now examine the $O(Re^{3/2})$ correction in order to show that the estimate for Re_c above, obtained by considering only the $O(Re)$ contribution, is not altered at leading order. One first needs an estimate for $\dot{\phi}_{c2}$, which may be obtained from the definition $\Delta T_{tumb} = Re^{3/2}\int_0^{T_{jeff}} \mathrm{d}t(\dot{\phi}_{c2}/\dot{\phi}_{jeff})$ and the fact that $\Delta T_{tumb} \sim O(Re^{3/2}\kappa/\log\kappa)$, as shown in § 5.5. For the aligned phase, $\mathrm{d}t \sim O(\kappa)$ and $\dot{\phi}_{jeff} \sim O(1/\kappa^2)$, and this leads to $\dot{\phi}_{c2} \sim 1/(\kappa^2\log\kappa)$. Using this, the higher-order inertial correction in (8.2) is $O(Re^{3/2}/\kappa^2\log\kappa)$. It should be noted that the singular origin of this contribution implies that the angular velocity at this order remains finite even for an aligned spheroid; this is unlike the regular $O(Re)$ contribution, which goes to zero as $O(\phi_j)$, being proportional to the instantaneous angular acceleration of the fluid elements

(approximated based on the Stokesian field). Using the aforementioned estimate of Re_c, one finds that the $O(Re^{3/2})$ correction is $O[(\log\kappa)^{1/2}/\kappa^{7/2}]$ at arrest, while the Stokesian and $O(Re)$ inertial contributions are $O(1/\kappa^2)$, and, therefore, asymptotically larger. Thus, the inclusion of the $O(Re^{3/2})$ contribution only decreases Re_c, relative to its leading-order estimate, by $O[(\log\kappa)^{1/2}/\kappa^{3/2}]$. In summary, for a given Re, the analysis in this paper predicts an $O(Re^{3/2})$ inertia-induced increase in the time period of a prolate spheroid for $1 \ll \kappa \ll \kappa_c$, with $\log \kappa_c/\kappa_c \sim Re$ (or $\kappa_c \sim Re \log Re$ at leading logarithmic order). However, the arrest of rotation for large κ values of $O(\kappa_c)$ is still controlled by the $O(Re)$ inertial correction first obtained by Subramanian & Koch (2005). For a flat disk, similar arguments show that the threshold for arrest corresponds to $Re_c = 15\kappa$, based on the $O(Re)$ correction, and inclusion of the $O(Re^{3/2})$ contribution obtained here only decreases Re_c by $O(\kappa^{1/2})$ relative to this estimate. This in turn implies that the $O(Re^{3/2})$ analysis given here for oblate spheroids is only valid provided that $\kappa \gg O(Re)$. Thus, the $O(Re^{3/2})$ analysis for a spheroid is valid only for $Re \ll \kappa \ll Re \log Re$. This Re-dependent aspect-ratio interval makes the limitation of order-unity aspect ratios mentioned earlier precise. Importantly, combination of the $O(Re^{3/2})$ contribution with the $O(Re)$ contribution given in Dabade *et al.* (2016) allows one to predict the first effects of inertia for all aspect ratios, including the arrest of rotation of extreme-aspect-ratio spheroids.

Appendix A. The integrals in (5.47)

The four-dimensional and five-dimensional integrals for the terms proportional to $\hat{u}_1^{fi}$ ($i = $ '0','$t\cos$','$t\sin$'), $\hat{u}_3^{fi}$ ($i = $ '0','$t\cos$','$t\sin$') and the four-dimensional integral for $\hat{u}_2^{fi}$ ('$t\cos$','$t\sin$') in (5.47) are given below in the spherical coordinate system.

The integral proportional to $\hat{u}_2^{f0}$ is written using (5.35) and (5.4),

$$\begin{aligned}
&\int (-4\pi^2 k^2\, \hat{u}_2^{f0}(\boldsymbol{k})\, \mathbf{1}_2 \cdot \boldsymbol{T}_1^{tumb})\, \mathrm{d}\boldsymbol{k} \\
&\quad = -\int_0^{2\pi}\int_0^{\pi}\int_0^{\infty} 4\pi^2 \left\{ k^2 \left[\frac{\mathrm{i}B_3 k_1}{2k^2\pi} \frac{(1+\kappa^2)^2}{2\kappa^2} \right.\right. \\
&\qquad \left.\left. + \frac{\mathrm{i}B_1 k_1 (k^2 - 2k_2^2)}{2k^4\pi} \frac{(1-\kappa^4)}{2\kappa^2} \right] \frac{k^2 + k_1^2 s^2 + 2k_1 k_2 s}{k^2} Q_2^0(\boldsymbol{k}') \right\} \\
&\qquad \times \int_0^{\infty} k^2 \exp\left(-4\pi^2 \left(k^2 s + k_1 k_2 s^2 + \frac{k_1^2 s^3}{3} \right) \right) \mathrm{d}k\, \mathrm{d}s\, \sin\theta\, \mathrm{d}\theta\, \mathrm{d}\phi. \qquad \text{(A 1)}
\end{aligned}$$

The integral proportional to $\hat{u}_3^{f0}$ is written using (5.41) and (5.4),

$$\begin{aligned}
&\int (-4\pi^2 k^2\, \hat{u}_3^{f0}(\boldsymbol{k})\, \mathbf{1}_3 \cdot \boldsymbol{T}_1^{tumb})\, \mathrm{d}\boldsymbol{k} \\
&\quad = -\int_0^{2\pi}\int_0^{\pi}\int_0^{\infty} 4\pi^2 \left\{ k^2 \left[-\frac{\mathrm{i}B_1 k_1 k_2 k_3}{k^4\pi} \frac{(1-\kappa^4)}{2\kappa^2} \right] Q_3^0(\boldsymbol{k}') \right\} \\
&\qquad \times \int_0^{\infty} k^2 \exp\left(-4\pi^2 \left(k^2 s + k_1 k_2 s^2 + \frac{k_1^2 s^3}{3} \right) \right) \mathrm{d}k\, \mathrm{d}s\, \sin\theta\, \mathrm{d}\theta\, \mathrm{d}\phi \\
&\qquad - \int_0^{2\pi}\int_0^{\pi}\int_0^{\infty}\int_0^{\infty} 4\pi^2 \left\{ k^2 \left[-\frac{\mathrm{i}B_1 k_1 k_2 k_3}{k^4\pi} \frac{(1-\kappa^4)}{2\kappa^2} \right] \right.
\end{aligned}$$

$$\times \frac{2k_1k_3}{k'^2}\left(\frac{k'^2+k_1^2s'^2+2k_1k_2's'}{k'^2}\right)Q_2^0(\boldsymbol{k}'')\Big\}$$
$$\times \int_0^\infty \exp\left(-4\pi^2\left(k^2s+k_1k_2s^2+\frac{k_1^2s^3}{3}\right)\right)$$
$$\times \exp\left(-4\pi^2\left(k'^2s'+k_1k_2's'^2+\frac{k_1^2s'^3}{3}\right)\right)k^2\,\mathrm{d}k\,\mathrm{d}s\,\mathrm{d}s'\,\sin\theta\,\mathrm{d}\theta\,\mathrm{d}\phi. \quad (A\,2)$$

The integral proportional to $\hat{u}_1^{ftcos}$ is written using (5.39) and (5.4),

$$\int(-4\pi^2k^2\,\hat{u}_1^{ftcos}(\boldsymbol{k})\,\mathbf{1}_1\cdot\boldsymbol{T}_2^{tumb})\,\mathrm{d}\boldsymbol{k} = -\int_0^{2\pi}\int_0^{\pi}\int_0^{\infty}4\pi^2\left\{k^2\left[\frac{(\kappa^4-1)}{2\kappa^2}\frac{\mathrm{i}B_3k_2}{2k^2\pi}\right.\right.$$
$$\left.\left.+\frac{\mathrm{i}B_1(k^2-2k_1^2)k_2}{2k^4\pi}\frac{(1+\kappa^2)^2}{2\kappa^2}\right]\left(Q_1^{2i}(\boldsymbol{k}')\cos(2\omega_gs)-Q_1^{2Re}(\boldsymbol{k}')\sin(2\omega_gs)\right)\right\}$$
$$\times\int_0^\infty \mathrm{i}2k^2\exp\left(-4\pi^2\left(k^2s+k_1k_2s^2+\frac{k_1^2s^3}{3}\right)\right)\mathrm{d}k\,\mathrm{d}s\,\sin\theta\,\mathrm{d}\theta\,\mathrm{d}\phi$$
$$+\int_0^{2\pi}\int_0^{\pi}\int_0^{\infty}\int_0^{\infty}4\pi^2k^2\left\{\left[\frac{(\kappa^4-1)}{2\kappa^2}\frac{\mathrm{i}B_3k_2}{2k^2\pi}+\frac{\mathrm{i}B_1(k^2-2k_1^2)k_2}{2k^4\pi}\frac{(1+\kappa^2)^2}{2\kappa^2}\right]\right.$$
$$\times\left(1-\frac{2k_1^2}{k'^2}\right)\left(Q_2^{2i}(\boldsymbol{k}'')\cos(2\omega_g(s+s'))-Q_2^{2Re}(\boldsymbol{k}'')\sin(2\omega_g(s+s'))\right)$$
$$\left.\times\left(\frac{k'^2+k_1^2s'^2+2k_1k_2's'}{k'^2}\right)\right\}\int_0^\infty\exp\left(-4\pi^2\left(k^2s+k_1k_2s^2+\frac{k_1^2s^3}{3}\right)\right)$$
$$\times\mathrm{i}2\exp\left(-4\pi^2\left(k'^2s'+k_1k_2's'^2+\frac{k_1^2s'^3}{3}\right)\right)k^2\,\mathrm{d}k\,\mathrm{d}s'\,\mathrm{d}s\,\sin\theta\,\mathrm{d}\theta\,\mathrm{d}\phi. \quad (A\,3)$$

The integral proportional to $\hat{u}_2^{ftcos}$ is written using (5.36) and (5.4),

$$\int(-4\pi^2k^2\,\hat{u}_2^{ftcos}(\boldsymbol{k})\mathbf{1}_2\cdot\boldsymbol{T}_2^{tumb})\,\mathrm{d}\boldsymbol{k}$$
$$=-\int_0^{2\pi}\int_0^{\pi}\int_0^{\infty}4\pi^2\left\{k^2\left[\frac{-\mathrm{i}B_3k_1}{2k^2\pi}\frac{(\kappa^4-1)}{2\kappa^2}+\frac{\mathrm{i}B_1k_1(k^2-2k_2^2)}{2k^4\pi}\frac{(1+\kappa^2)^2}{2\kappa^2}\right]\right.$$
$$\left.\times\left(\frac{k^2+k_1^2s^2+2k_1k_2s}{k^2}\right)\left(Q_2^{2i}(\boldsymbol{k}')\cos(2\omega_gs)-Q_2^{2Re}(\boldsymbol{k}')\sin(2\omega_gs)\right)\right\}$$
$$\times\int_0^\infty\mathrm{i}2\exp\left(-4\pi^2\left(k^2s+k_1k_2s^2+\frac{k_1^2s^3}{3}\right)\right)k^2\,\mathrm{d}k\,\mathrm{d}s\,\sin\theta\,\mathrm{d}\theta\,\mathrm{d}\phi. \quad (A\,4)$$

The integral proportional to $\hat{u}_3^{ftcos}$ is written using (5.42) and (5.6),

$$\int(-4\pi^2k^2\,\hat{u}_3^{ftcos}(\boldsymbol{k})\,\mathbf{1}_3\cdot\boldsymbol{T}_2^{tumb})\,\mathrm{d}\boldsymbol{k} = -\int_0^{2\pi}\int_0^{\pi}\int_0^{\infty}4\pi^2\left\{k^2\left[-\frac{\mathrm{i}B_1k_1k_2k_3}{k^4\pi}\frac{(1+\kappa^2)^2}{2\kappa^2}\right]\right.$$
$$\left.\times\left(Q_3^{2i}(\boldsymbol{k}')\cos(2\omega_gs)-Q_3^{2Re}(\boldsymbol{k}')\sin(2\omega_gs)\right)\right\}$$
$$\times\int_0^\infty\mathrm{i}2\exp\left(-4\pi^2\left(k^2s+k_1k_2s^2+\frac{k_1^2s^3}{3}\right)\right)k^2\,\mathrm{d}k\,\mathrm{d}s\,\sin\theta\,\mathrm{d}\theta\,\mathrm{d}\phi$$

$$
\begin{aligned}
&- \int_0^{2\pi}\int_0^{\pi}\int_0^{\infty}\int_0^{\infty} \left\{ 4\pi^2 k^2 \left[-\frac{\mathrm{i}B_1 k_1 k_2 k_3}{k^4 \pi} \frac{(1+\kappa^2)^2}{2\kappa^2} \right] \left(\frac{2k_1 k_3}{k'^2} \right) \right. \\
&\times \left(\frac{k'^2 + k_1^2 s'^2 + 2k_1 k_2' s'}{k'^2} \right) \\
&\left. \times \left(Q_2^{2i}(\boldsymbol{k}'') \cos(2\omega_g (s+s')) - Q_2^{2Re}(\boldsymbol{k}'') \sin(2\omega_g (s+s')) \right) \right\} \qquad \text{(A 5)} \\
&\times \int_0^{\infty} \exp\left(-4\pi^2 \left(k^2 s + k_1 k_2 s^2 + \frac{k_1^2 s^3}{3} \right) \right) \\
&\times \mathrm{i}2 \exp\left(-4\pi^2 \left(k'^2 s' + k_1 k_2' s'^2 + \frac{k_1^2 s'^3}{3} \right) \right) k^2 \,\mathrm{d}k \,\mathrm{d}s' \,\mathrm{d}s \,\sin\theta \,\mathrm{d}\theta \,\mathrm{d}\phi. \qquad \text{(A 6)}
\end{aligned}
$$

The integral proportional to $\hat{u}_1^{ftsin}$ is written using (5.39) and (5.4),

$$
\begin{aligned}
&\int (-4\pi^2 k^2 \hat{u}_1^{ftsin}(\boldsymbol{k}) \mathbf{1}_1 \cdot \boldsymbol{T}_3^{tumb}) \,\mathrm{d}\boldsymbol{k} \\
&= - \int_0^{2\pi}\int_0^{\pi}\int_0^{\infty} 4\pi^2 \left\{ k^2 \left[\frac{\mathrm{i}B_1 (k^2 - k_1^2 + k_2^2) k_1}{2k^4 \pi} \right. \right. \\
&\left. \left. \times \left(\frac{\kappa^2 + 1}{\kappa} \right) \right] \left(Q_1^{2Re}(\boldsymbol{k}') \cos(2\omega_g s) + Q_1^{2i}(\boldsymbol{k}') \sin(2\omega_g s) \right) \right\} \\
&\times \int_0^{\infty} \mathrm{i}2 \exp\left(-4\pi^2 \left(k^2 s + k_1 k_2 s^2 + \frac{k_1^2 s^3}{3} \right) \right) k^2 \,\mathrm{d}k \,\mathrm{d}s \,\sin\theta \,\mathrm{d}\theta \,\mathrm{d}\phi \\
&+ \int_0^{2\pi}\int_0^{\pi}\int_0^{\infty}\int_0^{\infty} 4\pi^2 \left\{ k^2 \left[\frac{\mathrm{i}B_1 (k^2 - k_1^2 + k_2^2) k_1}{2k^4 \pi} \left(\frac{\kappa^2 + 1}{\kappa} \right) \right] \right. \\
&\times \left(1 - \frac{2k_1^2}{k'^2} \right) \left(\frac{k'^2 + k_1^2 s'^2 + 2k_1 k_2' s'}{k'^2} \right) \\
&\left. \times \left(Q_2^{2Re}(\boldsymbol{k}'') \cos(2\omega_g (s+s')) + Q_2^{2i}(\boldsymbol{k}'') \sin(2\omega_g (s+s')) \right) \right\} \\
&\times \int_0^{\infty} \exp\left(-4\pi^2 \left(k^2 s + k_1 k_2 s^2 + \frac{k_1^2 s^3}{3} \right) \right) \\
&\times \mathrm{i}2 \exp\left(-4\pi^2 \left(k'^2 s' + k_1 k_2' s'^2 + \frac{k_1^2 s'^3}{3} \right) \right) k^2 \,\mathrm{d}k \,\mathrm{d}s' \,\mathrm{d}s \,\sin\theta \,\mathrm{d}\theta \,\mathrm{d}\phi. \qquad \text{(A 7)}
\end{aligned}
$$

The integral proportional to $\hat{u}_2^{ftsin}$ is written using (5.36) and (5.4),

$$
\begin{aligned}
&\int (-4\pi^2 k^2 \hat{u}_2^{f0}(\boldsymbol{k}) \mathbf{1}_2 \cdot \boldsymbol{T}_3^{tumb}) \,\mathrm{d}\boldsymbol{k} \\
&= - \int_0^{2\pi}\int_0^{\pi}\int_0^{\infty} 4\pi^2 \left\{ k^2 \left[- \left(\frac{\kappa^2 + 1}{\kappa} \right) \frac{\mathrm{i}B_1 k_2 (k^2 + k_1^2 - k_2^2)}{2k^4 \pi} \right] \right. \\
&\left. \times \left(\frac{k^2 + k_1^2 s^2 + 2k_1 k_2 s}{k^2} \right) \left(Q_2^{2Re}(\boldsymbol{k}') \cos(2\omega_g s) + Q_2^{2i}(\boldsymbol{k}') \sin(2\omega_g s) \right) \right\} \\
&\times \int_0^{\infty} \mathrm{i}2 \exp\left(-4\pi^2 \left(k^2 s + k_1 k_2 s^2 + \frac{k_1^2 s^3}{3} \right) \right) k^2 \,\mathrm{d}k \,\mathrm{d}s \,\sin\theta \,\mathrm{d}\theta \,\mathrm{d}\phi. \qquad \text{(A 8)}
\end{aligned}
$$

The integral proportional to $\hat{u}_3^{ftsin}$ is written using (5.42) and (5.4),

$$\begin{aligned}
&\int (-4\pi^2 k^2\, \hat{u}_3^{ftsin}(\boldsymbol{k})\, \mathbf{1}_3 \cdot \boldsymbol{T}_3^{tumb})\, \mathrm{d}\boldsymbol{k} \\
&\quad = -\int_0^{2\pi}\int_0^{\pi}\int_0^{\infty} 4\pi^2 \left\{ k^2 \left[-\left(\frac{\kappa^2+1}{\kappa}\right) \frac{\mathrm{i}B_1(k_1^2-k_2^2)k_3}{2k^4\pi} \right] \right. \\
&\qquad \left. \times\, (Q_3^{2Re}(\boldsymbol{k}')\cos(2\omega_g s) + Q_3^{2i}(\boldsymbol{k}')\sin(2\omega_g s)) \right\} \\
&\qquad \times \int_0^{\infty} \mathrm{i}2 \exp\left(-4\pi^2 \left(k^2 s + k_1 k_2 s^2 + \frac{k_1^2 s^3}{3} \right) \right) k^2\, \mathrm{d}k\, \mathrm{d}s\, \sin\theta\, \mathrm{d}\theta\, \mathrm{d}\phi \\
&\qquad - \int_0^{2\pi}\int_0^{\pi}\int_0^{\infty}\int_0^{\infty} 4\pi^2 \left\{ k^2 \left[-\left(\frac{\kappa^2+1}{\kappa}\right) \frac{\mathrm{i}B_1(k_1^2-k_2^2)k_3}{2k^4\pi} \right] \right. \\
&\qquad \times \left(\frac{2k_1 k_3}{k'^2} \right) (Q_2^{2Re}(\boldsymbol{k}'')\cos(2\omega_g(s+s')) + Q_2^{2i}(\boldsymbol{k}'')\sin(2\omega_g(s+s'))) \\
&\qquad \left. \times \left(\frac{k'^2 + k_1^2 s'^2 + 2k_1 k_2' s'}{k'^2} \right) \right\} \\
&\qquad \times \int_0^{\infty} \exp\left(-4\pi^2 \left(k^2 s + k_1 k_2 s^2 + \frac{k_1^2 s^3}{3} \right) \right) \\
&\qquad \times \mathrm{i}2 \exp\left(-4\pi^2 \left(k'^2 s' + k_1 k_2' s'^2 + \frac{k_1^2 s'^3}{3} \right) \right) k^2\, \mathrm{d}k\, \mathrm{d}s'\, \mathrm{d}s\, \sin\theta\, \mathrm{d}\theta\, \mathrm{d}\phi. \qquad \text{(A 9)}
\end{aligned}$$

REFERENCES

ARFKEN, G. B., WEBER, H. J. & HARRIS, F. E. 2011 *Mathematical Methods for Physicists: A Comprehensive Guide*. Academic.

CHILDRESS, S. 1964 The slow motion of a sphere in a rotating, viscous fluid. *J. Fluid Mech.* **20** (02), 305–314.

DABADE, V., MARATH, N. K. & SUBRAMANIAN, G. 2016 The effect of inertia on the orientation dynamics of anisotropic particles in simple shear flow. *J. Fluid Mech.* **791**, 631703.

DE GENNES, P. G. 1974 Coil–stretch transition of dilute flexible polymers under ultrahigh velocity gradients. *J. Chem. Phys.* **60** (12), 5030–5042.

EINARSSON, J., CANDELIER, F., LUNDELL, F., ANGILELLA, J. & MEHLIG, B. 2015 Rotation of a spheroid in a simple shear at small Reynolds number. *Phys. Fluids* **27** (6), 063301.

HINCH, E. J. 1974 Mechanical models of dilute polymer solutions for strong flows with large polymer deformations. *Proc. Coll. Int. CNRS Polym. Lubrification* **233**, 241–247.

HINCH, E. J. 1991 *Perturbation Methods*. Cambridge University Press.

HINCH, E. J. & LEAL, L. G. 1979 Rotation of small non-axisymmetric particles in a simple shear flow. *J. Fluid Mech.* **92** (03), 591–607.

JEFFERY, G. B. 1922 The motion of ellipsoidal particles immersed in a viscous fluid. *Proc. R. Soc. Lond.* A **102**, 161–179.

KIM, S. & KARRILA, S. J. 1991 *Microhydrodynamics: Principles and Selected Applications*. Butterworth-Heinemann.

LEAL, L. G. 1979 The motion of small particles in non-Newtonian fluids. *J. Non-Newtonian Fluid Mech.* **5**, 33–78.

LEAL, L. G. & HINCH, E. J. 1971 The effect of weak Brownian rotations on particles in shear flow. *J. Fluid Mech.* **46**, 685–703.

LIN, C.-J., PEERY, J. H. & SCHOWALTER, W. R. 1970 Simple shear flow round a rigid sphere: inertial effects and suspension rheology. *J. Fluid Mech.* **44** (01), 1–17.

MAO, W. & ALEXEEV, A. 2014 Motion of spheroid particles in shear flow with inertia. *J. Fluid Mech.* **749**, 145–166.

MARATH, N. K., DWIVEDI, R. & SUBRAMANIAN, G. 2017 An orientational order transition in a sheared suspension of anisotropic particles. *J. Fluid Mech. (Rapids)* **811**, R3.

MARATH, N. K. & SUBRAMANIAN, G. 2017 The orientation dynamics of anisotropic particles in a planar linear flow. *J. Fluid Mech.* (submitted).

MEIBOHM, J., CANDELIER, F., ROSÉN, T., EINARSSON, J., LUNDELL, F. & MEHLIG, B. 2016 Angular velocity of a spheroid log rolling in a simple shear at small Reynolds number. *Phys. Rev. Fluids* **1**, 084203.

MIKULENCAK, D. R. & MORRIS, J. F. 2004 Stationary shear flow around fixed and free bodies at finite Reynolds number. *J. Fluid Mech.* **520**, 215–242.

ROBERTSON, C. R. & ACRIVOS, A. 1970 Low Reynolds number shear flow past a rotating circular cylinder. Part 1. Momentum transfer. *J. Fluid Mech.* **40** (04), 685–703.

ROSEN, T. 2016 Angular dynamics of non-spherical particles in linear flows related to production of biobased materials. PhD dissertation. Stockholm.

SAFFMAN, P. G. T 1965 The lift on a small sphere in a slow shear flow. *J. Fluid Mech.* **22** (02), 385–400.

STONE, H., BRADY, J. & LOVALENTI, P. M. 2000 Inertial effects on the rheology of suspensions and on the motion of individual particles (unpublished).

SUBRAMANIAN, G. & KOCH, D. L. 2005 Inertial effects on fibre motion in simple shear flow. *J. Fluid Mech.* **535**, 383–414.

SUBRAMANIAN, G. & KOCH, D. L. 2006*a* Inertial effects on the orientation of nearly spherical particles in simple shear flow. *J. Fluid Mech.* **557**, 257–296.

SUBRAMANIAN, G. & KOCH, D. L. 2006*b* Inertial effects on the transfer of heat or mass from neutrally buoyant spheres in a steady linear velocity field. *Phys. Fluids* **18** (7), 073302.

SUBRAMANIAN, G., KOCH, D. L., ZHANG, J. & YANG, C. 2011 The influence of the inertially dominated outer region on the rheology of a dilute dispersion of low-Reynolds-number drops or rigid particles. *J. Fluid Mech.* **674**, 307–358.

YARIN, A. L., GOTTLIEB, O. & ROISMAN, I. V. 1997 Chaotic rotation of triaxial ellipsoids in simple shear flow. *J. Fluid Mech.* **340**, 83–100.